

SEISMIC PERFORMANCE OF BAMBOO STRUCTURES

by

Bhavna Sharma

B.Arch., State University of New York at Buffalo, 2001

M.A., State University of New York at Buffalo, 2003

M.S., University of Hawaii at Manoa, 2006

Submitted to the Graduate Faculty of
Swanson School of Engineering in partial fulfillment
of the requirements for the degree of
Doctor of Philosophy

University of Pittsburgh

2010

UNIVERSITY OF PITTSBURGH

SWANSON SCHOOL OF ENGINEERING

This dissertation was presented

by

Bhavna Sharma

It was defended on

August 17, 2010

and approved by

Dr. Piervincenzo Rizzo, Assistant Professor, Civil and Environmental Engineering

Dr. Albert To, Assistant Professor, Civil and Environmental Engineering

Dr. Lisa M. Maillart, Associate Professor, Industrial Engineering

Dr. Khosrow Ghavami, Professor, Civil Engineering, PUC-Rio

Dissertation Director: Dr. Kent A. Harries, Associate Professor, Civil and Environmental Engineering

Copyright © by Bhavna Sharma
2010

SEISMIC PERFORMANCE OF BAMBOO STRUCTURES

Bhavna Sharma, Ph.D.

University of Pittsburgh, 2010

This dissertation describes a wide-ranging research program aimed at identifying a method through which vernacular bamboo construction methods may be formalized into a performance based design framework. This requires an understanding of both material and structural behavior and an appreciation of the social and engineering context in which the structure is built. A relatively brief background and literature review addressing a number of topics relevant to the research methodology adopted in the present work including: sustainability, bamboo availability, properties and construction techniques, the hazard environment considered in this study and approaches to hazard mitigation and performance based design are presented.

The prototype structure that is the focus of the dissertation is investigated in an experimental study to determine the prototype frame behavior. The behavior forms the basis for the analytical model developed in work. In the course of the research program it was determined that certain mechanical properties of bamboo are not well established and, furthermore, that there is no standard method for comparing these critical properties. The work, therefore, reports on an experimental program aimed at filling these gaps in available knowledge and data. Initially a fracture mechanics approach to quantifying bamboo behavior was attempted in an effort to normalize for the significant variation expected in a natural material. While this method was successful, it was not felt to be practical for application outside a well-equipped laboratory

environment. Thus a simpler, mechanics-based, materials test was pursued and an attempt to correlate results from this with the more reliable fracture mechanics approach was made. A finite element model (FEM) of the prototype structure was developed. Static pushover and nonlinear dynamic analyses were conducted on several models of the prototype structure. In addition to the seismic model, the effect of the variability of bamboo material properties identified in a statistical analysis of data collected by the Group for Non-Conventional Materials (GNOCMAT) at PUC-Rio and the author's group at the University of Pittsburgh was explored.

TABLE OF CONTENTS

NOMENCLATURE.....	XVIII
ACKNOWLEDGMENTS	XXIII
1.0 INTRODUCTION.....	1
1.1 MOTIVATION, HISTORY AND CONTEXT	1
1.1.1 Bamboo as a Sustainable Construction Material	3
1.1.2 Physical Properties and Terminology Associated with Bamboo.....	3
1.1.3 Darjeeling Region of Northeast India.....	4
1.2 SUSTAINABILITY OF THE BUILT ENVIRONMENT	6
1.2.1 Local Materials	6
1.3 CONSTRUCTION WITH BAMBOO	7
1.3.1 Performance Based Design	8
1.3.2 Hazard Mitigation	9
1.3.3 Vernacular Architecture.....	10
1.4 SUMMARY	10
1.5 SCOPE OF DOCUMENT.....	11
2.0 BACKGROUND, LITERATURE REVIEWAND RESEARCH	
METHODOLOGY	14
2.1 SUSTAINABILITY	14
2.1.1 Construction Materials	15

2.1.1.1	Local Materials – Bamboo	16
2.2	MATERIAL PROPERTIES OF BAMBOO	21
2.3	HAZARD MITIGATION FORMARGINALLY AND NON-ENGINEERED STRUCTURES	24
2.4	METHODOLOGY AND OBJECTIVES	27
2.4.1	Approach to Experimental Program	28
2.4.2	Analytical Model of Prototype Bamboo Frame	29
2.4.3	Fragility Analysis.....	30
3.0	BAMBOO PORTAL FRAME BEHAVIOR	31
3.1	STRUCTURAL APPLICATIONS OF BAMBOO.....	31
3.1.1	Joint and Connections	33
3.1.2	Current Standards and Codes.....	37
3.1.2.1	International Organization for Standardization (ISO)	38
3.1.2.2	National Building Code of India	39
3.1.3	Current Design Approach.....	40
3.2	PROTOTYPE STRUCTURE AND CURRENT PRACTICE	40
3.2.1	Bamboo Connection Details.....	44
3.2.1.1	Description of Prototype Column Base.....	45
3.2.1.2	Description of Prototype Joint	46
3.3	MATERIAL PROPERTIES.....	47
3.3.1	Tension Tests.....	47
3.3.1.1	Results	48
3.3.2	Pull-out Tests.....	50

3.3.2.1	Results	51
3.4	PROTOTYPE FRAME TEST STRUCTURE	53
3.4.1	Bamboo	53
3.4.2	Grouted-Bar Column Base	54
3.4.3	Frame Connections.....	55
3.4.4	Construction.....	55
3.5	PROTOTYPE FRAME TEST SET-UP	59
3.5.1	Instrumentation and Loading	60
3.6	TEST RESULTS.....	62
3.6.1	Load – Deflection Response	62
3.6.2	Load – Deflection of Columns	63
3.6.3	Column Displacement	64
3.6.4	Behavior of Joint Regions	66
3.6.5	Post-Test Forensics	67
3.7	SUMMARY	68
3.8	CONCLUSIONS	69
4.0	CHARACTERIZATION OF SPLITTING STRENGTH OF BAMBOO	70
4.1	LITERATURE REVIEW	71
4.2	STANDARD TEST METHODS FOR BAMBOO.....	74
4.3	ASSESSING BAMBOO SPLITTINGBEHAVIOR.....	74
4.3.1	Appropriate Test Methods for Technological Sustainability	80
4.4	BOLT SHEAR TEST	81
4.4.1	Experimental Method.....	82

4.4.2	Bolt Shear Results.....	83
4.5	EDGE BEARING TEST	86
4.5.1	Equations Governing the Edge Bearing Test.....	87
4.6	EDGE BEARING EXPERIMENTAL PROGRAM.....	91
4.6.1	<i>Phyllostachys aurea</i> at PUC-Rio	91
4.6.2	<i>Bambusa stenostachya</i> at the University of Pittsburgh.....	92
4.7	EDGE BEARING TEST RESULTS	93
4.7.1	<i>Phyllostachys aurea</i>	93
4.7.2	<i>Bambusa stenostachya</i>	99
4.7.3	Comparison of Edge Bearing Results for <i>P. aurea</i> and <i>B. stenostachya</i> .	104
4.8	SPLIT PIN TEST.....	104
4.8.1	Split Pin Test Results.....	105
4.9	CORRELATION BETWEEN EDGE BEARING AND SPLIT PIN TEST RESULTS.....	106
4.10	TRANSVERSE TENSION STRAIN	107
4.11	SUMMARY	109
5.0	STATISTICAL ANALYSIS OF MATERIAL PROPERTIES OF BAMBOO..	110
5.1	INTRODUCTION	110
5.2	EXPERIMENTAL DESIGN AND STUDY PROCEDURES.....	116
5.2.1	Tensile Properties	116
5.2.2	Compressive Properties	116
5.2.3	Transverse Shear Properties	117
5.2.4	Interlaminar Shear Properties	117

5.2.5	Geometric Properties	117
5.3	STATISTICAL METHODOLOGY	118
5.3.1	Preliminary Analysis	118
5.3.2	Primary analysis	122
5.3.2.1	Homogeneity of variances	122
5.3.2.2	Analysis of Variance for equal means	125
5.3.2.3	Results	126
5.3.2.4	Summary.....	127
5.3.3	Distribution	128
5.3.4	Normal distribution.....	129
5.3.5	Weibull Distribution.....	129
5.3.6	Results.....	130
5.3.7	Summary	135
6.0	SEISMIC ANALYSIS OF BAMBOO PORTAL FRAME	136
6.1	MODELING THE PROTOTYPE BAMBOO STRUCTURE	136
6.1.1	Modeling the Column Base.....	136
6.1.2	Validation Using Tested Prototype Portal Frame	137
6.1.3	Mungpoo Prototype Model Parameters	140
6.1.4	Moment-rotation bilinear hysteretic relationship	143
6.2	SEISMIC INPUT PARAMETERS	144
6.2.1	Ground Motion Suite for NE India.....	144
6.2.2	Response Spectra	147
6.2.3	Artificial Ground Motion.....	147

6.3	SEISMIC ANALYSIS	149
6.3.1	Nonlinear Static (Pushover) Analysis	149
6.3.2	Nonlinear Dynamic Analysis	150
6.4	PERFORMANCE ASSESSMENT	150
6.4.1	Nonlinear Dynamic Response.....	150
6.4.2	Capacity vs. Demand	153
6.4.3	Effect of Species Selection and Variation of Material Properties	155
6.4.4	Results.....	158
6.5	FRAGILITY FUNCTIONS	159
6.6	SUMMARY	160
7.0	CONCLUSIONS	162
7.1	PROTOTYPE STRUCTURE.....	162
7.2	CHARACTERIZATION OF DESIGN VALUES	163
7.3	STATISTICAL ANALYSIS OF BAMBOO PROPERTIES.....	163
7.4	SEISMIC ANALYSIS	164
7.5	FUTURE WORK.....	165
7.5.1	Material Characterization	165
7.5.2	Panel Shear.....	165
7.5.3	Column-roof joint	166
7.6	SUMMARY	167
APPENDIX.....		169
CITED REFERENCES		171

LIST OF TABLES

Table 3.1 Tensile specimen dimensions and test results.....	49
Table 3.2 Pull-out test results.....	51
Table 3.3 Prototype Frame Member Details.....	54
Table 3.4 Cement Mortar Mix Design.....	55
Table 4.1 Summary of material test methods for bamboo.....	76
Table 4.2 Bolt shear specimen geometrical properties and test results.	84
Table 4.3 Average geometric properties of edge bearing specimens.	92
Table 4.4 Measured and calculated results from edge bearing tests on <i>P. aurea</i>	97
Table 4.5 Measured and calculated results from edge bearing tests on <i>B. stenostachya</i>	100
Table 4.6 Split pin specimen results for <i>B. stenostachya</i>	106
Table 4.7 Observed tension rupture strain values.....	108
Table 5.1 Longitudinal tensile properties of bamboo coupon specimens.....	112
Table 5.2 Longitudinal compressive properties of full culm bamboo.	113
Table 5.3 Transverse shear properties determined from bamboo coupon specimens.	114
Table 5.4 Interlaminar shear properties	114
Table 5.5 Full culm geometrical properties.....	115
Table 5.6 Selected data sources for the longitudinal tensile stress and modulus.	120
Table 5.7 Selected data sources for longitudinal compressive stress and modulus.....	120

Table 5.8 ANOVA test for equal variances	123
Table 5.9 Summary of ANOVA test for <i>D. giganteus</i> and <i>P. aurea</i>	127
Table 5.10 Comparison of distributions for goodness-of-fit.	128
Table 5.11 Calculated and estimated parameters for the Normal and Weibull distributions.	131
Table 6.1 OpenSees model geometric and material properties for PUC-Rio comparison.	140
Table 6.2 OpenSees model geometric and material properties for Mungpoo.	141
Table 6.3 Structural materials and associated nodal masses.....	142
Table 6.4 OpenSees hysteretic model parameters	144
Table 6.5 Nonlinear dynamic response of the Mungpoo frame.....	151
Table 6.6 Summary of geometric and material properties for parametric analysis	156
Table 6.7 Summary of parametric analysis of material properties for <i>D. giganteus</i>	157
Table 6.8 Summary of parametric analysis of material properties for <i>P. aurea</i>	157

LIST OF FIGURES

Figure 1.1 Topographic map of Darjeeling Region with sites highlighted.....	5
Figure 2.1 Global map of available bamboo species.	17
Figure 2.2 Examples of engineered bamboo structures.	19
Figure 2.3 Bamboo connection designed by architect Renzo Piano.....	19
Figure 2.4 Bamboo frame house.....	20
Figure 2.5 Undamaged Ikra (bamboo frame construction) building	25
Figure 2.6 Damaged stone masonry building	26
Figure 2.7 Damage in reinforced concrete building.	26
Figure 2.8 National Building Code of India Seismic Hazard Zone Map.....	27
Figure 3.1 IPRITI (Banglore) and TRADA (UK) full-scale bamboo house.	32
Figure 3.2 Aluminum Plate Pin-end Joint.....	33
Figure 3.3 Bamboo connections and commercially available engineered bamboo connections..	35
Figure 3.4 Bolted bamboo connection.	36
Figure 3.5 Grouted internode with fastener connection.....	36
Figure 3.6 Grouted Rebar Connection and footing with rebar connection.....	37
Figure 3.7 Faber Maunsell Covered Walkway and Stage Project.	38
Figure 3.8 Details from St. Joseph’s School, Mungpoo, India	42
Figure 3.9 Floor Plan and Elevations of the St. Joseph’s North Point School	43

Figure 3.10 St. Josephs’ Mungpoo School, India	45
Figure 3.11 Column base connections	45
Figure 3.12 Prototype Column – Truss Joint	46
Figure 3.13 Details for tension test.	48
Figure 3.14 Results for T-PA Specimens.	49
Figure 3.15 Pull-out test set-up details.	51
Figure 3.16 Results from Prototype Frame Pull-out Tests.	52
Figure 3.17 Prototype Frame As-Built with Dimensions (cm) and Member Notations.	54
Figure 3.18 Preparation of the column bases.....	56
Figure 3.19 Placement of cement mortar in column bases.	57
Figure 3.20 Column bases after template is removed.....	57
Figure 3.21 Final assembled frame positioned in place.....	59
Figure 3.22 Details of frame bracing.	60
Figure 3.23 Prototype frame instrumentation and loading.	62
Figure 3.24 Lateral Load – Displacement of at the top of both left and right columns.....	63
Figure 3.25 Load – Deflection Response for Columns A and B.	64
Figure 3.26 Load – Displacement Graphs	65
Figure 3.27 Column displacements at select load levels.	66
Figure 3.28 Distortion of Joint at Top of Right Column.	67
Figure 3.29 Interior of column pull-out tests.	68
Figure 4.1 Split pin test set-up.	72
Figure 4.2 Examples of bamboo splitting observed at St. Joseph’s School.	79
Figure 4.3 Bolt shear test set-up.	83

Figure 4.4 Applied load-displacement curves for bolt shear tests.	84
Figure 4.5 Ultimate bearing stress at failure vs. loading angle for bolt shear tests.	85
Figure 4.6 Edge bearing test specimen geometry.	88
Figure 4.7 Edge bearing specimen failure.	89
Figure 4.8 Load-displacement results from edge bearing tests of all <i>P. aurea</i> specimens.	94
Figure 4.9 Location of failures and apparent modulus of rupture values for <i>P. aurea</i>	96
Figure 4.10 Apparent stress vs strain results for edge bearing specimens for <i>P. aurea</i>	98
Figure 4.11 Edge bearing tests results for <i>B. stenostachya</i>	99
Figure 4.12 Location of failures and apparent modulus of rupture values for <i>B. stenostachya</i>	101
Figure 4.13 Apparent stress vs strain results for edge bearing specimens for <i>B. stenostachya</i>	102
Figure 4.14 Strain distribution through wall thickness in edge bearing specimens.	103
Figure 4.15 Test results for <i>B. stenostachya</i> split pin specimens.	106
Figure 5.1 Mechanical properties boxplots for <i>D. giganteus</i> and <i>P. aurea</i>	121
Figure 5.2 ANOVA test for equal variances.	124
Figure 5.3 Normal and Weibull probability plots for <i>D. giganteus</i>	132
Figure 5.4 Normal and Weibull probability plots for <i>P. aurea</i>	133
Figure 5.5 Normal empirical cumulative distribution functions.	134
Figure 6.1 OpenSees model node and member (noted in squares) numbering	138
Figure 6.2 Pushover behavior of the experimental frame.	140
Figure 6.3 Location of nodal masses in OpenSees Mungpoo model.	143
Figure 6.4 Bilinear hysteretic material model input parameters for OpenSees.	144
Figure 6.5 Artificial accelerogram for the MW 8.3 scenario earthquake located at Jorthang.	146
Figure 6.6 Spectral acceleration based on ASCE 7-05 and NBCI (2005) for site class C.	147

Figure 6.7 SIMQKE intensity function used to generate artificial ground motions	148
Figure 6.8 Response spectrum and artificial ground motions generated by SIMQKE.....	148
Figure 6.9 Nonlinear static analysis results for Mungpoo frame.....	149
Figure 6.10 Kobe earthquake results	151
Figure 6.11 Northridge earthquake results.....	152
Figure 6.12 India Zone IV earthquake results	152
Figure 6.13 India Zone V earthquake results.....	153
Figure 6.14 Capacity vs. demand curve in ADRS format	154
Figure 6.15 Capacity-demand spectrum for all models.	158
Figure 7.1 Portal frame analysis including bamboo infill.....	166
Figure 7.2 Column-roof joint splitting failure and capacity curve.	167

NOMENCLATURE

$2a$	initial length of the crack
$2w$	specimen length
A_b	bolt area
A_c	area of the culm
A_l	area of the interlaminar shear plane
A_{net}	smallest area of the bolt engaged in shear (usually through the threads)
A_t	area in tension
A_{\perp}	area of the transverse shear specimen
b	breadth of tension coupon
C_s	ratio of base shear to seismic weight of the structure
c	distance from the midline of the culm wall to the edge of the wall section
c_r	distance from the midline of the culm wall to the edge of the wall section at the location of rupture
d_b	bolt diameter
df_B	degree of freedom between groups
df_w	degree of freedom within group
D_o	external diameter
D_v	vertical diametric deflection of a hollow cylinder
E	modulus of elasticity
E_b	bending modulus of elasticity

E_L	longitudinal modulus of elasticity
E_φ	circumferential modulus of elasticity
f_b	apparent modulus of rupture
f_{bearing}	bearing stress
f'_c	concrete compressive strength
f_r	modulus of rupture of the culm wall
f_{rNS}	modulus of rupture of the north-south culm wall
f_{rEW}	modulus of rupture of the east-west culm wall
f_y	material yield strength
F	ANOVA statistic
F	shape factor
F_b	bearing force
F_c	compressive force
F_{crit}	critical ANOVA statistic
F_l	interlaminar stress force
F_{stat}	ANOVA statistic
F_t	tensile force
F_{\parallel}	shear force parallel to the fiber direction
F_{\perp}	transverse shear force
G	shear modulus
h	distance from the culm wall midline to the elastic neutral axis measured toward the center of curvature
h_{col}	length of the column
h_r	distance from the culm wall midline to the elastic neutral axis measured toward the center of curvature at the location of rupture
H_0	null hypothesis

H_1	alternative hypothesis
I	moment of inertia
I_b	bending moment of inertia
I_r	moment of inertia at location of rupture
k_1	correction factor for hoop-stress deformation
k_2	correction factor for transverse shear deformation
K_{IC}	fracture toughness
K_I	Mode I stress intensity factor
KL/r	slenderness ratio
L	length
L_b	beam length
L_e	embedded length
m	mass of the structure
M	moment
M_{EW}	moment at the east-west location
M_{NS}	moment at the north-south location
n	number of specimens in group
N	total number of specimens in sample
p_{stat}	calculated alpha value
P_{max}	maximum tensile load
P_{split}	total applied load to cause splitting
q	material property under investigation
R	radius to the midline of the culm wall section
R_o	measured outside radius of the culm
R_x	horizontal reaction force

R_y	vertical reaction force
s	standard deviation
s_B	variance between groups
s_W	variance within groups
S	slope of the load-displacement line from edge bearing test
SS_B	sum of squares between groups
SS_W	sum of squares within groups
T_n	natural period of the structure
t	wall thickness
t_r	wall thickness at the location of rupture
V	base shear
W	seismic weight of the structure
wL	applied load along length of specimen
\bar{x}	average
α	Weibull scale parameter
α_c	confidence level
β	Weibull shape parameter
Δ	displacement
ε	strain
μ	mean
μ_k	k^{th} mean
ν	Poisson ratio
φ	modal displacement
σ_B	variance between groups
σ_c	compressive stress of the culm

σ_{failure}	direct tension rupture stress
σ_{gross}	tensile stress measured over the gross culm wall area
σ_t	tensile capacity parallel to the fiber
σ_w	variance within groups
τ_{\parallel}	shear strength parallel to the fiber
τ_{\perp}	transverse shear capacity

ACKNOWLEDGMENTS

I would like to thank and acknowledge Dr. Kent Harries for his support and guidance throughout this adventure. In addition, I would like to thank Dr. Khosrow Ghavami for hosting me during my research rotation at PUC-Rio. Also, I graciously acknowledge the members of the committee, Dr. Rizzo, Dr. To, Dr. Maillart. I would like to acknowledge and thank Derek Mitch for his interest, support and work in this area of research. Also, thanks to Ian McElhone, Amanda Oczkowski, and Amanda Barry, as well as the students, technicians, and staff of PUC-Rio for their support and assistance. Furthermore, I would like to acknowledge Gayatri Kharel for her support and the members of SHED for sharing their work and knowledge of the Indian hill region. I gratefully acknowledge the support of the Mascaro Center for Sustainable Innovation and the National Science Foundation IGERT program. Finally, I would like to thank my family for their encouragement and guidance, as well as Gurumayi for her love and support.

1.0 INTRODUCTION

1.1 MOTIVATION, HISTORY AND CONTEXT

A recent Rand Corporation report (Silberglitt et al. 2006 and “Civil” 2006) anticipates an increasing socio-technical-economic gap developing between scientifically ‘advanced’ countries (e.g.: United States, Western Europe) and those that are ‘proficient’ (e.g.: the so-called BRIC countries: Brazil, Russia, India and China), ‘developing’ (e.g.: Mexico, Turkey) and ‘lagging’ (e.g.: Egypt, Nepal). Additionally, particularly within scientifically proficient countries expected to experience great growth, a similar widening gap between urban and rural populations is anticipated. Sixteen so-called ‘new technologies’ are predicted to proliferate by 2020; most involve aspects of the civil infrastructure. Indeed, the Rand report cites the lack of stable infrastructure (including electricity, potable water, roads, schools and transportation systems) as the primary barrier to the adoption of technology. The report further cites the increased emphasis by advanced countries on ‘sustainable practices’ as being largely unattainable (by 2020) for proficient, developing or lagging regions. Two key new technologies cited in the Rand report are the focus of the present work: inexpensive, autonomous housing and “green” manufacturing [and construction].

A critical aspect of sustainable infrastructure is its ability to perform under both service conditions and extreme events. Safety in the built environment is a fundamental right.¹ Recent ‘great’ natural catastrophes have resulted in unacceptably high casualty tolls. The 2001 earthquake in Bhuj, India left over 19,700 dead; the 2003 Bam (Iran) earthquake: over 26,000 dead; the 2004 Aceh earthquake and subsequent tsunami: over 275,000 dead; the 2005 Kashmir earthquake: over 80,000 dead; the 2008 Sichuan earthquake: 70,000 dead; and the 2010 Haiti earthquake: over 170,000 dead. The injured are many times these numbers and the displaced are often an order of magnitude or two greater. In reviewing this litany of statistics, one must acknowledge the clear disparity between developed and less developed regions.²

As demonstrated by the October 8, 2005 Kashmir earthquake, the Himalayan region is at particular risk. It is exposed to a high seismic hazard, is relatively densely populated by relatively poor people, and is geographically remote. The Himalayan range has experienced approximately 20 devastating earthquakes since 1900. Indian seismological maps indicate high hazard regions as far south as Delhi. Of particular concern is the “Himalayan gap” – a 600 km long region of the central Himalayas extending across Nepal (including Katmandu) and East into the Darjeeling region of India – which has not experienced a recent major event. Seismologists suggest that this region is capable of generating multiple events having moment magnitudes greater than 8.0 (Bilham et al. 2001).

¹ Article 25 of the United Nations Universal Declaration of Human Rights states that “Everyone has the right to a standard of living adequate for the health and well-being of himself and of his family, including food, clothing, housing and medical care and necessary social services...”

Principle #10 of the 1994 Special Rapporteur’s Report to the United Nations Commission on Human Rights states: “All persons have the right to adequate housing, land tenure and living conditions in a secure, healthy and ecologically sound environment.”

² The 2010 Chilean earthquake, the largest event of those listed and the fifth largest recorded since 1900, resulted in less than 521 casualties (Radio Coopertiva, May 15, 2010) primarily due to the adoption of advanced building codes and earthquake-hazard mitigating technology.

1.1.1 Bamboo as a Sustainable Construction Material

In 2004, the International Organization for Standardization (ISO), in partnership with the International Network for Bamboo and Rattan (INBAR), a Beijing-based agency whose aim is to promote bamboo and rattan for poverty alleviation in developing countries, published a model standard on structural design using bamboo (ISO 2004a) and a series of methods for determining the mechanical properties of bamboo (ISO 2004b). If the use of bamboo is limited to rural areas, the ISO standard recognizes established “experience from previous generations” as being an adequate basis for design. However, if bamboo is to realize its full potential as a sustainably obtained and utilized building material on an international scale, issues of the basis for design, prefabrication, industrialization, finance and insurance of building projects, and export and import of materials all require some degree of standardization (Janssen 2005).

The intent of the ISO (2004a) standard is to establish a modern limit states design approach while recognizing traditional design and practices. Precisely because of this dichotomy, however, the standard is simultaneously inadequate on both counts in the context of application in developing regions. A limit states approach requires specialized knowledge and engineering which may not be readily available. The traditional approach, while often adequate for service conditions, is unable to address ultimate limit states, particularly those associated with extreme events such as earthquakes.

1.1.2 Physical Properties and Terminology Associated with Bamboo

Bamboo is not a material well known to civil engineers. Nonetheless, it is not the intent of this work to describe or quantify all physical properties of bamboo. For an overview of the properties of bamboo as they relate to structural applications, the reader is directed to Janssen (1981) and

Arce-Villalobos (1993). Both Janssen and Arce-Villalobos also provide reviews of the extensive nomenclature associated with bamboo. Nonetheless, a brief glossary of relevant terms is provided in Appendix A: *Definitions and Nomenclature* of this document.

1.1.3 Darjeeling Region of Northeast India

For the sake of appropriate contextualization, this project considers the hill region of the Darjeeling area in northern West Bengal state. This area is an economically depressed region of a rapidly emerging country, India. It epitomizes what Silbergliitt et al. (2006) refer to as “the widening gap between urban and rural populations”. The selection of this region for context is largely independent of the technical goals of this work. Nonetheless, the author feels that it is important to provide context, if only to better define the scope of the work. The selection of this region is supported by contact with Ms. Gayatri Kharel and a number of other contacts made during a three week visit to Darjeeling, Kalimpong, Mungpoo and Gangtok (Sikkim) in May 2008 (Sharma et al. 2008). The author returned to this region in May 2010 to follow-up on some goals identified in 2008 and since. Figure 1.1 provides an overview of the Darjeeling area visited in 2008 and 2010 that forms the contextual basis for this work.

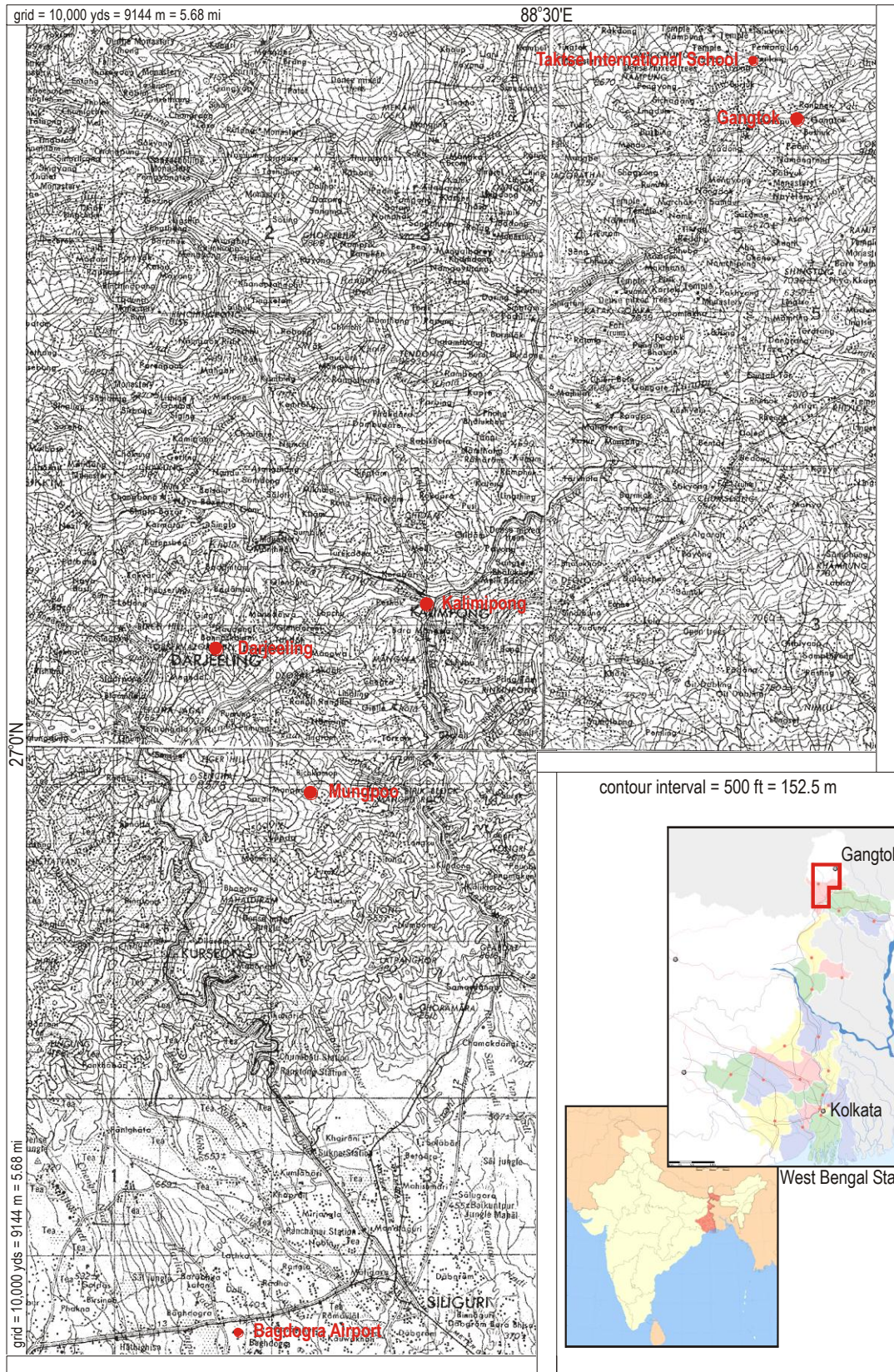


Figure 1.1 Topographic map of Darjeeling Region with sites highlighted.

1.2 SUSTAINABILITY OF THE BUILT ENVIRONMENT

The ability of the built environment to sustain infrastructure and the surrounding natural environment largely depends on the way it is engineered. A key topic in the world today is how to be 'green' and more importantly how to do so in a sustainable manner and provide for future generations. A significant area in need of transformative technology is the built environment and infrastructure. Consumption of natural resources for construction and use of energy are typically the primary concerns. Additionally, the ability of the current infrastructure to withstand natural hazards, such as earthquakes and flooding, is quickly emerging as a priority in developing and developed countries, not least due to recent disasters such as those in Aceh and Haiti.

Typically, sustainability of the built environment is centered on the use of local materials and adaptation to utilize the natural resources of the local environment. By adapting to the surroundings, for example, the building utilizes the natural resources of light, ventilation, as well as vegetation to allow it to operate more efficiently. The main goal is to reduce the impact on the environment of the building and its use and occupancy, as well as to minimize the operation costs of the building during its lifespan.

1.2.1 Local Materials

Historically, use of local materials was *de facto* due to the ease of transportation and appropriateness to local climates. Structures were built in response to the surrounding environment using materials that would provide the best shelter. For instance, the adobe houses of the southwestern United States provide thermal comfort in a desert climate; Icelandic turf houses were built into the hillside which utilized the ground for insulation and cooling, as well as

providing a unique form that reduced the forces from the wind. The effects of globalization have impacted these concepts, particularly in respect to the use of materials in residential construction.

The use of modern materials, such as reinforced concrete and steel, is often preferred over traditional methods of construction. Modern materials, however, are not always suited to a particular environment, and more importantly are not constructed using proper design approaches or the necessary tools. The failure of poorly designed or constructed structures is a major problem, especially in areas of high seismic risk. The structure itself becomes the cause of what would otherwise be preventable casualties in event of an earthquake. The relationship between construction materials and methods and seismic hazard risk needs to be further explored.

1.3 CONSTRUCTION WITH BAMBOO

Recognition of bamboo as a sustainable construction material is growing, with research and construction not limited to developing countries but being initiated worldwide. Structural applications of bamboo are diverse and include flooring, ‘particle board’, reinforcement (culms and partial culms for concrete and masonry and fibers for mortars and polymers), and framing. Nonetheless, the majority of knowledge of bamboo construction is based on cultural tradition. To develop bamboo as a sustainable construction material, in both an engineering and cultural sense, one must evaluate traditional building techniques in terms of engineering standards and develop equivalent methods of design and performance assessment. The performance based design (PBD) paradigm provides a basis for the formalization and codification of vernacular and non-engineered structures. The approach begins in the initial design phase and develops goals that

reflect the desired performance of the structure. Different objectives or ‘performance metrics’ are used to reflect the performance of the structure in terms of structural, social or economic goals. This method is gaining traction but has only been applied sparingly to the design and evaluation of building and bridge infrastructure.

1.3.1 Performance Based Design

Performance based design has been most widely adapted to address performance of structures subject to extreme loading, most typically earthquake loading. Performance based seismic design (PBSD) has been formulated into a four stage methodology: hazard analysis, structural analysis, damage analysis and loss analysis (Porter et al. 2007). Hazard analysis, in the context of seismic design, represents a geophysical assessment of anticipated ground motion parameters. Due to the highly probabilistic nature of the hazard input and eventual damage analysis output, the structural analysis is typically simple, although for seismic design, it must capture nonlinear effects. Damage analysis is based on the use of engineering demand parameters (EDP) to determine a level of damage, or damage measure (DM), in the structural components of a building. Finally, the loss analysis applies metrics (often cost) to the damage measure to allow assessment of the performance.

The probabilistic nature of the damage analysis, in particular, accounts for the uncertainty of the impact an earthquake has on the integrity of a structure. Damage analysis is conducted using fragility functions which describe the probability of a structure being damaged beyond a specified damage state as a function of the level of ground shaking. The method utilizes probability functions based on structural demand and capacity, which determine the damage state of the components in the structure (Porter et al. 2007). The DM of the structure is based on the

strength and capacity of the structural components. For seismic analysis, the demand, or EDP, are ground motion parameters representative of the area under investigation.

Fragility curves portray the vulnerability of structures in terms of service level decision basis variables: “dollars [cost], death [casualty], and downtime” (Porter et al. 2007). These variables facilitate the implementation of hazard mitigation policy and provide a relationship between structural damage and seismic intensity. Typically applied to the performance of modern structures, fragility analyses provide for the assessment of buildings, transportation networks and other infrastructure, and assist in the prioritization of disaster response for infrastructure. The method, therefore, demonstrates the adequate or inadequate response of a structure or inventory of structures and the probable impact of a seismic event.

Current seismic risk analysis research focuses on modern materials and construction methods with little research dedicated towards traditional building methods. Exploration of traditional building methods is essential to hazard mitigation in developing countries, due to the lack of standards and proliferation of non-engineered structures. The probabilistic framework of seismic risk analysis provides an opportunity to verify the structural performance of marginally and non-engineered structures. Use of fragility functions demonstrates the vulnerability of traditional structures and provides a foundation for developing risk assessments and can lead to seismic guidelines and standards.

1.3.2 Hazard Mitigation

Hazard mitigation is typically addressed through building standards or codes and community planning. Hazard mitigation is defined as any sustained action taken to reduce or eliminate long-term risk to life and property from a hazard event (HAZUS 2003). To assess the vulnerability of

a structure to a natural hazard, the structure can be analyzed to determine its performance. The HAZUS-defined approach has been applied to evaluate the seismic risk to bridges and buildings on the west coast and in the southeast U.S.

1.3.3 Vernacular Architecture

Traditional or non-engineered building techniques represent a heritage that has evolved over generations and has the potential to make significant contributions to engineering research due to the depth of experience from which they have been developed. Such structures are often referred to as ‘vernacular architecture’, a term which has various meanings and interpretations. For the purpose of this work, the definition of ‘vernacular’ is taken to mean a cultural form of building developed in response to the surrounding context. From a PBD perspective, the importance of vernacular structures is that the form has evolved in response to the demands of the environment. Research has shown that some vernacular buildings perform well in seismic events while others are susceptible to severe damage (Gutierrez 2004). Assessment of traditional building methods will facilitate further understanding of the performance of vernacular structures in areas of high seismic risk. Additionally such an assessment will help to place these previously unconsidered structures into a building code or similarly formal engineering context thereby facilitating socio-economic objectives of emerging and developing communities and countries.

1.4 SUMMARY

Development of sustainable construction methods is growing, with research and construction being initiated worldwide. Use of indigenous materials and vernacular non-engineered building

methods constitute a large portion of housing in the world. Nonetheless, the majority of knowledge of non-engineered structures is based only on cultural tradition. Vernacular structures must be evaluated in terms of engineering standards in order to develop equivalent design methods, which both assess and improve performance. Performance based design provides a basis for the formalization and codification of non-engineered structures. Damage analysis using fragility curves provides a tool for assessing the performance of structures in terms of service level decision basis variables.

Due to the lack of standardization of construction methods, understanding of traditional building materials and methods is essential to hazard mitigation in developing countries. Fragility functions may be used to assess the vulnerability of marginally and non-engineered structures and demonstrate a foundation for further development of seismic guidelines and standards. The significance of this study is to demonstrate the performance of bamboo frame structures in the event of an earthquake. Using a performance-based approach, codification of bamboo structures will help to standardize the construction process and decrease vulnerability of bamboo housing. Seismic risk assessment of vernacular structures will facilitate further understanding of building performance in areas of high seismic risk and development of hazard mitigation policies.

1.5 SCOPE OF DOCUMENT

This dissertation describes a wide-ranging research program aimed at identifying a method through which vernacular bamboo construction methods may be formalized into a performance based design framework. This requires an understanding of both material and structural behavior

and an appreciation of the social and engineering context in which the structure is built. The document is divided into largely self-contained chapters as follows:

While each subsequent chapter provides a review of immediately relevant literature, Chapter 2.0 provides a relatively brief background and literature review addressing a number of topics relevant to the research methodology adopted in the present work including: sustainability, bamboo availability, properties and construction techniques, the hazard environment considered in this study and approaches to hazard mitigation and performance based design.

Chapter 3.0 introduces the prototype structure considered in the remainder of the dissertation and reports on an experimental study of prototype frame behavior. This behavior will form the basis for the analytical model developed in Chapter 6.0. In the course of the research program described in Chapter 3.0 and in a parallel study (Mitch 2009), it was determined that certain mechanical properties of bamboo are not well established and, furthermore, that there is no standard method for comparing these critical properties. Chapter 4.0, therefore, reports on an experimental program aimed at filling these gaps in available knowledge and data. Initially a fracture mechanics approach to quantifying bamboo behavior was attempted in an effort to normalize for the significant variation expected in a natural material. While this method was successful, it was not felt to be practical for application outside a well-equipped laboratory environment. Thus a simpler, mechanics-based, materials test was pursued and an attempt to correlate results from this with the more reliable fracture mechanics approach was made.

The work presented in Chapter 5.0 considers data collected by the Group for Non-Conventional Materials (GNOCMAT) at PUC-Rio and the author's group at the University of Pittsburgh. In total, the data collected represents nine bamboo species, and a variety of geometric and mechanical properties. The sources present tests on a variety of bamboo species, however

the available data sets are limited for most of the species. Only two species, *Phyllostachys aurea* and *Dendrocalamus giganteus*, which represent the two data sets with the largest number of samples, were examined in detailed. Significance of the statistical variability between these species was assessed and provides at least one benchmark for interspecies variation. The objective of the chapter is to reduce the epistemic uncertainty, due to variations in geometry and material properties, for the finite element model presented in Chapter 6.0 .

In Chapter 6.0 , a finite element model (FEM) of the prototype structure described in Chapter 3.0 is developed. Static pushover and nonlinear dynamic analyses were conducted on several models of the prototype structure. In addition to the seismic model, the effect of the variability of bamboo material properties identified in Chapter 5.0 was explored. Chapter 7.0 presents a summary of the research program and several topics for future work.

2.0 BACKGROUND, LITERATURE REVIEW AND RESEARCH METHODOLOGY

This chapter provides a relatively brief background and literature review addressing a number of topics relevant to the research methodology adopted in the present work including: sustainability, bamboo availability, properties and construction techniques, the hazard environment considered in this study and approaches to hazard mitigation and performance based design. Subsequent chapters provide focused reviews of literature relevant to the material presented in each chapter.

2.1 SUSTAINABILITY

Sustainability of a community is heavily reliant on available infrastructure. For building construction, the issue may be further exacerbated by reliance on transported and imported materials. Particularly in rural areas, non-engineered and marginal construction methods typically rely on local materials due to their availability and ease of transport. Nonetheless, an increasing trend toward the use of modern, typically imported, materials, such as reinforced concrete and steel is emerging. Anecdotally, this trend is a byproduct of globalization and the increasing affluence of emerging and developing economies. “Bamboo is a poor-man’s material” whereas the use of concrete, for instance, is an indication of status.³ The disadvantage of this shift toward ‘modern’ materials is not only associated with increased reliance on products associated with large CO₂ emissions and other harbingers of environmental change, but also the

³Paraphrased from discussions with Gayatri Kharel relating to the experience in NE India.

need to import the materials from often remote locations. Use of such materials requires not only vehicular transportation but also a need to carry the materials to the actual site which is an energy intensive task in, for example, the Indian hill regions. Furthermore, the structural performance of such materials, especially in the event of a natural hazard, is highly reliant on the method of construction and technical expertise of the workers.

The importance of infrastructure was seen in the remote areas of northern Pakistan devastated by the October 8, 2005 Kashmir earthquake. Ali (2007) noted that the earthquake caused landslides that limited access to affected areas. As a result, the local people were living in temporary shelters. The shelters became somewhat permanent due to the materials that were provided for reconstruction, mainly reinforced concrete, brick and stone masonry. The disaster relief was further aggravated by the difficulty in transporting these materials to the rural areas. Furthermore, the presumed design for replacement shelter was largely inappropriate for homes above specific altitudes which comprised much of the damaged building inventory. While some of the problems were associated with policy, the understanding and use of local, sustainable materials is not presently used as an alternative for post-disaster rural construction.

2.1.1 Construction Materials

The importance of the use of local materials for construction emphasizes the connection between the built and natural environments. With increasing population the need for renewable, low cost, local materials in developing countries is greater than ever. Some examples of sustainable local materials include mud-brick, natural fiber reinforced masonry and bamboo. Often these building materials are part of the traditional or vernacular style, which in many cases is disappearing in favor of modern materials such as concrete. While use of reinforced-concrete is advantageous in

many ways, the availability and economic and environmental costs of the material represent significant disadvantages. Furthermore, the technical expertise required for design and construction may not be locally available. Traditional building materials, such as bamboo, can contribute to sustainability on many levels.

2.1.1.1 Local Materials – Bamboo

Bamboo is a sustainable material that is available globally (Figure 2.1). Bamboo species suitable for structural applications are indigenous primarily between the tropics, although cultivation of some appropriate species has been successfully transplanted in very diverse environments including the Pacific Northwest of the United States. At Washington State University's (WSU) Mount Vernon Northwestern Washington Research and Extension Center, a successful bamboo plantation has been established (Miles 2002). The WSU research center has explored primarily the horticultural aspects of bamboo cultivation and only briefly explored the production of bamboo shoots and poles.⁴

⁴ The pole production is assumed to be used for non-structural purposes based on the species that were selected and listed in the Miles (2002) report.

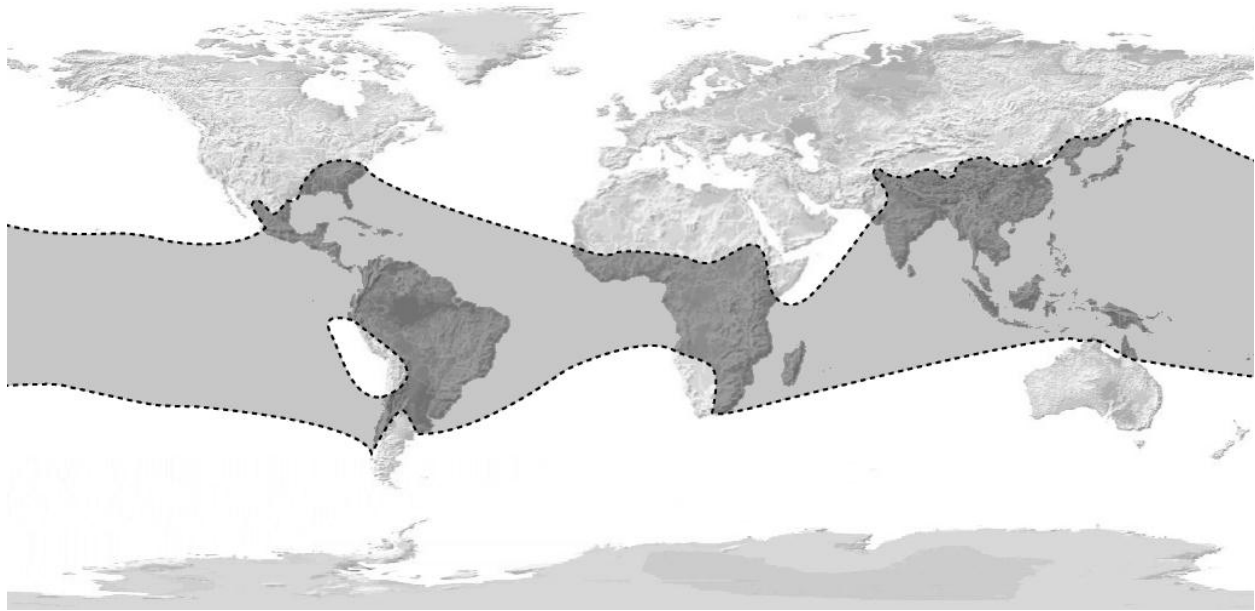


Figure 2.1 Global map of available bamboo species (Laroque 2007).

Research and development of bamboo for construction has been conducted for years and is increasing with pressure to find alternative renewable building materials. Bamboo is widely promoted as a construction material for its environmental and physical advantages (Liese and Kumar 2003). The disadvantages, however, can be significant and include the degradation of the material, variation in geometric and mechanical properties within and between species, as well as the difficulty in fabricating connections and joints due to the cylindrical culm shape, dimensional variability and highly isotropic material properties leading to limitation in mechanical strength, particularly the resistance to splitting (Janssen 1981). Although these are daunting challenges, research and development of bamboo building materials continues to progress and the use of bamboo is being accepted more widely than in the past.

Bamboo is a global renewable resource. Lobovikov et al. (2007) published a study on world bamboo resources for the Food and Agriculture Organization (FAO) of the United Nations (UN). This study noted that bamboo is a resource found in Africa, Asia, Central and South

America. The bamboo resources of Asia are significant, containing over 60% of the global bamboo resources and continuing to rise with China's increasing plantation of Moso, or *Phyllostachys heterocycla pubescens*, a sympodial bamboo. Bamboo-based consumer products are growing worldwide and include bamboo charcoal which is widely used in Asia and is growing in Africa as an alternative fuel source. The calorific value of bamboo is comparable or better than conventional charcoal sources and coal (Lobovikov et al. 2007).

The primary use of bamboo, however, is for construction. Bamboo structures are classified into two types: traditional and engineered structures. Over one billion people live in vernacular housing in which bamboo is the primary building material (Lobovikov et al. 2007). Engineered structures also use bamboo, but typically in the form of engineered products such as laminates and panels. There is a very small cadre of engineered bamboo structures which use bamboo in its native form (Figure 2.2). These are niche markets, championed by such architects as Simon Velez and Jörg Stamm (Rohrbach and Gillmann 2002). In such engineered bamboo structures, connections are generally engineered fabricated components based on space-frame nodes. The connection shown in Figure 2.3, for instance, was developed by architect Renzo Piano. The connection supports light loads and uses wires to connect bamboo members to a steel node element (Laroque 2007). While innovative, such approaches are not generally viable for application in the vernacular housing stock.



a) ZERI Pavillion by Simon Velez



b) Pedestrian Bridge by Jörg Stamm

Figure 2.2 Examples of engineered bamboo structures (Rohrbach & Gillmann 2002).



Figure 2.3 Bamboo connection designed by architect Renzo Piano (Laroque 2007).

Bamboo is a sustainable construction material found in many regions of India and an example of traditional, or vernacular, bamboo construction is found in northeast India. In the northeastern Indian state of Assam, traditional building techniques utilize bamboo for construction of different structures, such as houses and schools (Ranjan et al. 1986). The houses are single-story and are constructed on a platform of rammed earth. The frame of the building consists of bamboo posts that are embedded vertically in the ground around the platform. Posts are typically large diameter whole culms, with a large wall thickness and short internodes (Ranjan et al. 1986). The posts are linked together by a method similar to post and lintel construction. A saddle joint is constructed at the top of the post and the beam, or lintel, rests in

the joint and is secured by tying the components together with natural fiber material. The roof is constructed from rafters and purlins that are fastened together and covered with grass thatch. The wall structure consists of smaller diameter bamboo culms attached horizontally to the posts at uniform intervals (Ranjan et al. 1986). The wall members have a smaller wall thickness and larger internodal distance. The walls are covered with woven bamboo mats that are connected by portions of bamboo culms. Plaster is sometimes applied to the exterior to finish the wall. Figure 2.4 shows an axonometric drawing of such a traditional bamboo house.

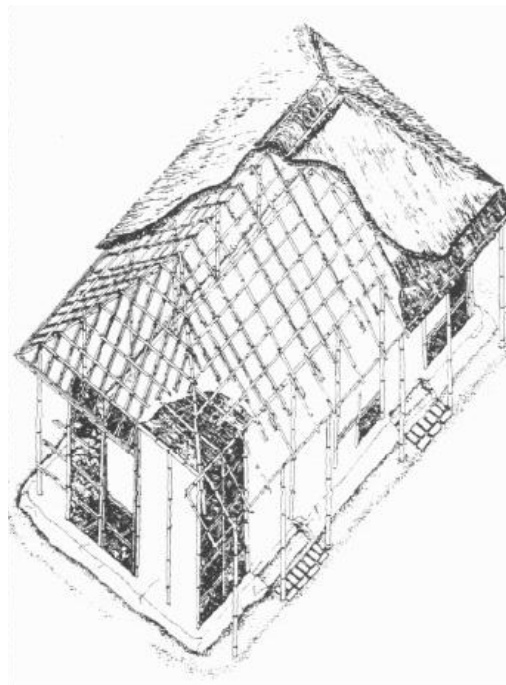


Figure 2.4 Bamboo frame house (Ranjan et al. 1986).

Similar types of bamboo construction and housing are found globally, in regions such as Latin America and Africa. Due to relatively their light weight and flexible connections, such housing is recognized to perform well in earthquakes. Buildings that are constructed to be resistant to vertical gravitational forces and horizontal seismic forces are based on the following principles: (1) regular height and plan with continuous walls from foundation to roof; (2) light

structural weight (particularly the roof system); and (3) include effective features for protection against weather decay such as roof eaves and stone foundations (Gutierrez 2004). Due to their relative simplicity, bamboo structures generally satisfy these requirements.

2.2 MATERIAL PROPERTIES OF BAMBOO

The study of the engineering material properties of bamboo is surprisingly nascent. Janssen (1981) first explored the composition of a bamboo culm. He developed a mathematical model of the culm by considering it to be a structure composed of a number of ‘substructure cells’. Janssen then assessed different mechanical properties of bamboo including bending, shear, tension and compression. Finally, he investigated different truss systems and various ways to connect bamboo elements. From his work on the composition of bamboo, Janssen drew several conclusions relevant to the present work:

1. The angle that the microfibrils of bamboo make with the cell axis has a large impact on the stresses and displacements observed in mechanical tests.
2. A numerical model of a single substructure cell may be used to predict the Poisson ratio and tensile strength, but cannot be used to predict the compressive strength as pectin prevents the buckling of individual fibers; a more complex model is required to accurately predict compressive strength.

In addition to simple mechanical tests of bamboo, Janssen applied statistics and linear models in an attempt to discover which physical parameters are related to bamboo’s material properties. Some of Janssen’s relevant conclusions are as follows:

3. An increase in moisture content decreases compressive strength, and the compressive strength increases with the height along the culm from which sample was taken.
4. Shear stress is the cause of failure for smaller spans, and the limiting shear stress is much lower than a typical shear test would indicate.
5. In bending, dry bamboo behaves better; strength decreases with the height along the culm from which the sample is taken. Additionally, there is a possible relationship between ultimate bending stress and density.
6. A new shear test was developed to determine the shear strength of bamboo. This four-plane shear test was later adopted by the ISO guideline (ISO 2004b).
7. Shear strength and density are related.
8. A new test method is needed to determine the tensile strength of bamboo.

Arce-Villalobos (1993) extended the work of Janssen by providing a more in-depth examination of the tensile properties of bamboo both parallel (along culm) and perpendicular (transverse) to the primary orientation of the fibers. Arce-Villalobos also attempted to relate different mechanical properties; his most relevant conclusions are as follows:

1. Transverse tension capacity and density are not correlated whereas longitudinal tension capacity and density are.
2. Tension modulus, E , in the transverse direction is about $1/8^{\text{th}}$ that measured in the longitudinal direction.
3. There may be a universal maximum transverse strain at which bamboo fails (splits longitudinally). Three different species exhibited similar values during testing, approximately 0.0012.

4. Variation in cross-section and modulus of elasticity produce a reduction of no more than 15% in the bending strength and axial stiffness compared to the values a theoretical uniform member would yield.
5. Variation in cross-section and the presence of nodes can reduce bending stiffness by 50%, and axial strength by 80%.
6. The slenderness ratio (KL/r) of compression elements should be kept below 50 to avoid global buckling or splitting resulting from flexural behavior.

The present understanding of the material properties of bamboo, as expressed in the ISO Standard (2004a) and the Indian National Building Code (NBCI 2005), for instance, stem largely from the work done by Janssen (1981) and Arce-Villalobos (1993). While these standards are a start, there are many areas that still require further exploration. Janssen quotes several researchers who claimed that “the collapse of the bamboo was always sudden and the material was split into pieces parallel to the longitudinal axis”. Arce-Villalobos concludes “Bamboo culms do not fail in compression, in bending or shear, but do fail when a maximum tangential tensile stress is reached.” Despite these acknowledgements, the splitting behavior of bamboo has not been adequately addressed in present standards.

Ghavami et al. (2003a) investigated different bamboo species on a micro-scale using digital image analysis. The analysis indicated that the fibers are functionally graded through the wall thickness of the culm. The authors developed equations for the modulus of the fibers and matrix. The equations were based on the modulus of composites and modified to account for the volume gradation within the culm. An additional study by Ghavami et al. (2003b) explored the fiber orientation within the culm and more specifically at the nodes of *Phyllostachys edulis* Riv. or Moso bamboo. Longitudinal and azimuthally oriented fibers were noted to be only located at

the nodes and diaphragm. Analysis using Atomic Force Microscopy (AFM) discovered that the gradation of the fibers is in three sections, with similar fiber volume within each section. The fibers are assumed to form the various sections during growth and develop as a functionally graded material in response to natural loads on the culm.

Amada et al. (1997) noted that the nodes on the bamboo culm help to mitigate buckling, as well as to arrest longitudinal cracks. The authors proposed to model bamboo as a fiber-reinforced, composite cylinder with a hollow cross-section. The paper focuses on Moso, or *Phyllostachys edulis* Riv. Over the entire height of the bamboo culm, the maximum internodal length occurs at the midheight and the outer diameter decreases with height. The volume fraction of the bamboo culm demonstrates that it is a functionally graded material. The fiber volume percentage also increases in the upper portion of the culm. Amada and Untao (2001) also explored the fracture properties of Moso (*Phyllostachys edulis* Riv.) bamboo. The experiment was carried out through a series of notched longitudinally oriented tension tests from different sections of the bamboo culm. The results indicated that the fracture toughness (K_{IC}) of Moso bamboo averaged across the radius was comparable to aluminum alloy 2014-T6.

2.3 HAZARD MITIGATION FORMARGINALLY AND NON-ENGINEERED STRUCTURES

Marginally and non-engineered structures that populate the vernacular are adapted to their surroundings and their design has evolved to mitigate damage caused by natural hazards. The seismic performance of long-lasting traditional construction methods has been tested in various earthquakes around the world. Ranjan et al. (1986) explored the use and seismic performance of

timber-laced masonry structures, noting that such traditional structures in the 1999 Marmara and Düzce (Turkey) earthquakes experienced little or no-damage in comparison to newer concrete structures which collapsed. Additionally, newly constructed bamboo housing in Costa Rica, performed exceptionally well in a large seismic event, experiencing little or no structural damage in the 1991 Limon (Costa Rica) earthquake (Gutierrez 2004). In the northeast Indian hill region, the recent 2004 Sikkim earthquake demonstrated the vulnerability of existing and newly constructed masonry and concrete structures while traditional bamboo structures experienced little or no damage (Figure 2.5 to Figure 2.7) (Kaushik et al. 2006).



Figure 2.5 Undamaged Ikra (bamboo frame construction) building following 2006 Sikkim earthquake (Kaushik et al. 2006).



Figure 2.6 Damaged stone masonry building following 2006 Sikkim earthquake (Kaushik et al. 2006).



Figure 2.7 Damage in reinforced concrete building at Deorali resulting from 2006 Sikkim earthquake (Kaushik et al. 2006).

Vulnerability increases when the design and construction of structures is not capable of resisting the seismic demand of the area. Vulnerability may also increase as inappropriate building forms are transported from one region to another. In northeast India, for instance, seismic threat is very localized (see Figure 2.8) along the Himalayan belt and the threat is perceived to diminish quickly as one moves south. Thus construction details suitable in southern

West Bengal (Kolkata area) may be entirely unsuitable in the Darjeeling, Sikkim or Assam regions only a few hundred miles north. Hazard mitigation focuses on reducing the impact of natural hazards through planning, construction, application of building codes and standards, as well as through sound structural design. Primary hazard mitigation design considers life safety and collapse prevention, however more sophisticated designs can also account for post-event occupancy and operation, repair costs and other performance goals.

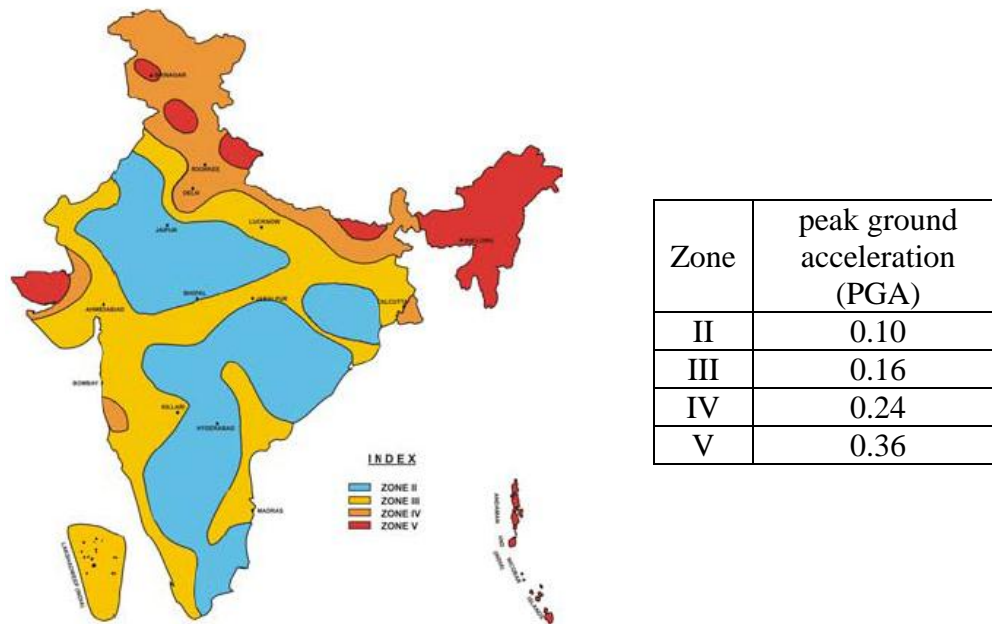


Figure 2.8 National Building Code of India Seismic Hazard Zone Map (NBCI 2005).

2.4 METHODOLOGY AND OBJECTIVES

The present study relies on both quantitative and qualitative results to provide a seismic performance assessment of bamboo frame structures. The following sections detail the methodology and objectives associated with the present work.

2.4.1 Approach to Experimental Program

Bamboo structures are constructed worldwide using a variety of methods and supplementary materials. To construct a model of a bamboo structure, an assessment of existing structures, as well as an assessment of typical site location and conditions, and building construction methods must be conducted (ATC-58 2007). Analysis of joints and methods for processing structural bamboo will further add to the understanding of the building process as a whole. The material properties of bamboo, as well as the behavior of various joints and connections, have been explored in previous research (e.g.: Janssen 1981; Arce-Villalobos 1993; Ghavami and Moreira 1996). Variations in species and geometric properties have also been investigated to determine the effect on the structural properties of bamboo (Ghavami et al. 2003b; Naik 2005). Determination and verification of the material properties and failure modes provide a necessary foundation for developing any model. Estimation of parameters, such as material strength, increases the uncertainty in the model. Thus the behavior of material will be determined from existing data and experimental tests conducted as part of this study to properly reflect the characteristics of the material.

The variability between bamboo species and thus the inherent epistemic uncertainty in the material and geometric properties will be addressed using a sampling technique and assigning properties that result in a ‘nominally identical but statistically different’ bamboo culm for the model (Shinozuka et al. 2000a). Investigation of various test methods will also be explored to determine the factors related to bamboo material properties and particularly splitting failure in bamboo culms (see Chapter 4.0).

The objective of the experimental study (see Chapter 3.0) is to establish the physical behavior of a selected prototype structure. The results will be used to form the basis for the

modeling tasks of this study (see Chapter 6.0). The experimental program will utilize the available data of a variety of species, as well as available species of bamboo for experimental testing.

2.4.2 Analytical Model of Prototype Bamboo Frame

The prototype bamboo frame, tested in the experimental program, provides the basis for the analytical model (Chapter 6.0), and will represent the geometry of structural components and joints, as well as the material properties. Ideally, the model will characterize the material and structure exactly, however some generalization will be required. Due to the degree of uncertainty and simplification required, modeling will be limited to two-dimensional frame and panel structures. Considering analogous timber-frame construction, for instance, Li and Ellingwood (2007) used a two-dimensional plane wall shear model with the assumption that the structure has a regular configuration and torsional effects can be neglected. This approach eliminates the significant additional uncertainty associated with three-dimensional modeling and has been used extensively in studies having similar goals addressing timber construction (e.g. Rosowsky 2002; Li and Ellingwood 2007). The accuracy of the model will be reflected in the detail of building components and in the performance of the structure.

Several commercial analysis programs have been used to analyze bamboo structures. Most recently, bamboo structures have been successfully modeled using *OASYS GSA* (Laroque 2007). Alternatively, the flexibility of *OpenSees*, which is based on *Tcl/Tk*, a string based scripting language, allows integration of new components into the framework without the need to change the existing code and provides an opportunity to create a more specialized model (Mazzoni et al. 2006; Nielson and DesRoches 2007). *OpenSees* has the capability of reliability

analysis using a module developed for the code (Scott and Haukass 2006). The availability of a built-in reliability module is a significant advantage in comparison with the other available programs.

2.4.3 Fragility Analysis

The performance-based earthquake engineering approach provides the impetus for recognition and formalization of marginally and non-engineered structures within a building code context. Past research has demonstrated the use of derived fragility functions to assess seismic performance of structures (Nielson and DesRoches 2003; Kim and Rosokowsky 2005; Ellingwood et al. 2004). The probability of damage can be further correlated to environmental, social and economic cost metrics and serve as the basis for developing hazard mitigation policy. This is beyond the scope of the present work although some discussion and direction will be provided to guide future policy-related work founded on the present study.

3.0 BAMBOO PORTAL FRAME BEHAVIOR

Bamboo research has been conducted for years, ranging from studies on vernacular structures to modern engineered structures and connections. Janssen (1981) published a significant dissertation describing bamboo construction in detail. Arce-Villalobos (1993) followed with another dissertation on bamboo structural design. Arce-Villalobos attempted to demonstrate the structural viability and necessary standardization of bamboo. His research investigated adhesive-based connections of bamboo and explored the effect of loading reversals; thus suggesting the use of bamboo frame, rather than truss, structures. The author explored bamboo connections through a design methodology that focused on the transfer of stresses and practicality of construction. Both seminal studies, Janssen and Arce-Villalobos, demonstrated that the geometric and material variation of bamboo reduces the reliability of the material, thus affecting the appeal of bamboo as a material for engineered structures.

3.1 STRUCTURAL APPLICATIONS OF BAMBOO

Ghavami (2005) investigated the use of bamboo as reinforcement in reinforced concrete. The bamboo culms were treated to prevent water absorption and alkali attack which can deteriorate the bond between the bamboo and the concrete. The method used to reduce the water absorption of the bamboo culms included a thin layer of epoxy with a coating of sand to enhance bond

characteristics. Ghavami notes that more economical treatment methods such as asphalt, tar paints, or other bituminous materials, may also be used. The study explored bamboo culms as internal reinforcement and half-culms as external stay-in-place (SIP) forms, or ‘shutter slabs’. Experimental results indicated that slab failure was through debonding of the concrete from the SIP forms followed by compression failure of the concrete. In beam tests, internal bamboo reinforcing failed in tension, while the shutter slabs, having no internal reinforcing, failed in shear.

Bamboo structures have been constructed in variety of forms, from single story residential homes to elaborate exhibition halls. In 2004, the Indian Plywood Industries Research and Training Institute (IPRITI) in Bangalore and TRADA (UK) developed and tested a pre-fabricated bamboo house in a series of shake table tests (Jayanetti 2004). The full-scale structure, shown in Figure 3.1, was 2.7 m square in plan. Regional ground motions, as well as ground motions from the 1995 Kobe earthquake were used to evaluate the performance of the house.



Figure 3.1 IPRITI (Bangalore) and TRADA (UK) full-scale bamboo house (Jayanetti 2004).

Brown (2004) noted that the test house utilized bamboo composite materials and was analyzed and designed for seismic performance. The limited information available on these tests suggests that the house performed well, however details of the experiment results were not found

at the time of writing (August 2010). Additional research has explored the application of bamboo for infrastructure, such as a low-cost footbridge constructed with *Guadua angustifolia*, a species widely used for construction in Columbia (Laroque 2007).

3.1.1 Joint and Connections

Ghavami and Moreira (1996) investigated the use of *Dendrocalamus giganteus* for nodal space structures. The study developed an aluminum plate pin-end joint that served as a nodal connection for multiple bamboo culms (Figure 3.2).

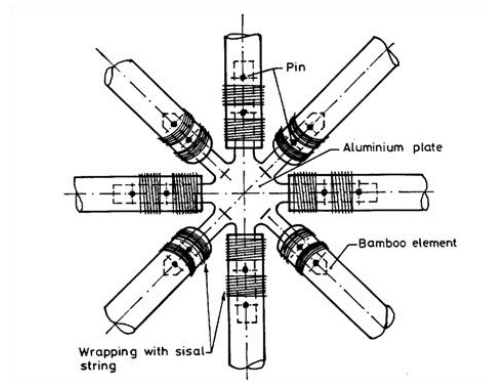


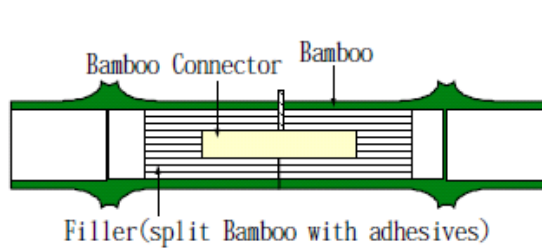
Figure 3.2 Aluminum Plate Pin-end Joint (Ghavami and Moreira 1996).

Longitudinal splitting failure (i.e. shear) of the connection region was mitigated using a sisal fiber wrap to reinforce the end of each culm. Ghavami and Moreira also carried out a finite element analysis to investigate the effect of the required boring of the culm on the failure of the connections. The model used isoparametric elements within a mesh that was discretized to represent the connection without the sisal wrap. The analysis studied the crushing, shearing and splitting failure of the pin connection. The results were used to produce a series of design equations for the connection type.

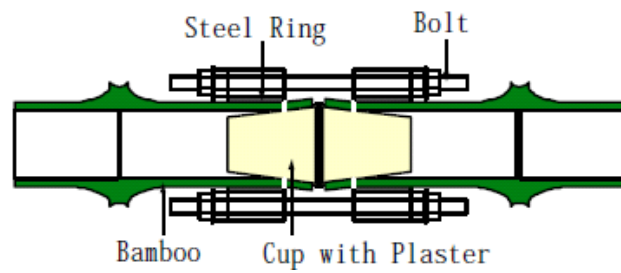
The use of fiber reinforced polymers is increasing in bamboo structures, due the advantages of strength, as well flexibility of the material for reinforcing connections. Guzman and Morel (2005) explored the use of glass fiber reinforced polymer (GFRP) composites as reinforcement for bamboo. The GFRP allowed for a more ductile response in compression tests parallel and perpendicular to the grain.

Inoue et al. (2004) developed two methods of fabricating joints using Madake bamboo: a pin secured in a laminated bamboo filler and a bolted steel ring with plaster cup fillers. The first joint type, shown in Figure 3.3a, tested in tension, exhibited pull-out failure and had the highest maximum load. The second joint, shown in Figure 3.3b, failed through slippage of the steel ring. Three additional steel-reinforced connections, utilizing sheaths, rings, and internal reinforcing steel were also designed and tested by Inoue et al. (Figure 3.3c-e). The connections performed similarly to the first two joints, however their weight increased significantly.

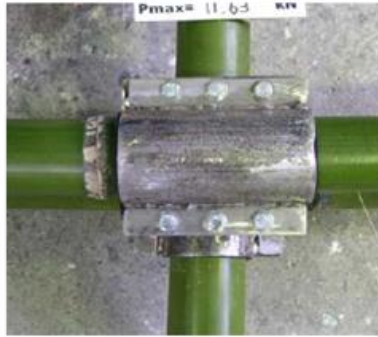
Laroque (2007) explored different commercially produced connections. Bambu-Tec produces pre-fabricated poles that are capped with a resin and connector (Figure 3.3). Nodal connections, such as the Pan frame-works, use a metal rod to carry forces from the member to the node (Figure 3.3g). Induo is a system that uses a spherical connection that is screwed to the bamboo member and grouted (Figure 3.3h). Shoei Yoh developed a system where tubes are inserted into the culm and connected with clevises and bolts (Figure 3.3i). This connection can be designed following traditional steel codes. Wood-core connections (Figure 3.3j) use a slot in the bamboo member that is filled with an adhesively bonded wood dowel. This type of connection may be designed using typical wood construction methods.



a) Laminated bamboo connection and split bamboo filler



b) Steel ring and cup with plaster



c) Steel sleeve connection



d) Steel ring connection



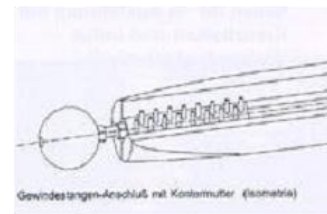
e) Mechanical hook connection



f) Bambu-Tec connection



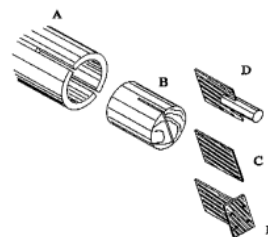
g) Pan Frame-works connection



h) Induo connection



i) Shoei Yoh connection



j) Wood-core connections

Figure 3.3 Bamboo connections proposed by Inoue et al. (2004) and commercially available engineered bamboo connections (Laroque 2007).

Bolted connections have also been used (Figure 3.4), however they are not typical due to the potential splitting of the bamboo culm. Laroque (2007) noted that bolted connections typically failed by splitting or local crushing. The strongest connection reported by Laroque was a grouted internode with a fastener (Figure 3.5); this connection failed by local crushing and bolt bending. For column-to-foundation connections, the most common joint is a steel reinforcing bar extended from the foundation and embedded in the bamboo culm using concrete or mortar (Figure 3.6). This is referred to as a ‘grouted-bar’ connection.



Figure 3.4 Bolted bamboo connection (photo by author).

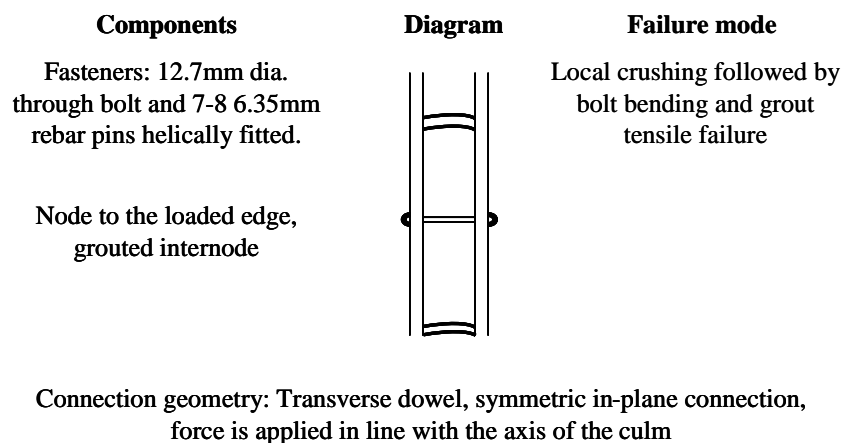


Figure 3.5 Grouted internode with fastener connection (adopted from Trujillo 2007).



Figure 3.6 Grouted Rebar Connection (Mitch 2010) and footing with rebar connection (photo by author).

3.1.2 Current Standards and Codes

Engineered bamboo structures have been designed and constructed worldwide (Figure 2.2), however a difficulty lies in the available standards which vary by country. Finch (2005) described the difficulties that faced engineers from Faber Maunsell when designing a bamboo covered stage and walkway for a community in India (Figure 3.7). The project required proof testing of bamboo connections to determine appropriate capacities for the design of the structure. The ISO Standards (see below) were not applicable in India due to their reference of other codes that are not currently available in the country.⁵ Furthermore, neither the Uniform nor British timber codes applied to the sections being designed. Available standards for bamboo are briefly described in the following sections.

⁵Identifying another roadblock to implantation in developing regions: the availability of standard documents, texts and other technical documentation.

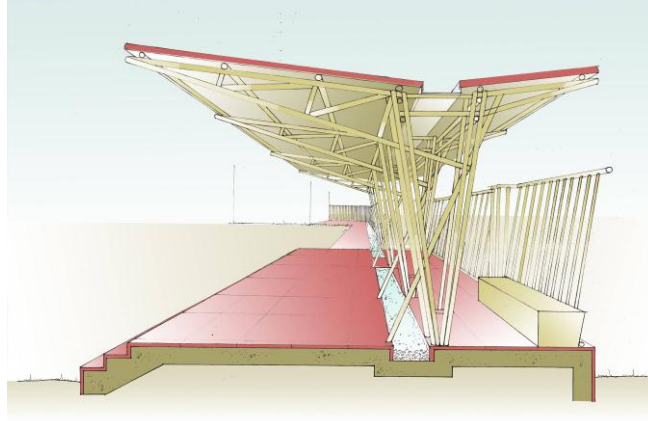


Figure 3.7 Faber Maunsell Covered Walkway and Stage Project (Faber Maunsell 2005).

3.1.2.1 International Organization for Standardization (ISO)

Janssen (2005) summarized the International Organization for Standardization (ISO) publications on structural bamboo (ISO 2004a and 2004b). The standards were supplemented by a technical report (ISO 2004c) and described the necessary design and material properties of bamboo. The first standard, *ISO 22157-1:2004 Bamboo – Determination of physical and mechanical properties Part 1: Requirements* (ISO 2004b), provides the testing methodology used to obtain properties necessary for establishing design values (some tests from this standard are described in Table 4.1). The second standard, *ISO 22156:2004 Bamboo – Structural Design* (ISO 2004a), is based on a limit states design approach and refers to round, split and glue-laminated bamboo materials. The technical report (ISO 22157-2:2004) (ISO 2004c) represents the laboratory manual, or Part 2 of the standard on bamboo properties, and provides a more detailed description of proposed testing methods and data collection. Janssen (2005) describes the ISO standards as necessary tools that build upon existing traditional knowledge. The standards reference existing ISO timber standards, however the testing methods provided were specifically intended to derive properties of bamboo. The ISO standards compile past research

and testing knowledge (primarily from Janssen 1981 and Arce-Villalobos 1993) to incorporate the subtle differences between bamboo and timber testing. The ISO documents serve as a basis for further standardization of bamboo as a structural material.

3.1.2.2 National Building Code of India

The *National Building Code of India* (NBCI) (2005) addresses the use of bamboo in Part 6: *Structural Design, Section 3 – Timber and Bamboo: 3B Bamboo*. The scope of this section covers the use of bamboo for structures and provides requirements to satisfy acceptable performance. The NBCI provides strength limits for three classes of bamboo. The NBCI additionally provides some examples of bamboo joints and connections, however the detailing (including dimensions and capacities) of such joints is not addressed. It must therefore be inferred that proof testing is required to qualify connection methods and joint types. Such an approach is obviously prohibitive when applied to residential construction. Furthermore, the NBCI refers to other Indian Standards (IS 6874:1973, 9096:1979, and 8242:1976) which refer to test methods and preservation of structural bamboo.

The 2005 NBCI also includes seismic design guidelines that coincide and cross-referenced with additional Indian Standards. The design approach uses an equivalent lateral force approach that is comparable to the equivalent lateral force (ELF) method found in ASCE 7-05 (ASCE 2005). The ground motion parameters (Figure 2.8) are ‘second generation’ zonations rather than the third (USGS maps and the basis for ASCE 7-05) or fourth (micronization, becoming more commonly used in California, for instance) generation approaches used in North America.

3.1.3 Current Design Approach

The Faber Maunsell bamboo project (Faber Maunsell 2005) for Chennai, India serves as a good example of the engineering design process for bamboo structures (Figure 3.7). Faber Maunsell conducted a *Madras Project Feasibility Study* in 2005 for a cantilevered covered walkway. The study explored the available material properties for different species of bamboo including the locally available *Bambusa bambos*. The study also investigated the available standards and codes. The ISO standard on *Bamboo Structural Design* (ISO 2004a) referenced ‘relevant national standards’ (Faber Maunsell 2005) for limit states design. The study also examined the British Timber code, *BS 5268 Structural Use of Timber* (British Standards 2002), for comparative calculations of stresses, as well as connection design. The design criterion was outlined as a combination of British, Indian and ISO standards since no comprehensive standard was available. The loading cases and deflections were calculated based on British Standards. The computer analysis of the structure required the bamboo culms to be discretized into internodal sections which were represented by two-node elements with internal fully-fixed joints (Faber Maunsell 2005). A linear analysis was conducted on the structure and was iterated upon until an acceptable design was obtained.

3.2 PROTOTYPE STRUCTURE AND CURRENT PRACTICE

The prototype structure, which serves as the basis for this study, is a single story four-classroom building located at St Joseph’s School in Mungpoo (Figure 3.8). The structure consists of a reinforced concrete grade-beam foundation with rubble infill (Figure 3.8c) supporting reinforced concrete plinths with multiple (two or four) bamboo culms forming single columns (Figure

3.8d). The bamboo culms are connected to the footing using a grouted reinforcing bar connection. Bolted connections are used to connect primary roof framing (Figure 3.8e) and infill panels to the columns. The resulting structure consists of five two-dimensional portal frames in the ‘short direction’ and two multi-bay frames in the long direction as shown in Figure 3.9. Infill wall panels consist of framed sections with fish mouth or saddle joints and woven bamboo infills.

Drawings for the structure were made available by the design engineer, Gayatri Kharel (Figure 3.9). The bamboo species used was *Bambus nutan* (Mala Bans). Other bamboo species appropriate for structural applications available in the area include *B. maling* (Malingo Bans), *B. vulgaris*, *Dendrocalamus hamiltonii* (Choya Bans), *Dendrocalamus sikkiminfis* (Bhalu Bans), and *Dendrocalamus strictus* (Kattha Bans). The local names are given parenthetically.



a) front elevation



b) end elevation



c) Reinforced concrete grade-beam foundation with rubble infill.

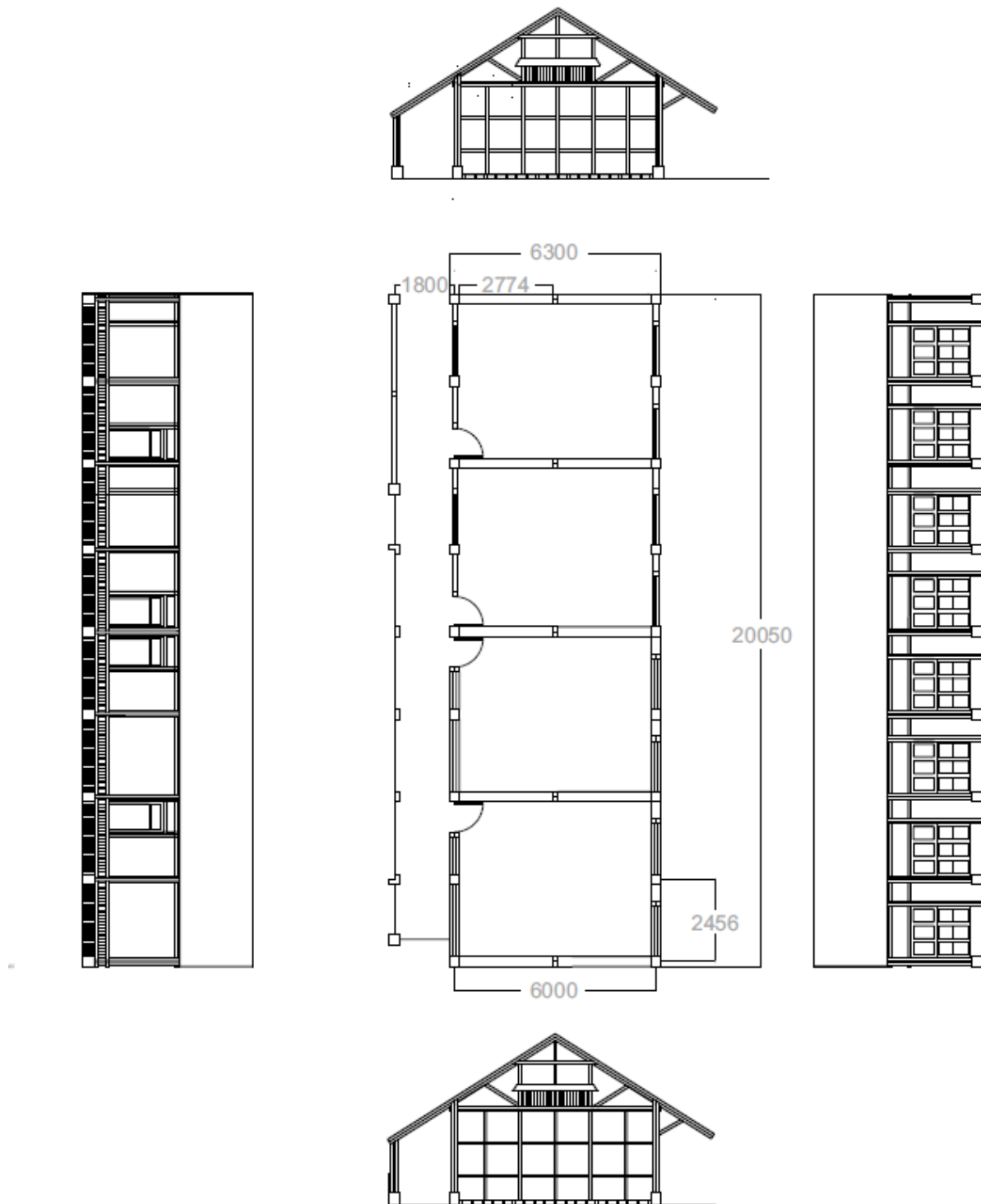


d) Reinforced concrete column plinths with four bamboo culms forming one column.



e) Bolted connections used to connect primary framing.

Figure 3.8 Details from St. Joseph's School, Mungpoo, India (photos by author).



**Figure 3.9 Floor Plan and Elevations of the St. Joseph's North Point School with dimensions in mm.
(drawing provided by Gayatri Kharel).**

3.2.1 Bamboo Connection Details

Bamboo structures utilize a variety of connection details. Traditional details vary from lashing to dowel connections while more contemporary non-engineered structures use simple mechanical connectors, such as steel bolts and wire. Engineered bamboo structures often employ proprietary mechanical connections such as those shown in Figure 3.3.

The use of nodal connections for bamboo is intended to enforce a ‘truss-like’ structural behavior: ensuring that only tension and compression forces are carried by the bamboo members. Connection details affect the failure mechanisms associated with the joints. Splitting of bamboo is often a critical limit state; thus a connection that limits the flexure that may be imparted into the connected culm helps to mitigate shear-flow induced splitting(i.e.: VQ/I). Nonetheless splitting, ‘block shear’ and local crushing failures resulting from the manner by which the culm is connected to the node may also occur (Ghavami and Moreira 1996).

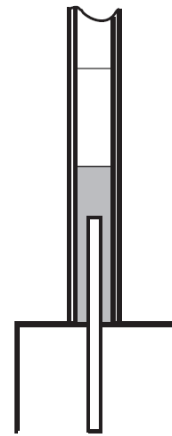
The objective of the present work is to define an engineering basis for non- or marginally-engineered connections appropriate for indigenous vernacular construction. Use of indigenous materials and vernacular non-engineered building methods constitute a large portion of housing in the world. It is not believed that engineered nodal connections (such as those shown in Figure 3.3) represent practical alternatives for widespread indigenous adoption. Therefore, the experimental programme focuses on the bamboo connection details used at the St. Joseph’s School in Mungpoo. Through this experimental study, the physical behavior of the prototype structure will be established. The results are used to form the basis for the modeling tasks presented in subsequent chapters.

3.2.1.1 Description of Prototype Column Base

The prototype structural system to be investigated is best described as a portal frame having a four-culm column base connection. The column base is a doweled and grouted connection to the concrete plinth (see Figure 3.10). An alternative column base detail is to embed the culm(s) directly into the plinth although this requires a larger plinth. Such a system was used at the Community Center at Camburi, Brazil (Figure 3.11).



a) St. Joseph's Mungpoo School

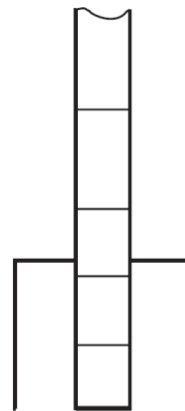


b) grouted-bar base connection

Figure 3.10 St. Josephs' Mungpoo School, India (photos by author).



a) Columns at Camburi



b) embedded-culm base connection

Figure 3.11 Column base connections (photos: Camburi – Bamboostic).

3.2.1.2 Description of Prototype Joint

The column-to-roof joist connection is comprised of multiple single bolt connections. Individually, each connection is a pin, however, the multi-culm geometry results in a moment resisting connection as a couple may be generated between bolts and culms comprising the transverse framing (see Figure 3.12). The pinned nature of the individual culm connections limits the introduction of flexure into the culms. The ‘staggered’ bolt pattern limits the high local shear and flexure that would occur between adjacent bolts in a single culm. The resulting connection is a three dimensional connection, with the header beams (long direction of building) connecting out-of plane. The experimental program, however, is limited to two-dimensional frame behavior in the short direction of the building. Nonetheless, the out-of-plane headers must be included to both enforce the geometry of the connection and to affect the correct in-plane behavior. It is anticipated that as the joint deforms, the out-of-plane culms provide resistance to shear distortion of the connection (racking) thereby enhancing the in-plane moment behavior.

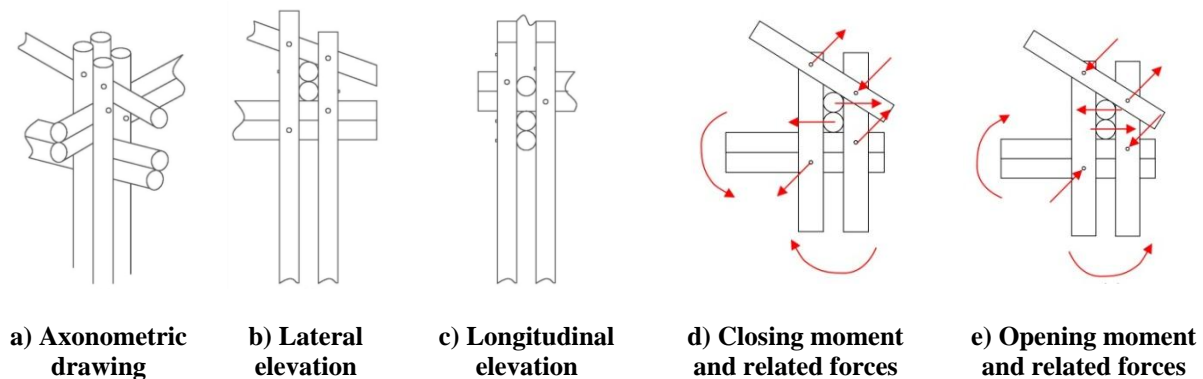


Figure 3.12 Prototype Column – Truss Joint.

3.3 MATERIAL PROPERTIES

To supplement the bamboo portal frame test, additional material testing was conducted. Tension tests were conducted to obtain basic material properties for the *Phyllostachys aurea* used for the scaled portal frame test described in Section 3.4. Additional tests to determine the pull-out strength of the grouted-bar column bases were also conducted. All testing reported in this section was carried out by the author at Pontifícia Universidade Católica do Rio de Janeiro (PUC-Rio).

3.3.1 Tension Tests

Bamboo specimens of water-treated *Phyllostachys aurea* were tested in longitudinal tension (Figure 3.13). Thirteen coupon specimens each consisting of a radial ‘slice’ (approximately 10 mm wide) of the full culm wall thickness (approximately 4.5 mm) were prepared as shown in Figure 3.14b. The specimens were cut into a ‘dogbone’ shape having a neck width of approximately 2.5 mm. Measured specimen dimensions are given in Table 3.1. Aluminum plates were bonded to the specimen ends to distribute the gripping loads and prevent crushing of the specimen in the grips. The specimen labels provided in Table 3.1 refer to the type of test (T = tension), species (PA = *Phyllostachys aurea*) and specimen identifier.

The tests were conducted using an EMIC universal test frame. The tests were run in displacement control at a rate of 0.02 mm per second. The global displacement of the test head was measured using an LDVT, while the local elongation of the specimen was measured with LDVTs on either side of the specimen. The test setup is shown in Figure 3.13a. An additional group of three specimens was tested with 0-90° strain gage rosettes.

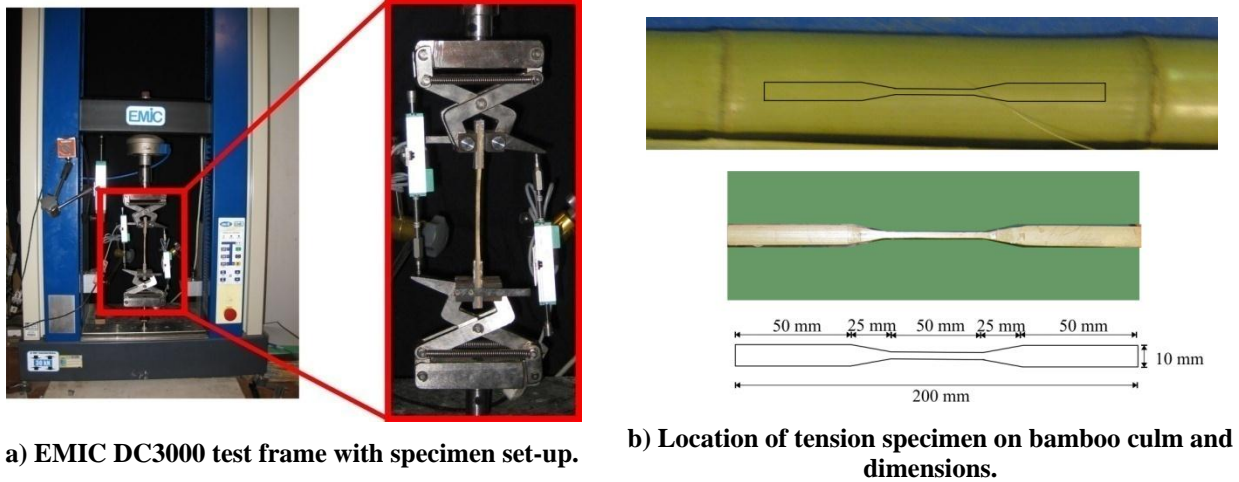


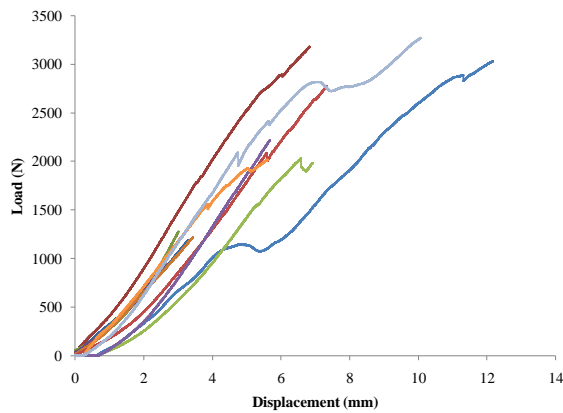
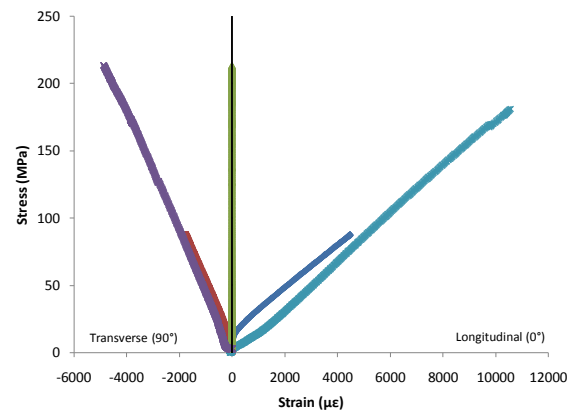
Figure 3.13 Details for tension test.

3.3.1.1 Results

The resulting longitudinal tension load-displacement curves are shown in Figure 3.14a and summarized in Table 3.1. The average tensile stress at failure was 233 MPa. The maximum tensile stress occurred in specimen T-PA-13: 296 MPa. Most specimens failed in the region were the specimen tapers from the grip to the neck of the dogbone. Several specimens broke in the grip region of the specimen; these are noted with a superscript ^g in Table 3.1. Three specimens (T-PA-14 to T-PA-16) were instrumented with strain gages. The average longitudinal tensile modulus of elasticity (E_L), calculated between 20-80% of the ultimate stress of the specimens was found to be 16167 MPa. Based on the recorded strain gage values the average Poisson's ratio was 0.34.

Table 3.1 Tensile specimen dimensions and test results.

Specimen	Neck Width (mm)	Culm Wall Thickness (mm)	Area (mm ²)	P _{max} (N)	σ _{max} (MPa)
T-PA-1 ^g	2.5	4.3	10.75	2793	260
T-PA-2	2.7	4.2	11.34	3183	281
T-PA-3	2.5	4.4	11.00	3280	298
T-PA-4	2.0	4.9	9.80	2253	230
T-PA-5	2.6	4.6	11.96	2658	222
T-PA-6	2.8	4.1	11.48	2369	206
T-PA-7	2.8	4.3	12.04	3034	252
T-PA-8 ^g	2.7	4.4	11.88	3375	284
T-PA-9 ^g	2.8	4.5	12.60	2249	178
T-PA-10	2.7	4.5	12.15	3096	255
T-PA-11	2.3	4.2	9.66	2622	271
T-PA-12	2.3	4.1	9.43	2058	218
T-PA-13	2.6	4.3	11.18	3307	296
T-PA-14	2.8	4.3	11.69	1018	87
T-PA-15	3.0	4.0	12.00	2171	151
T-PA-16	2.8	5.0	13.75	2934	213
\bar{x}	2.6	4.4	11.4	2650	233
s	0.25	0.28	1.13	618	54
COV (%)	9.4	6.3	9.9	23.3	23.3

**(a) load-displacement curves (n=11)****(b) strain gage specimens (n=3)****Figure 3.14 Results for T-PA Specimens.**

By comparison, Cruz (2002) also reports tension tests of *Phyllostachys aurea*. Cruz reported four values for water treated bamboo, based on the location of the specimen along the

culm length and the presence of the node. The average values of ultimate tensile stress and modulus reported by Cruz were 222 MPa and 21600 MPa, respectively, as well as a Poisson's ratio of 0.3. These values are in good agreement with the results presented. The modulus obtained experimentally and reported in Cruz (2002) is the apparent modulus, which is averaged over the wall thickness.

3.3.2 Pull-out Tests

Pull-out tests were conducted on bamboo culms having a steel reinforcement bar embedded in cement mortar. The culms were cut to a one meter length, ensuring there was a node at the top of the culm when possible. A 12 mm diameter reinforcing bar was grouted into the culm using a neat mortar. The bar was embedded a length of L_e as indicated in Table 3.2. The culms had a nominal outside diameter of 50 mm (D_o in Table 3.2) and an average wall thickness of 4.4 mm. Thus the grouted socket was approximately 41 mm in diameter or 3.4 times the bar diameter.

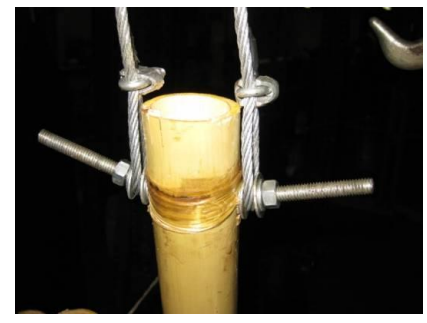
The load was applied using a 2 ton engine hoist secured to the strong floor (Figure 3.15a). The load was applied manually using the engine hoist jack connected to a 6 mm steel cable looped around an 8 mm threaded rod and secured with washers and bolts (Figure 3.15b and c). The load was applied below the upper node and above the grouted embedment height. The load-pull-out displacement (slip) data was acquired using a 50 kN tension load cell and a LVDT at the base of the culm. Additional reinforcement of bolt hole area was necessary to mitigate a tear-out failure of the loading bolt. Two strands of Kevlar fiber were applied with a coating of resin below the nearest node to prevent failure.



a) Pull-out test set-up: engine hoist



b) Load cell with attachment to culm.



c) Detail of Kevlar fiber reinforcement with bent threaded rod.

Figure 3.15 Pull-out test set-up details.

3.3.2.1 Results

The results of the pull-out tests, presented in Table 3.2, were two pull-out failures (culms P-PA-3 and P-PA-4) and two tear-out failures of the loading bolt (P-PA-1 and P-PA-2). The pull-out failures are characterized by the entire grout plug slipping out of the bamboo culm, while the tear-out failures represent lower bound pull-out capacities. Figure 3.16 shows the load-displacement curve for the four culms. The tear-out failures are indicated by dashed lines, while the solid lines represent the pull-out failures. Culms P-PA-1 and P-PA-2 demonstrated the highest loads, with very little displacement prior to tear-out of the bolt associated with the shear failure of the bamboo surrounding the bolt hole. In both cases, a region of bamboo the width of the bolt was removed as a single piece (i.e. block shear failure of single bolt connection).

Table 3.2 Pull-out test results.

Specimen	L_e (mm)	D_o (mm)	Failure	P_{max} (N)	Δ (mm)	Nodes
P-PA-1	528	45	Tear-out	9410	1.04	2
P-PA-2	824	50	Tear-out	13570	4.34	5
P-PA-3	541	50	Pull-out	8849	3.98	2
P-PA-4	706	49	Pull-out	6590	20.97	4

The pull-out failures of culm P-PA-3 and P-PA-4 demonstrated two different behaviors. Specimen P-PA-3 exhibited little slip prior to a rather sudden failure. This behavior may be classified as being relatively stiff. The failure of culm P-PA-4 demonstrated a much softer behavior; exhibiting a relatively uniform slip through the course of loading.

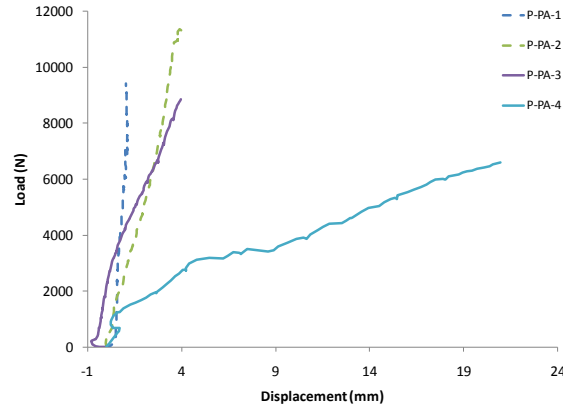


Figure 3.16 Results from Prototype Frame Pull-out Tests.

After the tests were completed the culms were split open using a hammer and chisel to inspect the interior. The bond of the mortar to the interior of the bamboo culm showed greater resistance than expected. The mortar molded to the interior of the culm, forming a mechanical ‘shear key’ at each culm diaphragm. Additionally, this well-formed interface results in considerable available friction once slip of the mortar plug is engaged. This can be seen in the response of P-PA-4 (Figure 3.16) as a softening at a slip of about 4 mm followed by engaging the friction component and associated stiffening at a slip of about 8 mm. Mitch (2010) continued the study of the pull-out behavior of grouted-bar connections and developed a behavior model, of sorts, for this type of connection.

3.4 PROTOTYPE FRAME TEST STRUCTURE

The prototype structure system was constructed in the Laboratório de Estruturas e Materiais (LEM-DEC) at PUC-Rio. The frame was based on the prototype structure described previously and shown in Figure 3.8 and Figure 3.9. The scale of the structure was reduced to approximately half the original dimensions. The frame was constructed in phases. The following sections provide details on each of the materials used, as well as the construction process.

3.4.1 Bamboo

The prototype frame was constructed with water treated *Phyllostachys aurea*. The bamboo was selected based on outer diameter, length and straightness of the member. The diameters of the members were 50 mm for the columns and 40 mm for the lateral, roof and tension tie members. The measurement details and notable defects of the bamboo members are listed in Table 3.3 and a diagram of the as-built frame is shown with dimensions in centimeters in Figure 3.17. The nomenclature in the table refers to the members by: column, location and number (C-A1); roof truss, left or right (RT-L); and tension tie, front or back (TT-F).

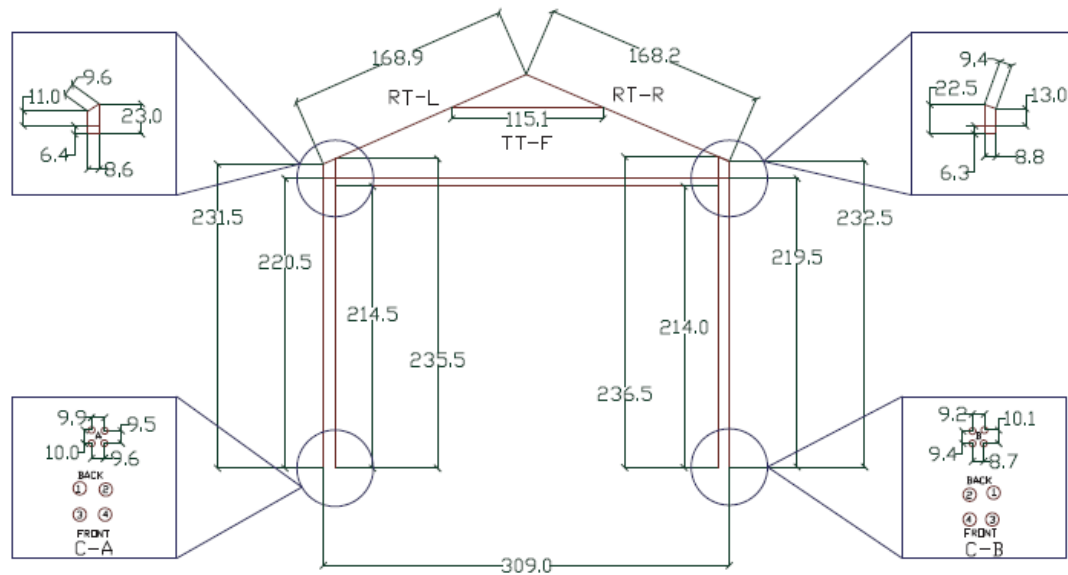


Figure 3.17 Prototype Frame As-Built with Dimensions (cm) and Member Notations.

Table 3.3 Prototype Frame Member Details.

Member	L (cm)	D _o (mm)	t (mm)	Defects
C-A1	231.5	50	5.5	Slight curvature of member 40 cm from base
C-A2	235.0	45	5.0	--
C-A3	231.0	50	4.0	Oval section; slight curvature at mid-height
C-A4	235.0	50	4.0	Very light member; significant taper of section.
C-B1	232.0	42	4.5	Oval section; slight curvature 60 cm from base
C-B2	236.0	48	4.5	Oval section; split in member at mid-height
C-B3	232.0	50	7.0	Out-of-straightness 32 cm from base
C-B4	236.0	49	6.0	Oval section
RT-L	182.0	39	5.0	--
RT-R	182.0	37	4.5	--
TT-F	132.0	41	4.5	--
TT-B	132.0	44	5.0	--

3.4.2 Grouted-Bar Column Base

To replicate the grade-beam foundation and the column-plinth joint, the base of the prototype frame was formed using two steel channels, each measuring 1 m long by 0.15 m in width. Bolt holes were drilled in the channels for the frame reinforcement, as well as the connection to the

strong floor. The channels were bolted to the floor using 12 mm threaded rod. The reinforcement for the bamboo columns utilized 12 mm steel threaded rod with a 50 cm embedded length. The rods extended below the culm base (see Figure 3.20) and were bolted to the center of the steel channel, thereby affecting a ‘fixed’ connection at the base of each culm.

The column reinforcement was embedded in the bamboo culm using a cement mortar. The ratio of cement to sand to water was 1:2.25:0.5 and quantities used are listed in Table 3.4. The mix water was reduced to account for the approximate water content of the sand.

Table 3.4 Cement Mortar Mix Design.

	Ratio	Batch (3x)	mL	Weight (kg)
Cement	1	3	3000	2
Sand	2.25	6.75	6750	2.6
Water	0.5	1.5	1250	1.25

3.4.3 Frame Connections

The single bolt frame connections were made with 8 mm diameter steel threaded rod. The dimension was determined by scaling down the original bolt size in relation to the diameter of the bamboo culm. Nuts and washers were installed only ‘finger tight’ so as not to crush the culms. This practice is consistent with that observed in Mungpoo (Figure 3.4, Figure 3.8 and Figure 3.12).

3.4.4 Construction

The construction process of the prototype test frame progressed in phases. The initial phase was selection of the bamboo. Once the members were selected and ‘graded’ as shown in Table 3.3, they were cut, using a hand saw, to their required lengths. The species used in the test, *Phyllostachys aurea*, has completely closed nodal walls (Figure 3.18b). To allow for the

embedment of the base reinforcement, nodal walls were knocked out using a steel reinforcement bar and mallet, as shown in Figure 3.18a. The nodal walls were only removed to allow for the reinforcement, the remaining walls were left intact.



a) Removal of Nodal Wall for Embedment of Reinforcement



b) Bamboo cross-section with closed and removed nodal diaphragm.

Figure 3.18 Preparation of the column bases.

The next phase of construction was to embed the reinforcement in the culms. To maintain the spacing between the culms for the lateral and roof connections, the columns were formed using bamboo spacers, made from two crossing pieces of bamboo (see Figure 3.19a and Figure 3.20). The columns were secured using tape and inverted for placement of the cement mortar.

The cement mortar was mixed according to the design proportions noted in Table 3.4. The culm bases were filled with the mortar by hand using a steel rod for compaction as the culm was filled (Figure 3.19a). Some of the culms required more cement mortar due to the location of the first closed nodal diaphragm beyond the embedment length. The reinforcement was placed in a template to secure the bars in the center of the culm (Figure 3.20) and was pushed into the mortar-filled culms and ‘vibrated’ to ensure good consolidation by tapping the template.

The column bases were covered with a plastic bag and taped to maintain the humidity for 48 hours (Figure 3.19b and c). The template was removed after 4 days to verify the curing

process of the cement mortar. There were some gaps between the cement mortar and reinforcement at the culm base. Additional mortar was placed in the culms to fill the gaps at the base around the reinforcement as shown in Figure 3.20. Despite the minor difficulties in placing the mortar, the quality of the resulting connection is believed to be equal to or possibly superior to those fabricated in the field. In a full-scale application, the annular space between the bar and culm wall will be larger and will permit better consolidation of the mortar.



Figure 3.19 Placement of cement mortar in column bases.



Figure 3.20 Column bases after template is removed: a) visibly filled bases, b) bases not completely filled, voids visible.

The roof truss was formed by embedding a wood angle to connect the two roof members at the ‘peak’. The angle was inserted into the culms to fix the roof pitch. Finally, this connection was secured using glass fiber reinforced polymer (GFRP) fabric wrapped around the joint. This connection is not reflective of that used in the St Joseph School prototype but was deemed

necessary to provide stability to the two-dimensional test frame which would otherwise be provided by the three-dimensional structure.

Several construction modifications occurred with the final frame assembly. The bolted connections were initially made using a hand drill to make the holes. The difficulty occurred in assembling the connection between three adjacent members. The length of the drill bit needed to be long enough to drill through all three members, which was achieved. However, the straightness of the hole was not exact and the bolt would not pass through the final connections. The previously drilled region of the columns was removed and a second attempt using a drill press to drill through all three members, was successful. This experience illustrates a practical aspect of using bolted connections: the need to align holes through single and adjacent culms. At reduced scale, this was possible using a long drill bit in a drill press. In the field at full scale, enlarging (or overdrilling) the holes to provide the tolerance necessary for assembly will likely be necessary. Enlarged holes will result in some 'slack' in the structural system, requiring some degree of deformation before the connection is fully engaged.

The column culms were bolted to the base and secured. The lateral members were then bolted into place. The roof truss was assembled on the ground, with the tension tie bolted in place, and then was placed in the column joint and bolt holes were drilled. The final assembled frame is shown in Figure 3.21.



Figure 3.21 Final assembled frame positioned in place.

3.5 PROTOTYPE FRAME TEST SET-UP

The prototype frame was braced to prevent out-of-plane movement (Figure 3.22). The lateral members were braced using two steel channels that were cantilevered from an existing laboratory reaction frame. The channels served as a guide for the lateral members of the frame (Figure 3.22c). Steel angles were placed at four points along the length of the lateral members to center these within the guide channels as shown in Figure 3.22d. Additional bracing was formed using pieces of Unistrut create a guide for the columns (Figure 3.22b). Again, the guide was secured to an of the existing reaction frame.

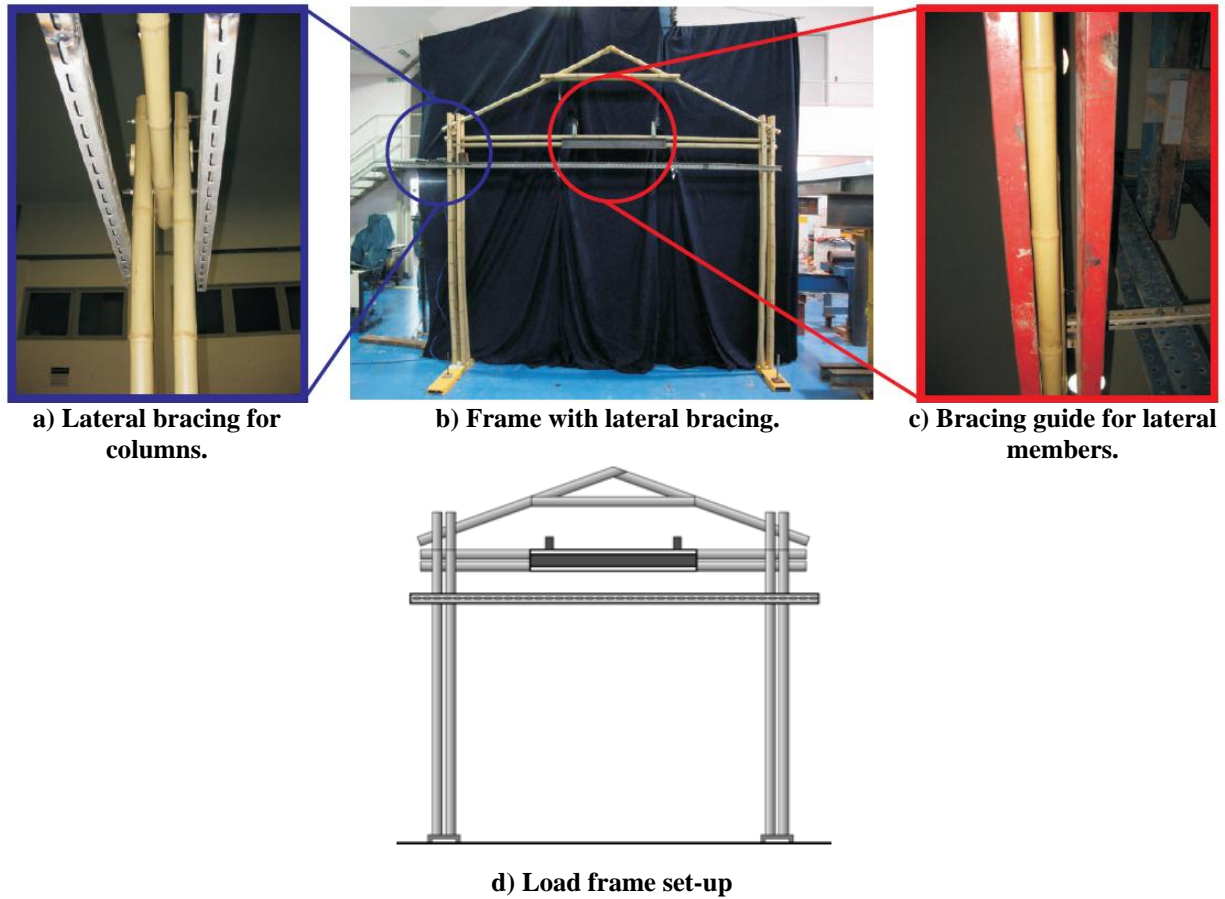


Figure 3.22 Details of frame bracing.

3.5.1 Instrumentation and Loading

The frame was instrumented with linear variable displacement transducers (LVDTs). Two horizontally-oriented LVDTs, having a 30 cm stroke length, were placed at the top of both columns below the lateral members. These LVDTs were located at the same elevation as the applied load (see below). Additional horizontally-oriented LVDTs, with a 15 cm stroke length, were placed at the peak of the roof truss and at mid-height elevation of both columns. Finally, dial gages were used to monitor the displacements of the columns bases. Instrumentation is shown in Figure 3.23.

The lateral load was applied using a 6 mm steel tension cable (so-called aircraft cable) anchored to an external reaction frame. The cable was directed through pulley blocks and onto a hand-operated ratchet winch. A 50 kN capacity tension load cell was placed in series with the cable and the eye bolt assembly used to connect to the bamboo frame. Load was transmitted to the bamboo frame using an eye bolt connected to a steel ‘spreader plate’ the plate was anchored behind the column culms with a piece of neoprene rubber placed between the bamboo and the steel plate to eliminate any local damage to the bamboo fibers in the load application area. A schematic representation of the loading arrangement is shown in Figure 3.23.

The lateral load was applied manually using the winch crank. Control over the load steps was limited to the ratchet spacing; a load step typically consisted of three or four ‘teeth’ on the winch ratchet gear. At each load step, the visual and LVDT measurements were recorded and a photo was taken. The frame was loaded and unloaded multiple times to capture the cyclic behavior of the prototype frame and connections. The LVDTs and the load were recorded using a LabView-based data acquisition system. Data was also acquired using manual measurements. Rulers and markers were placed on the frame set-up and readings were taken during the test. Photographs were also taken at each load step; these were used, in combination with fixed reference markers and markers affixed to the frame, to determine some displacements through a process of digital image correlation (DIC). The DIC was conducted manually for the tests reported.

The majority of the test data was collected manually or recorded with photographs. The LVDTs provided some initial information, however the deflections quickly exceeded the instrument capacity. The photographic data was processed by creating a uniform template for the photographs in order to maintain continuity of scale between photographs. Additionally,

stationary reference markers were used to position (and scale) the photos to ensure that all DIC measurements used the same frame of reference. These were verified with rulers placed in all photos. The resulting precision of the DIC approach was on the order of 1 mm; more than sufficient to assess the behavior of a bamboo frame.

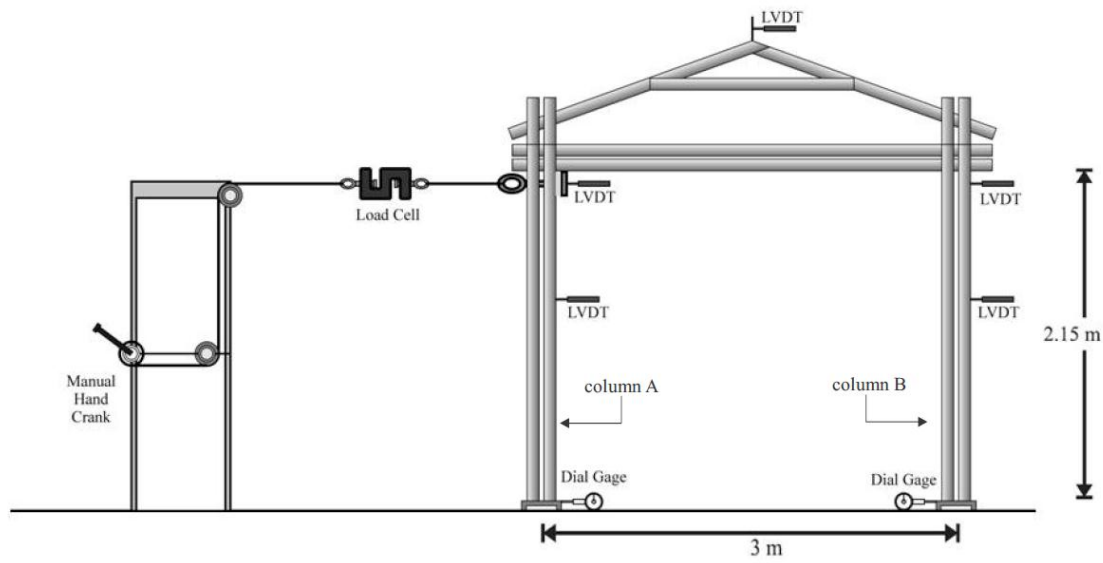


Figure 3.23 Prototype frame instrumentation and loading.

3.6 TEST RESULTS

3.6.1 Load – Deflection Response

The load-deflection response of the prototype frame shown in Figure 3.24 illustrates the behavior at the top of both columns A and B under the load cycles that were applied. The maximum deflection was 562 mm at a lateral load of 760 N. The load was recorded at the final load steps, but the displacement of the frame exceeded the visual measurements, as well as the scope of the camera and thus was not recorded. The column A and B traces are virtually identical indicating little axial distortion of the horizontal members.

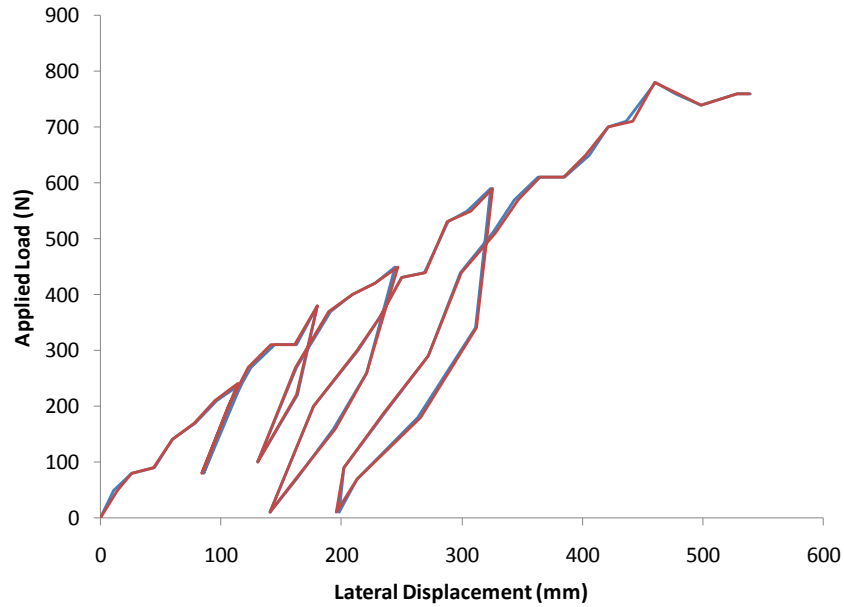


Figure 3.24 Lateral Load – Displacement of at the top of both left and right columns of the Prototype Frame. The two traces are essentially identical.

3.6.2 Load – Deflection of Columns

For the individual columns, the displacements of the outer and inner culms were determined at each load step (Figure 3.25). Initially, the displacements of each culm in a column are the same, although following the first load release, a small difference in culm displacements becomes evident. This shift is likely associated with a ‘shakedown’ effect in the bolted connections as culms and bolts ‘settle’ into their local equilibrium conditions. Some of this effect may also be attributed to the load being applied directly to the inner culms of column A (Figure 3.23). Nonetheless, based on the overall behavior shown in Figure 3.24, the relative behavior of the individual culms has a negligible effect on the overall frame response.

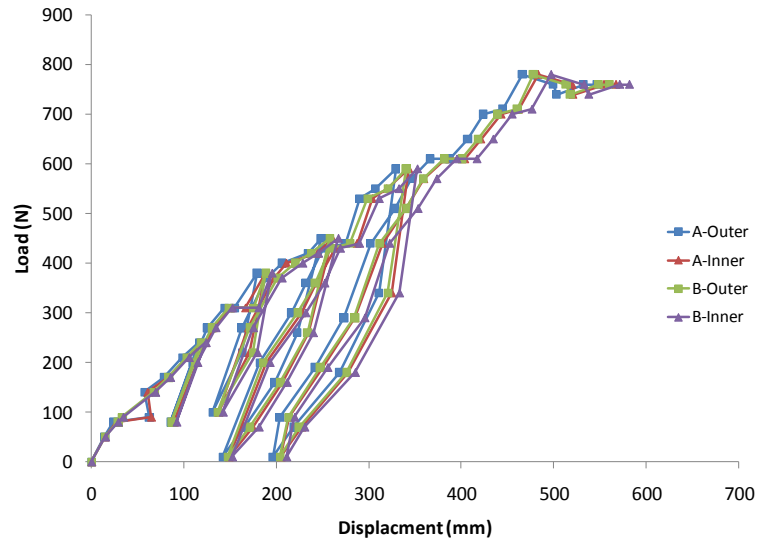


Figure 3.25 Load – Deflection Response for Columns A and B.

3.6.3 Column Displacement

The column displacement was measured using DIC at four points along the columns: at the base, mid-height of the column, the location of the lower horizontal member and at the roof truss bolt connections. Figure 3.26 illustrates the increase in displacement at the base (Figure 3.26a), mid-height (Figure 3.26b), the lower joint (Figure 3.26c), and top joint (Figure 3.26d). The nomenclature of the graphs indicate the column, A or B, and the position of the column, Outer (O) or Inner (I), along with the location of the measurement.

Figure 3.26a clearly illustrates no movement (slip) of the column base. The displacement of the mid-height of the columns were increased, although not in proportion to the height along the column and with the inner culms (AI and BI) demonstrating a larger displacement (Figure 3.26b). Figure 3.26c and d illustrate the bottom and top joint load-displacement curves. The figures indicate the maximum displacement occurred at the top joint with the largest displacement occurring at the top of column B (BO and BI). Figure 3.27 show the column

displacements at select load levels. The non-proportional displacements along the height indicate a some degree of fixity at the column base although the behavior is clearly dominated by rigid body rotation at the column base. The figure also illustrates the behavior of the roof-column connection, illustrated in Figure 3.12c and d.

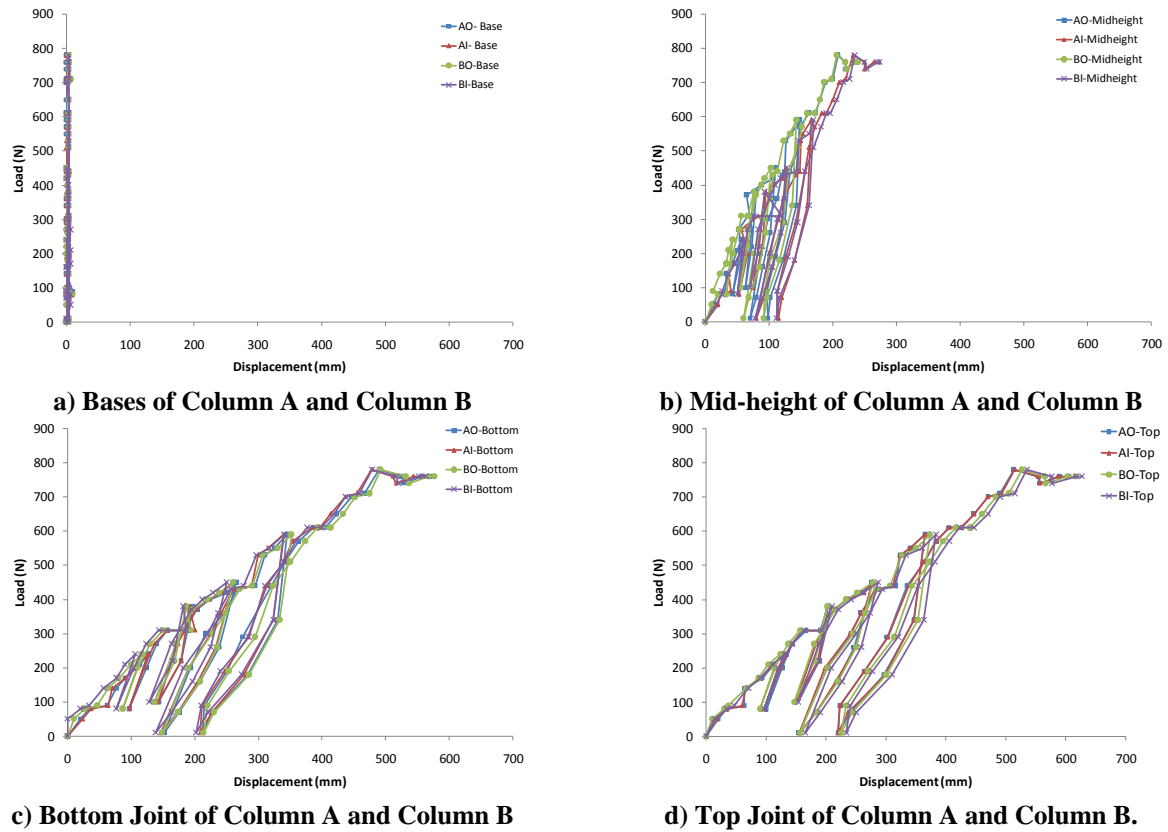


Figure 3.26 Load – Displacement Graphs

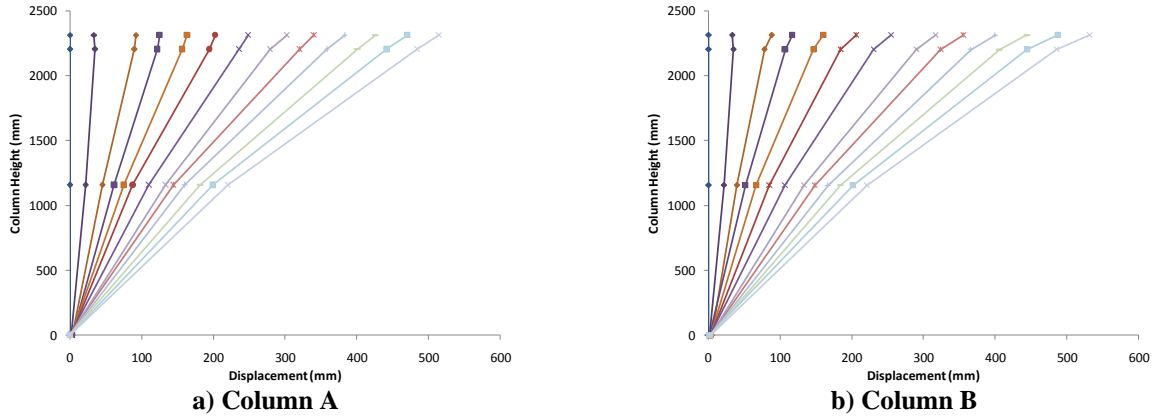


Figure 3.27 Column displacements at select load levels.

3.6.4 Behavior of Joint Regions

The displacement of the top joint induced sufficient stress on the out-of-plane members to cause fracture of the bottom culm. Figure 3.28b shows the top joint of Column B, before and after the crack occurred at an average lateral displacement of 422 mm and a lateral load of 700 N. The before and after images of the out-of-plane members are shown in Figure 3.28a and Figure 3.28c. The bottom culm continued to displace with increased load, however the member did not fully fracture. The flexibility of the culm to resist load after fracture and regain its original shape was demonstrated. Further tests to explore the edge bearing strength of *Phyllostachys aurea* need to be conducted to determine the contribution of the out-of-plane members to the overall stiffness of the column-roof connection. A method is presented in Chapter 4.0 .

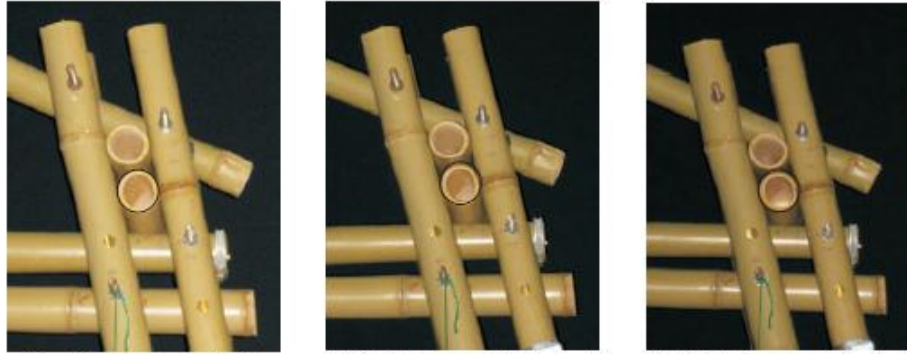


Figure 3.28 Distortion of Joint at Top of Right Column. Sequence shows distortion and fracture of the out-of-plane members.

The frame test was conducted to determine the behavior of the column bases and the roof-column joint. The anticipated fixed base boundary condition did not occur. Instead the boundary condition of the frame base was between those of a fixed base and a pinned base. There was some vertical displacement at the base of the columns, however it was minimal and the center line of the column culms rotated about a single point.

3.6.5 Post-Test Forensics

Further examination of the columns was conducted after the frame test. The culm was split open with a chisel using existing cracks when possible. The examination indicated that the cement mortar in the bamboo culm was either: (a) well consolidated, (b) broken up at the base, or (c) there were significant gaps in the embedment length. Figure 3.29 shows the embedded reinforcement bar and cement mortar within the culms.

The images in Figure 3.29 illustrate the variation in the embedment length. The variation between the culms is attributed to the method used to grout and embed the threaded rod. In some cases, the mortar broke through the closed nodal wall and leaked into the next internode region, as seen in culm A1. Additionally, the mortar separated leaving gaps of the reinforcing bar

exposed (culms A1, B2, and B4). In the case of specimen B4, the mortar slipped off the rod and broke through the nodal wall, coming to rest at the next nodal wall. The explanation for the lack of embedment is the breakage of the nodal wall due to the weight of the cement mortar and embedment rod. The rod itself did not slip due to the template used to hold the reinforcement bars in place.

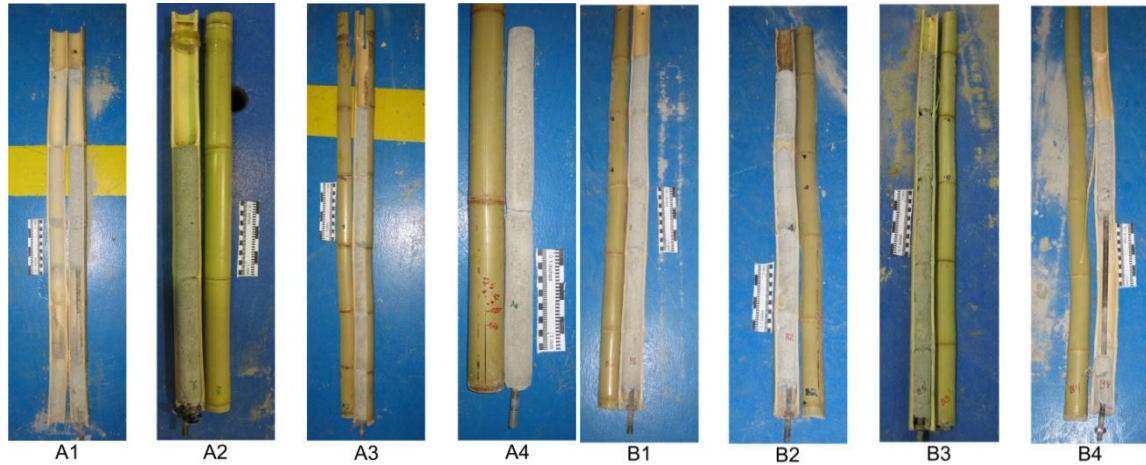


Figure 3.29 Interior of column pull-out tests.

3.7 SUMMARY

The prototype frame test provided useful information for the further study of the behavior of a plane frame constructed from bamboo. The results will be used to form the basis for the additional modeling tasks of this study. The data will serve as input for the *OpenSees* model, which will provide further detailed analysis of the seismic behavior. Some initial observations include the boundary condition at the base and the global frame behavior. The rotation of the base indicates that a rotational spring will best describe the boundary condition for the column base. The racking behavior of the frame suggests that bracing may be eventually required.

Additional tests were conducted to obtain data on the bond interface between the bamboo and cement mortar, as well as the tensile material properties of the species used in the tests.

3.8 CONCLUSIONS

The Mungpoo frame test provided significant details for the modeling tasks of this work. The results provided input parameters and basis for validating the *OpenSees* model described in Chapter 6.0 . Additional testing on the pull-out strength of the column bases indicated that the interface between the bamboo and cement mortar is good. Also, the resistance of the nodal walls to prevent pull-out failure of the bamboo is very high. Finally, the tensile strength of *Pylostachys aurea* was determined and the results will be added to the data sets which will be statistically sampled to determine nominal material properties (Chapter 5.0). The Mungpoo frame experiment illustrated the potential behavior of bamboo in areas of high seismic risk. Future research will be conducted to explore the behavior of the column bases (Mitch 2010).

4.0 CHARACTERIZATION OF SPLITTING STRENGTH OF BAMBOO

Conventionally reported material properties of bamboo typically focus on the strength parallel to the fibers; these include tension, compression and flexural (modulus of rupture) capacities (ISO 2004b). Transverse material properties such as longitudinal shear (ISO 2004b) and tension perpendicular to the fibers (Mitch et al. 2009), while arguably more relevant to the behavior of assembled bamboo structures, are reported less often.

The present understanding of the material properties of bamboo, as expressed in the ISO Design Standard (2004a) and the Indian National Building Code (2005), for instance, stem largely from the work done by Janssen (1981) and Arce-Villalobos (1993). While these standards are a start, there are many areas that still require further exploration. Janssen quotes several researchers who claimed that “the collapse of the bamboo was always sudden and the material was split into pieces parallel to the longitudinal axis”. Arce-Villalobos concludes “Bamboo culms do not fail in compression, in bending or shear, but do fail when a maximum tangential tensile stress is reached.” Despite these acknowledgements, the splitting behavior of bamboo has not been adequately addressed in present standards.

The present work explores the so-called ‘diametric compression strength’, technically the edge bearing strength of the bamboo culm (shown schematically in Figure 4.6a). One objective of this work is to investigate the potential for adopting the relatively simple-to-conduct edge bearing test as a surrogate for the critical, although more difficult-to-obtain transverse material properties. The objective of the study is to use the edge bearing test to determine the modulus of

elasticity, ultimate diametric compressive stress and culm wall modulus of rupture. The study is carried out using specimens of *Phyllostachys aurea* and *Bambusa stenostachya* bamboo.

4.1 LITERATURE REVIEW

The splitting behavior of bamboo (Figure 4.2) has not been adequately addressed in present standards. Arce-Villalobos (1993) concluded that there is no correlation between the density of bamboo and its transverse tensile strength. This is important because the dominant limit state of bamboo is splitting, and the resistance to splitting is based on the transverse tensile strength. With wood, for instance, there is a strong correlation between strength and density. The fact that this relationship is absent from bamboo makes the determination of its strength much less intuitive.

Mitch (2009; reported in Mitch et al. 2010) explored various test methods to characterize the splitting capacity of bamboo basing his analysis on the transversely oriented Mode I stress intensity factor, K_I , which provides a measure of the material's "fracture toughness". A fracture mechanics approach was selected on the premise that this might 'normalize' the quantification of material properties thereby reducing the significant scatter inherent in establishing mechanical properties of bamboo. A fracture mechanics approach should, it was hypothesized, result in more comparable measures of behavior allowing, for instance, more rational interspecies comparison. Mitch explored multiple test configurations and selected the configuration thought to introduce the least unnecessary variation: a full culm split pin test. The test configuration selected is shown in Figure 4.1.

The test configuration includes a split steel pin to which a tensile load is applied inducing a splitting failure in the test specimen. Specimens have a notch located at the edges of the hole drilled through the culm, perpendicular to the load direction (Figure 4.1b) in order to initiate the failure – allowing for the most reliable calculation of K_I . Mitch also conducted compression and “bowtie” shear tests (ISO 2004b) to compare and assess the variation in test results. The proposed split pin test showed the least variation in results. The average K_I value obtained for *Bambusa stenostachya* treated with a borate solution was $0.174 \text{ MPa}\cdot\text{m}^{1/2}$ (COV = 0.22). Additional tests were conducted to determine the influence of the pin diameter, which was shown to have little influence on the average K_I value as should be expected for a fracture mechanics test.

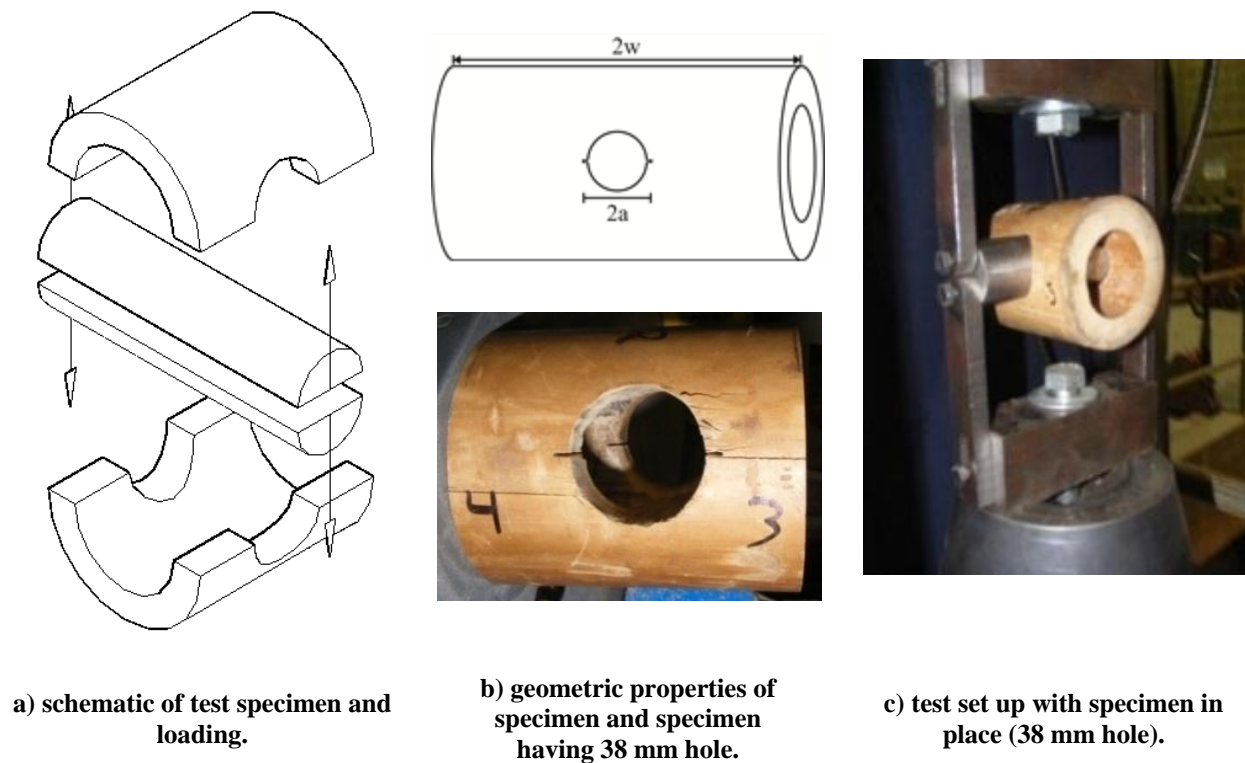


Figure 4.1 Split pin test set-up (Mitch 2009).

The split pin test also permits the direct tension capacity perpendicular to the fibers to be determined. For the *B. stenostachya* tested by Mitch (2009), the average tensile rupture stress perpendicular to the fibers was found to be 1.06 MPa (COV = 0.22). The split pin test is adopted in the present work and calculations associated with its use are presented later in this chapter.

Amada and Untao (2001) investigated the fracture properties of Moso (*Phyllostachys edulis* Riv.) bamboo. The experiment was carried out through a series of notched longitudinal tension tests from different sections of the bamboo culm. The results indicated that the fracture toughness (K_I) of Moso bamboo, averaged across the radius, was $56.8 \text{ MPa}\cdot\text{m}^{1/2}$. Low et al. (2006) in contrast, used flexural tests to calculate K_I values for young (1 yr) and old (5 yr) *Sinocalamus affinis* bamboo; the values obtained were 8.0 and $5.5 \text{ MPa}\cdot\text{m}^{1/2}$, respectively. Additional data was obtained from Guatibonza (2009), where longitudinal tension tests were used to obtain K_I values for *Dendrocalamus giganteus*. The average value obtained in this case was $53 \text{ MPa}\cdot\text{m}^{1/2}$. The variation in reported values of ‘fracture toughness’ results from each study using a different test arrangement and therefore calculating a different parameter, although all defined this parameter as K_I based on their selected test orientation. Amada and Untao (2001) and Guatibonza (2009) report the behavior of longitudinal tension tests; Low et al. (2006) reports what amounts to a modulus of rupture test; while Mitch (2009) addresses tension perpendicular to the fiber. The results reflect the hierarchy of bamboo material properties: it is very strong and tough in tension parallel to the fibers; approximately an order of magnitude weaker in flexure; and another order of magnitude less robust in perpendicular tension. It is this last property that most influences the splitting capacity of bamboo. It is interesting to note, however, that the calculated variation in test results using fracture properties is generally less than that reported for

conventional mechanical properties suggesting that regardless of orientation, a fracture approach may provide a better method for comparing bamboo behaviors.

4.2 STANDARD TEST METHODS FOR BAMBOO

Material properties of bamboo are typically obtained based on the ISO 22517-1 *Bamboo – Determination of physical and mechanical properties* guidelines (ISO 2004b). This document provides general guidance on specimen preparation and testing. Information is also given on determination of moisture content, mass, and shrinkage. ISO tests for mechanical properties are described in Table 4.1. Also shown in Table 4.1 are two non-ISO tests that have been adopted for bamboo materials. Specimens are typically taken from the top, bottom and middle regions of the culm to establish an average value over the height of the culm. The author contends that tests using full culm specimens are preferable since they eliminate any bias associated with sampling from a culm cross section. Factors that may affect tested properties include the curvature of the culm wall and the through-thickness gradient of material properties of the culm wall.

4.3 ASSESSING BAMBOO SPLITTING BEHAVIOR

As described previously, the dominant failure mode of bamboo is longitudinal splitting associated with the lower strength of the matrix of the culm (Mitch et al. 2010). Splitting behavior has not been fully addressed and the need for additional work in this area was identified by Janssen (1981), in which he notes the modulus perpendicular to the fiber as being very low and unknown. Splitting failure also occurs in bending tests; Janssen describes the bending

stresses in a culm as the maximum compressive stress and lateral strain in the compression zone of the culm, with failure occurring due to longitudinal splitting. This is ideally a Mode II longitudinal shear failure characterized by the VQ/I shear flow equation; however, in the presence of flexure, there is a Mode I component stress which significantly reduces the apparent pure Mode II capacity. Janssen (1981) developed and standardized (ISO 2004b) the ‘bowtie’ test (see Table 4.1) in an attempt to quantify this material behavior. This test, however, neglects the modest Mode I contribution which is believed to drive the splitting failure. Mitch et al. (2010) proposed the split pin test method to assess the tensile behavior of full culm bamboo perpendicular to the culm longitudinal axis.

Table 4.1 Summary of material test methods for bamboo.

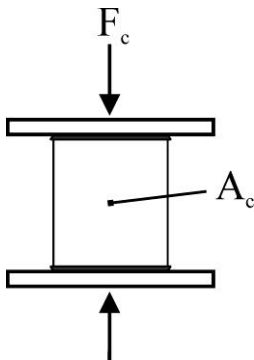



Test Method	Schematic representation of test	Photo	Material Property	Test description
Compression Parallel to the Fiber (ISO 2004b)	 $A_c = \pi/4 [D_o^2 - (D_o - 2t)^2]$	 <p>(Mitch 2009)</p>	$\sigma_c = \frac{F_c}{A_c}$	<p>The ultimate compressive stress of the culm (σ_c) is found from a compressive test of a length of culm no longer than twice its outside diameter ($L \leq 2D_o$). The net area of the culm (A_c) is used in this calculation. The compressive modulus of elasticity (E_c) can be obtained using electrical resistance strain gages placed at mid-height at either side of the culm. The strain is averaged and the compressive modulus is calculated between 20-80% of the resulting stress-strain curve. Care must be taken to minimize friction between the loading head and culm which affects results. Steel shims or sulphur capping compound have been shown to be adequate to minimize friction. Rigid loading blocks are required to ensure that F_c is distributed uniformly to the culm section.</p>
Tension Parallel to the Fiber (ISO 2004b)			$\sigma_t = \frac{F_t}{A_t}$	<p>A 'dogbone' style tension test is used to determine the tension capacity parallel to the fibers (σ_t). The coupon thickness (t) corresponds to the culm wall thickness (t) and the coupon breadth (b) is a circumferential chord of the culm. The reduced area gage length is typically 50 to 100 mm in length. Additional specimen length is provided for wider clamping tabs. The tensile stress is calculated over the reduced gage length area ($A_t = bt$). Tensile modulus of elasticity (E_t) can also be calculated using clip gages or strain gages. Care must be taken so that gripping stresses do not cause local damage to the specimen affecting results.</p>

Table 4.1 (continued)

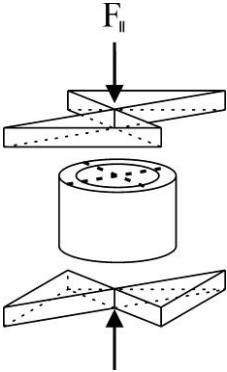

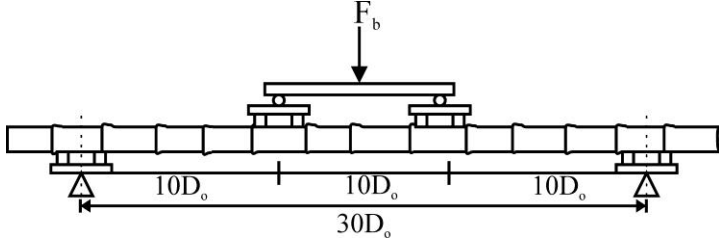
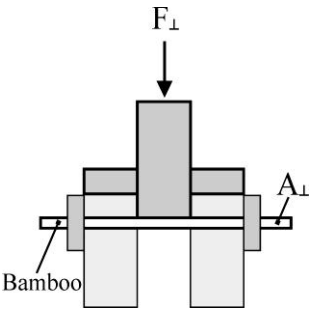
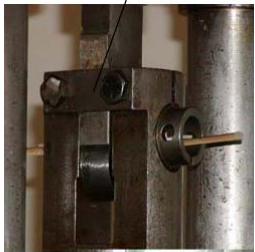
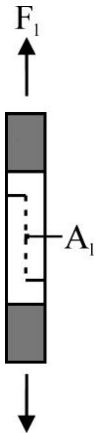

Test Method	Schematic representation of test	Photo	Material Property	Test description
Shear Parallel to the Fiber (ISO 2004b)		 <p>(Mitch 2009)</p>	$\tau_{\parallel} = \frac{F_{\parallel}}{4Lt}$	<p>To measure shear strength parallel to the fibers (τ_{\parallel}) a “butterfly” or ‘bowtie” shear test is used. The specimen length is equal to the outer culm diameter ($L = D_o$). The ultimate shear stress is calculated based on the applied load (F_{\parallel}) distributed over the sum of the shear areas (Lt) of all four failure planes (i.e.: $4Lt$). Separate tests are required for specimens that include nodes and those that do not since their capacities will differ. Care must be taken that the ends of the culm are smooth, parallel and at right angles to the culm longitudinal axis. Rigid loading blocks are required to ensure that load is distributed uniformly to the culm section.</p>
Bending Perpendicular to the Fiber (ISO 2004b)	 $I_b = \pi/64 [D_o^4 - (D_o - 2t)^4]$		$f_b = \frac{F_b L D_o}{12 I_b}$ $E_b \approx \frac{L^3}{56 I_b \Delta}$	<p>Flexural properties of a bamboo culm are determined from a third-point bending test as shown. The specimen length is $L \geq 30D_o$ to ensure a flexure-dominated behavior (minimizing the effects of shear). The apparent modulus of rupture (f_b) is calculated from the applied moment in the constant moment span ($M_b = F_b L/6$) and the moment of inertia of the culm (I_b). The bending modulus of elasticity (E_b) is calculated from the measured mid-span deflection (Δ). In this test, calculated values are ‘apparent’ or ‘effective’ since the calculations do not account for the non-uniform section material properties (grading) of the bamboo. Nonetheless, the results may be used directly in design using full culm bamboo.</p>

Table 4.1 (continued)

Test Method	Schematic representation of test	Photo	Material Property	Test description
Shear Perpendicular to the Fiber (Cruz 2002)		 (Cruz 2002)	$\tau_{\perp} = \frac{F_{\perp}}{2A_{\perp}}$	Transverse shear capacity (τ_{\perp}) of a coupon cut from a culm wall is obtained using a simple two-plane shear arrangement which restrains the flexure of the specimen. The test results in the specimen being broken into three pieces, providing the transverse shear strength of the coupon having an area A_{\perp} .
Interlaminar Shear (INBAR 1999)		 (Cruz 2002)	$\tau_l = \frac{F_l}{A_l}$	<p>The interlaminar shear tests based on ASTM D2733-70 (1976), Method of Test for Interlaminar Shear Strength of Structural Reinforced Plastics at Elevated Temperatures and were conducted by Moreira (1991). INBAR (1999) standardized this test for bamboo.</p> <p>Interlaminar shear (τ_l) tests may involve coupons oriented to assess either the shear parallel or perpendicular to the through-thickness direction of the culm. Shear perpendicular to the through-thickness dimension may also be assessed using the previously described ‘bowtie’ test.</p> <p>An ‘S-type’ shear specimen is used consisting of a tension coupon cut from the culm wall. This coupon is scored halfway through its depth perpendicular to the loading direction at two locations resulting in shear plane having an area A_l. The shear plane is at the middle of the specimen and therefore subject to pure shear when the specimen is loaded in tension as shown. Care must be taken so that gripping stresses do not cause local damage to the specimen affecting results.</p>



a) column splitting near sawn end



b) beam splitting near sawn end at dowelled and lashed joint



c) severe splitting at sawn ends of roof rafters



d) severe splitting initiated by presence of bolted connection



e) initiation of splitting at bolted connection

Figure 4.2 Examples of bamboo splitting observed at St. Joseph's School (Mitch et al. 2009).

Since splitting is also often associated with bolted connections (see Figure 4.2). The split pin test is analogous to a bolt shear test if the small crack initiators (Figure 4.1b) are not included. To address the effect of the angle of bolt loading (which varies in a real structure), an adaptation of the split pin test was developed to determine the behavior of bolt-induced forces and assess their contribution to the splitting behavior of the bolted culm. This is discussed in Section 4.4.

4.3.1 Appropriate Test Methods for Technological Sustainability

An important and often overlooked consideration in developing test methods is that the method must be usable and reliably repeatable in the environment in which it is to be used. For tests intended to characterize the material properties of bamboo, the tests need to be simple enough to be conducted in the field by non-technical personnel and not require cumbersome or complex test equipment. Some issues that should be considered in developing an appropriate field test include:

1. Compression tests are simpler to conduct than tension tests; they do not require gripping mechanisms and may usually be accomplished with a simple frame and hydraulic piston.
2. Tests that require special components such as the compression test (steel shims or capping), the flexure test ('whiffle tree' for load distribution), or the perpendicular shear test (test jig) will be less likely to be conducted correctly in the field.
3. Tests requiring accurate specimen fabrication such as the tension test (specimen machining); 'bowtie' test (parallel ends machined for bearing) or the split pin test (through culm drilling) are more difficult to prepare and therefore may be less reliable when conducted outside of a laboratory environment.

Thus the most appropriate test uses a full culm specimen (no machining apart from cutting to length), requires no special test apparatus, and is based on a compression test. The edge-bearing test reported in Section 4.5 meets these requirements.

Most importantly, however, a material characterization test must yield a useful metric of material performance. This metric, preferably must correlate with useful design values but, at a minimum, must be sufficiently consistent to permit it to be used to compare bamboo from different batches or species. An analogy to this is the standard concrete compression test: from a

single value of ultimate compressive stress (f_c'), modulus ($E \approx 4750\sqrt{f_c'}$), tension ($f_t \approx 0.33\sqrt{f_c'}$) and modulus of rupture ($f_b \approx 0.60\sqrt{f_c'}$) values may be reliably calculated (f_c' values in MPa in all cases).

The following sections describe the bolt shear and edge bearing tests and present data from pilot applications of these. A companion test series illustrating the split pin test is also presented. Finally a discussion of the correlation between the relatively complex split pin test and the simple edge bearing test is presented. It is hypothesized that the former may be an appropriate simple-to-conduct surrogate for the latter.

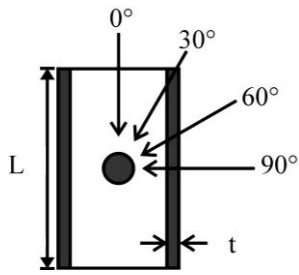
4.4 BOLT SHEAR TEST

The bolt shear tests are based on the typical the column-to-roof joist connection from St. Joseph's school in Mungpoo, India (Figure 3.10). The joint consists of multiple single bolt connections (Figure 3.10e). Bolted connections are commonly used in bamboo construction, although the connection often induces a splitting failure. Janssen (1981) investigated the potential uses of bamboo pins in lieu of metallic bolts on the premise that the softer pin will distribute the damage between the pin and surrounding bamboo. The study included shifting the angle of loading to determine the failure strength of the connection. Researchers have also explored the location of the bolt hole with respect to the edge of the culm (Arce-Villalobos 1993; Ghavami and Moreira 1999). The present study investigates bolt shear behavior of a steel bolt connection in the center of a bamboo culm. This is thought to represent the simplest possible connection requiring the least degree of workmanship (bamboo or wooden pin connections require relatively precise fabrication). Finally, it is important to note that the bolt shear test is not

testing the bolt/pin itself – this is assumed in all cases to sufficiently strong to allow a bamboo failure to develop. No reports of shear failures of metallic pins/bolts in such joints are known. In any event, the shear capacity of a bolt/pin may be determined as: $V = 0.577A_{\text{net}}f_y$, where A_{net} is the smallest area of the bolt engaged in shear (usually through the threads) and f_y is the material yield strength.

4.4.1 Experimental Method

The bolt shear specimens to be tested were loaded at 0, 30, 60, and 90 degrees relative to the longitudinal axis of the culm, as shown in Figure 4.3. The bamboo specimens are *Bambusa stenostachya*, which is treated with a borate solution. The specimens were taken only from the internodal regions and were randomly cut from eight different culms. Table 4.2 summarizes the average specimen length and wall thickness of the specimens in each angle group. A 25.4 mm hole was drilled through both sides of the culm in a single pass and was located at mid-height of the specimens. Supports were fabricated for the 30, 60 and 90-degree specimen groups to ensure the specimen was positioned at the correct angle, while also distributing the load to reduce effects of eccentricity (Figure 4.3c, b and d). The compressive load was applied to the extended ends of the bolt (see Figure 4.3) in displacement control at a rate of 0.005 mm/sec.



a) loading angles and section



b) 0 degrees



c) 60 degrees



d) 90 degrees

Figure 4.3 Bolt shear test set-up.

4.4.2 Bolt Shear Results

A total of thirty-three specimens were tested and the summary of the tests are presented in Table 4.2. The bearing stress that the bolt applies to culm wall is determined as:

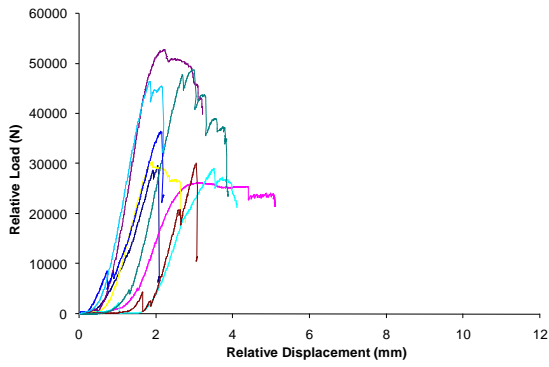
$$f_{bearing} = P_{split} / 2d_b t \quad (\text{Eq. 4.1})$$

where P_{split} is the total applied load to cause splitting, d_b is the bolt diameter and t is the culm wall thickness. It is noted that for the tests conducted, bolt threads were not included in the specimen span and thus the bolt area is: $A_b = \pi d_b^2 / 4$.

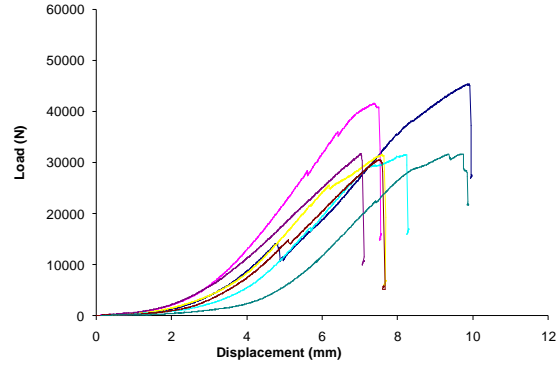
Plots of the applied load versus displacement of the bolt (in the direction of loading) for all specimens are shown in Figure 4.4. The ultimate failure of all specimens involved longitudinal splitting of the culm initiating at the bolt hole. The applied load to cause this failure decreased as the loading angle varied from 0° (loading parallel to longitudinal axis and splitting failure) to 90° (loading perpendicular to splitting) as shown in Figure 4.5.

Table 4.2 Bolt shear specimen geometrical properties and test results.

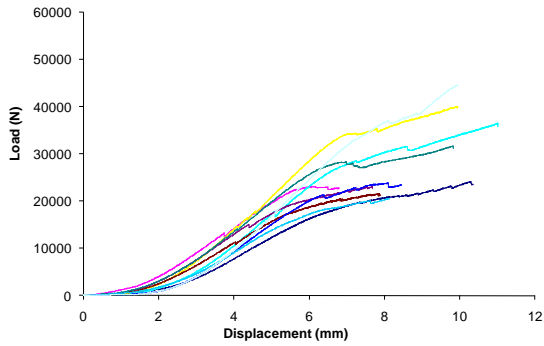
Angle	0°			30°			60°			90°		
n	9			7			10			7		
	\bar{x}	s	COV (%)	\bar{x}	s	COV (%)	\bar{x}	s	COV (%)	\bar{x}	s	COV (%)
L (mm)	157	0.7	0	157.5	0.7	0	157.6	0.9	1	157.4	1.0	1
t (mm)	18.3	3.6	20	21.6	1.7	8	18.6	4.2	23	17.6	5.8	33
P (N)	36704	10711	29	34894	6002	17	28905	8686	30	26856	6545	24
$f_{bearing}$ (MPa)	39.5	11.0	28	31.8	4.7	15	30.6	4.7	15	30.0	7.7	26



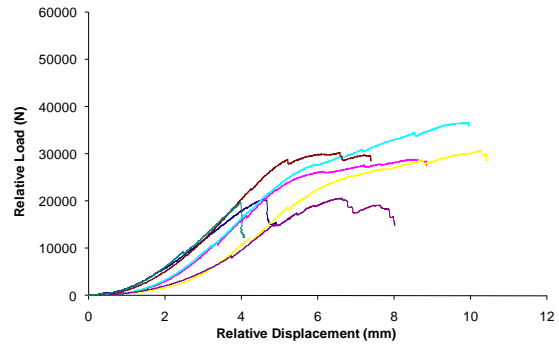
a) 0 Degree (n = 9 tests)



b) 30 Degree (n = 7 tests)



c) 60 Degree (n = 10 tests)



d) 90 degree (n = 7 tests)

Figure 4.4 Applied load-displacement curves for bolt shear tests.

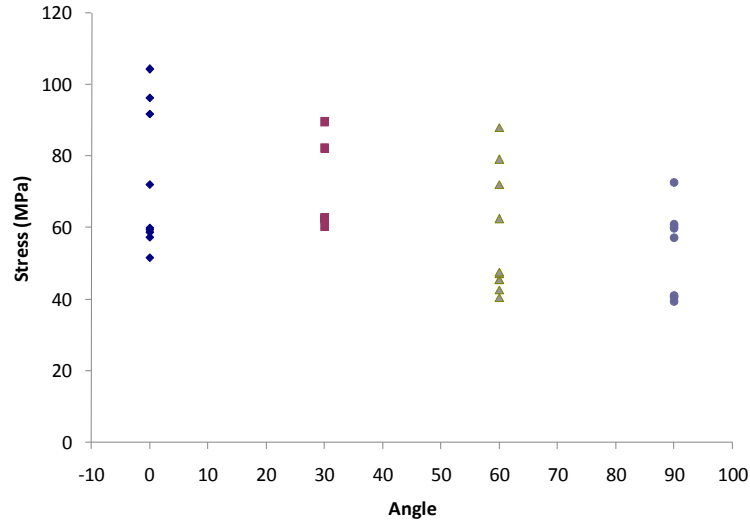


Figure 4.5 Ultimate bearing stress at failure vs. loading angle for bolt shear tests.

Two distinct types of failures were documented: For the specimens having a load orientation of 0 and 30 degrees (Figure 4.4a and b), the behavior was brittle: loading increased to a point where the bamboo split (P_{split}) at which point bearing capacity was lost. For the specimens having loading oriented more transversely to the fibers – 60 and 90 degrees (Figure 4.4c and d) – a bilinear behavior was observed. This behavior is explained by the fact that splitting does not result in catastrophic failure at these ‘flatter’ orientations and some reserve capacity associated with bearing remains. This ‘reserve capacity’ is an artifact of the test set-up and the applied load to cause splitting (P_{split}) should be used in assessing the bolt shear capacity. This value is defined on the load-displacement curves (Figure 4.4) as the proportional limit for the initial loading portion of the test.

4.5 EDGE BEARING TEST

The edge bearing strength (sometimes referred to as diametric compression) of bamboo culms, is often not included in studies due to the low strength of the material and the difficulty of interpreting the test results. Trujillo (2007), for example, excluded edge bearing due to the nature of the failures that result from the test. The complex failure mechanism involves the formation of a multi-pinned arch around the culm diameter. Amada et al. (1996) noted the use of edge bearing tests to determine the circumferential properties for *Phyllostachys edulis* Riv. Amada et al. investigated the properties along the length of the culm. Torres et al. (2007) conducted edge bearing tests on *Guadua angustifolia* and *Phyllostachys pubescens* specimens, to determine the ‘circumferential modulus of elasticity, E_{ϕ} ’. Torres considered the difference in this modulus at various locations along the culm, as well as the variation of the modulus of specimens having different lengths.

Torres’ ‘circumferential modulus’, in fact, represents an apparent modulus of elasticity in the direction perpendicular to the longitudinal axis of the culm averaged for the tension and compression behaviors. It is noted that due to a misinterpretation of the mechanics equations governing this test arrangement⁶, Torres’ absolute values are incorrect although his comparisons between specimens remain valid (the error was consistent throughout and did not affect the proportionality of the results).

⁶ Torres misinterpreted the value h , substituting the culm wall thickness, t and therefore incorrectly calculated I . The present discussion corrects this error and has been verified using benchmark data tabulated by Nelson (1939).

4.5.1 Equations Governing the Edge Bearing Test

The vertical diametric deflection, D_V , of a hollow cylinder (i.e.: ‘squashing’) with an applied line load, w (Figure 4.6a) may be shown to be (Young 1989, Article 8.3):

$$D_V = -\frac{wLR^3}{E_\phi I} \left(\frac{\pi k_1}{4} - \frac{2k_2^2}{\pi} \right) \quad (\text{Eq. 4.2})$$

For a uniform culm wall thickness, t , Figure 4.6d and e illustrate that R_o = the measured outside radius of the culm; $R = R_o - t/2$ = the radius to the midline of the culm wall section; $c = t/2$ = the distance from the midline of the culm wall to the edge of the wall section; and h = distance from the culm wall midline to the elastic neutral axis measured toward the center of curvature (Figure 4.6e). The location of the neutral axis (h) for a curved beam in flexure having a solid rectangular section is estimated as (Young 1989, Table 16.1):

$$h = R - 2c / \ln \left(\frac{\frac{R}{c} + 1}{\frac{R}{c} - 1} \right) \quad (\text{Eq. 4.3})$$

As shown in Figure 4.6b, $A = L \times t$ = area of a single culm wall; and I = moment of inertia of area A calculated about the culm wall midline:

$$I = Lt^3/12 \quad (\text{Eq. 4.4})$$

The terms k_1 and k_2 are correction factors for hoop-stress deformation and transverse shear deformation, respectively. For thin-walled sections, these values are given as (Young 1989):

$$k_1 = \left(1 - \frac{I}{AR} + \frac{FEI}{GAR} \right) \text{ for thin-walled sections} \quad (\text{Eq. 4.5})$$

$$k_2 = \left(1 - \frac{I}{AR^2} \right) \quad (\text{Eq. 4.6})$$

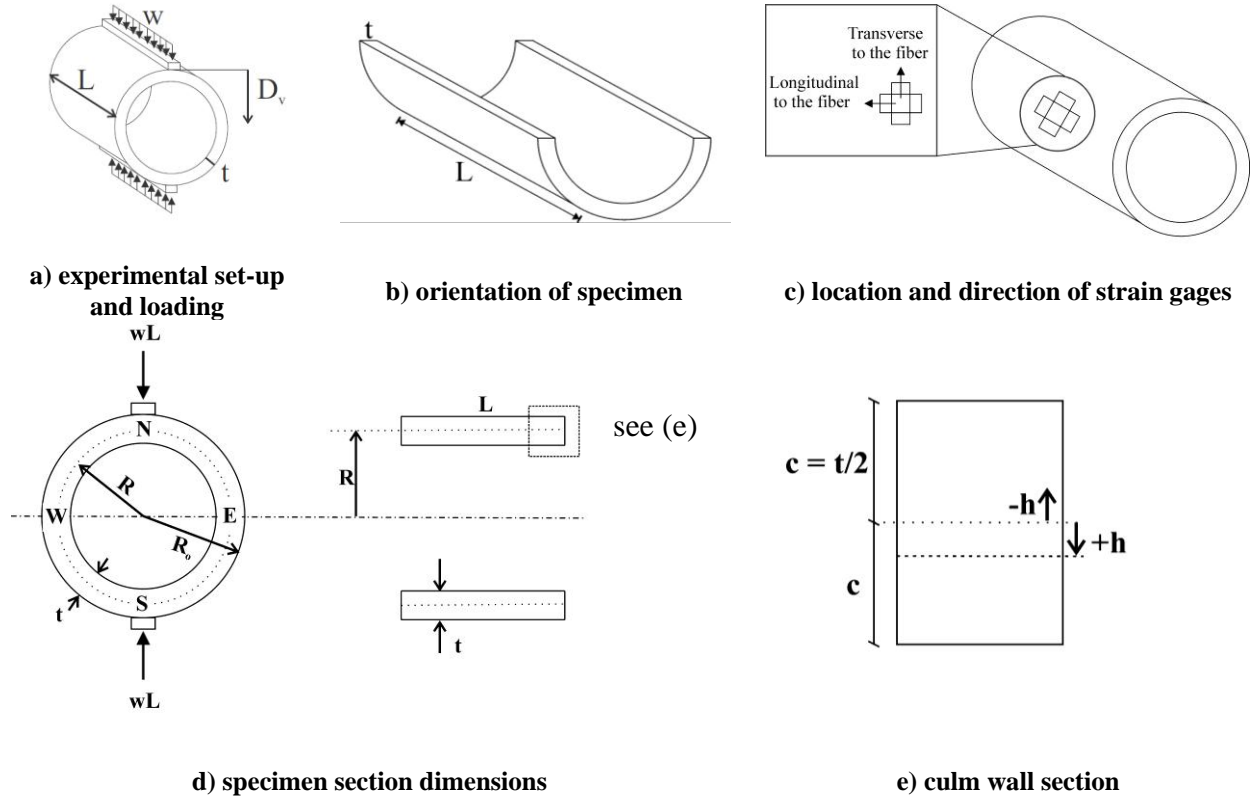


Figure 4.6 Edge bearing test specimen geometry.

To simplify equations 4.5 and 4.6, the ratio E/G is taken as $2(1+\nu)$ and ν is set equal to 0.3 (Cruz 2002). Additionally, the shape factor, F , for a rectangular section may be taken as 1.2 (Young 1989). Typically a section is defined as being thick or thin-walled based on the ratio of the wall thickness to outer diameter ($t/2R_o$). If this ratio is less than 0.1 the section is thin-walled (Vlasov 1961). The ratio $t/2R_o$, for the *Phyllostachys aurea* specimens tested is approximately 0.09 to 0.1, small in comparison to the ratios of other species of bamboo that vary from 0.08 to 0.21. The ratio of the *Bambusa stenostachya* specimens varied from 0.13 to 0.21 which, in contrast to *P. aurea* specimens, is in the upper range of the ratios. However, for the uniform wall section shape of a bamboo culm ($L \times t$ in Figure 4.6), the correction factors calculated for thick and thin walled sections are similar and relatively negligible. These corrections do not account

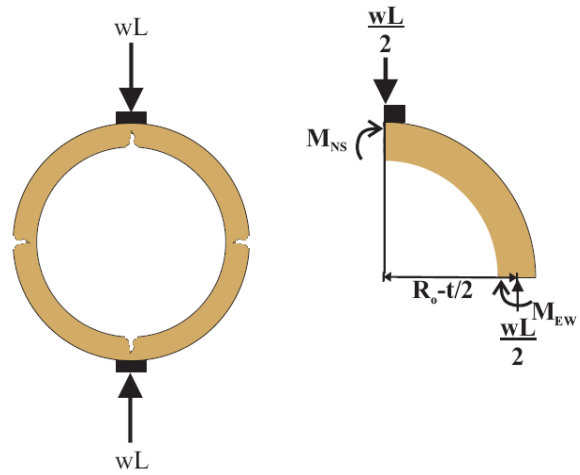
for local stresses associated with bearing stresses on thick walled sections (Young 1989). These are not addressed in the present study.

Substituting experimental data in the form of an applied load versus vertical displacement relationship (wL/D_V), into Equation 4.2, one obtains the apparent modulus of elasticity, E_ϕ . Again, it is noted that this value must be interpreted to represent the modulus of elasticity in the direction perpendicular to the longitudinal axis of the culm averaged for the tension and compression behaviors resulting from through-wall flexure.

Other pertinent data that may be obtained from the edge bearing test are the through culm wall bending properties. The culm wall modulus of rupture is clearly related to the transverse tension properties of the bamboo and therefore the splitting behavior. Considering the idealized failure shown in Figure 4.7, multi-pinned arches will form as a result of hinges forming at the locations of maximum moment around the circumference of the culm section. The maximum moments occur at the loading and reaction points (designated N and S in Figure 4.6d) and at the extreme edges (designated E and W).



a) Specimen PA-0.5-4 following failure showing rupture at North (top) location, under applied load.



b) expected cracking failures at different quadrants and calculation of resulting moment.

Figure 4.7 Edge bearing specimen failure.

The location of the rupture around the culm circumference is informative. As shown in Figure 4.7b, the cracks around the culm diameter result from local flexure of the culm wall. Arbitrarily identifying flexure resulting in tensile stress on the interior of the culm wall (and compression at the exterior) as being positive, results in the culm wall at the N and S locations being subject to positive flexure and the E and W locations being subject to negative flexure. This distinction is important when calculating the modulus of rupture since the properties of the bamboo vary through the wall thickness (Liese 1998) and different moduli of rupture would be expected depending on the orientation of the moment. The through culm wall moments at the critical sections are (Young 1989):

$$M_{NS} = \frac{wLR}{\pi} \left(1 - \frac{I}{AR^2} \right) \quad (\text{Eq. 4.7})$$

$$M_{EW} = \frac{wLR}{\pi} \left(1 - \frac{I}{AR^2} \right) - \frac{wLR}{2} \quad (\text{Eq. 4.8})$$

The apparent modulus of rupture of the culm wall, f_r , may therefore be calculated as:

$$f_{r\ NS} = \frac{M_{NS}(c_r + h_r)}{I_r} \quad (\text{Eq. 4.9a})$$

$$f_{r\ EW} = \frac{M_{EW}(c_r + h_r)}{I_r} - \frac{wL}{2Lt} \quad (\text{Eq. 4.9b})$$

In the calculation of the modulus of rupture, I_r , c_r , and h_r are calculated using the wall thickness at the location (N, S, E or W) of rupture, t_r . Similar calculations made at section quadrants that did not rupture may be interpreted as lower bound moduli of rupture for the same culm. The effect of the section orientation requires the additional axial load component to be included at the E and W locations (Equation 4.9b).

4.6 EDGE BEARING EXPERIMENTAL PROGRAM

Two series of edge bearing tests were conducted by the author in different laboratories. Thin-walled *Phyllostachys aurea* specimens were tested at PUC-Rio and thick-walled *Bambusa stenostachya* specimens were tested at the University of Pittsburgh. While the author conducted all tests, the different laboratories resulted in slightly different test protocols being used as described in the following sections.

4.6.1 *Phyllostachys aurea* at PUC-Rio

All specimens in this group were water treated *Phyllostachys aurea*. The specimens were cut from remnants; therefore their locations on the original culm are unknown. Four groups of four specimens each were tested. The lengths of the specimens in each group were $L = 2R_o$, $L = 1.5R_o$, $L = R_o$ and $L = 0.5R_o$. The average values (\bar{x}) and standard deviations (s) for the outside radius (R_o), wall thickness (t) and their ratio (R_o/t) for each specimen group are listed in Table 4.3. The radius and thickness measurements were taken at the four quadrants (N, S, E and W) of the culm as shown in Figure 4.6d. The specimen naming convention is as follows:

$$XX-Y-Z$$

where XX is the species of bamboo (PA – *P. aurea*; BS – *B. stenostachya*); Y is the length expressed as a multiple of the outer radius ($L = YR_o$); and Z is the unique specimen identifier. An additional two groups of three specimens each were tested with 0-90° strain gage rosettes as shown in Figure 4.6c. The two strain gage groups had lengths $L = 2R_o$ and $L = R_o$. The strain gages were placed on the W side of the specimens, centered at mid-height of the specimen and oriented such that the gages were parallel and perpendicular to the fiber direction.

Table 4.3 Average geometric properties of edge bearing specimens.

Length	PA-2			PA-1.5			PA-1			PA-0.5			BS-2		
n	6			4			6			4			10		
	\bar{x}	s	COV (%)	\bar{x}	s	COV (%)	\bar{x}	s	COV (%)	\bar{x}	s	COV (%)	\bar{x}	s	COV (%)
R_o (mm)	21.8	0.7	3.2	22.1	0.3	1.4	22.4	0.8	3.6	21.7	0.1	0.5	39.7	0.8	2.0
t (mm)	4.2	0.3	7.1	4.0	0.1	2.5	4.2	0.3	7.1	4.0	0.0	0.0	13.5	2.6	19.4
R_o/t	5.24	0.27	5.2	5.48	0.10	1.8	5.32	0.29	5.5	5.42	0.02	0.4	3.0	0.55	18.2

Thin pieces of particle board (4 mm thick) with dimensions L x 6 mm were used to distribute the load evenly across the specimen at both the load (N) and reaction (S) locations (Figure 4.6a and Figure 4.7a). The test was conducted using a universal testing machine operated in displacement control at a displacement rate of 1 mm/min. The load-displacement curves were obtained from the test frame controller, thus frame compliance and deformation of supports are included in the displacement value. While not technically correct, the small specimen size makes measuring actual diametric displacement difficult. The applied loads are all very small (greatest reported load is 410 N) and therefore the effects of compliance and elastic strains in the supports are negligible.

4.6.2 *Bambusa stenostachya* at the University of Pittsburgh

To directly compare the edge bearing and split pin test methods, additional test series of each test were performed using the same bamboo. All specimens in this study were taken from the same culm of borax treated *Bambusa stenostachya*. Ten specimens were tested for each test method and the specimens were taken from alternate adjacent locations along the culm (i.e: A-B-A-B-etc. where A specimens were edge bearing and B specimens were split-pin tests). Based on the previously conducted *P. aurea* results, the influence of the variation in specimen length was minimal, thus the edge-bearing specimens lengths were all taken as $L = 2R_o$ (Table 4.3). Four of

the specimens were instrumented with strain gages, placed on the W and E sides of the specimens, centered at mid-height of the specimen and oriented such that the gage was transverse to the fiber direction as shown in Figure 4.6c. An additional gage was placed on the interior surface opposite to the exterior gage on either the W or E side.

Thin pieces of neoprene (3 mm thick) with the dimensions L x 9.5 mm were used to distribute the load evenly across the specimen at both the N and S locations (Figure 4.6a and Figure 4.11b). The test was conducted using a universal test machine operated in displacement control at a displacement rate of 0.3 mm/min. The load-displacement curve was obtained from the test frame controller, thus frame compliance and deformation of supports are included in the displacement value. An additional test of a solid steel cylinder was conducted to determine the compliance of the frame and deformation of the neoprene supports. The test data was corrected by the calculated compliance in this case.

4.7 EDGE BEARING TEST RESULTS

4.7.1 *Phyllostachys aurea*

The load-displacement curves for the 16 specimens having no strain gages are presented in Figure 4.8. The traces, in general, show good repeatability within each of the groups and capacities that are proportional to specimen length. In Figure 4.8a, Specimen PA-2-3 had a pre-existing crack in the outer face of the specimen resulting in a reduced capacity and a softer load-displacement response.

All specimens were tested until failure. Failure was defined as the first local flexural failure of the culm wall at one of the four quadrants (N, S, E or W) of the culm. Table 4.4 lists

the location of the failure for each of the specimens. Figure 4.7a shows the failure of specimen PA-0.5-4. The photo was taken following failure but after the applied load had been reduced. The crack is visible at the top center (N) of the culm section.

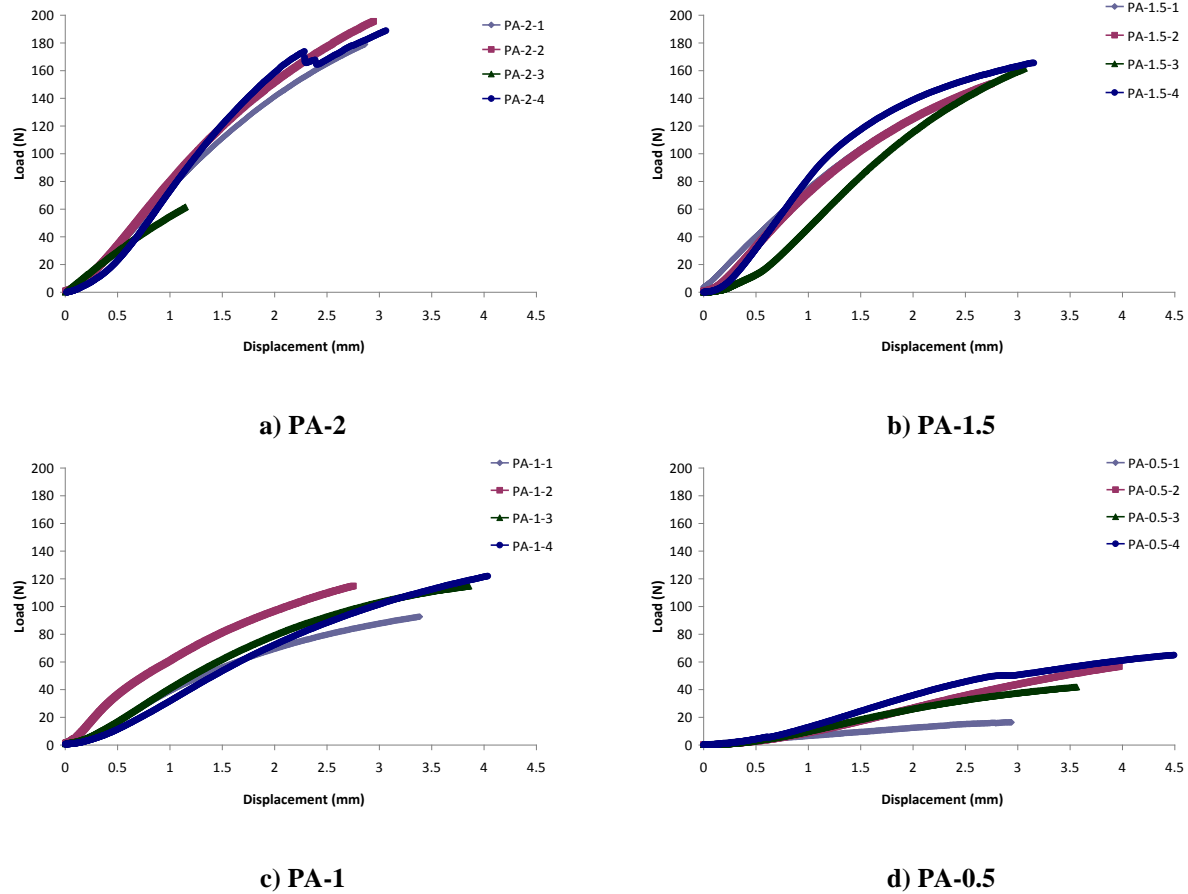


Figure 4.8 Load-displacement results from edge bearing tests of all *P. aurea* specimens.

The location of the rupture around the culm is informative. As shown in Figure 4.7b, the cracks around the culm circumference result from local flexure of the culm wall. Since the through-thickness properties of bamboo vary, one expects the flexural behavior to differ in the positive and negative directions. Additionally, one would expect this difference to be more pronounced with greater material property gradients through the wall thickness. Table 4.4 provides measured and calculated results from this test series. The value of the slope of the load-

deflection curve, $S = wL/D_V$, was determined from a best fit line between about 20% and 50% of the experimental data (Figure 4.8). While the modulus of rupture, f_r , may be calculated at the rupture location, corresponding lower bound values may be calculated at the other locations around the culm. These values are given in Table 4.4. Lower bound values are indicated using the ' $>$ ' inequality. The locations of the actual rupture failure (solid bars) and the lower bound values (open bars) are presented in Figure 4.9. Each graph represents the stress in each specimen at the designated location at the time of rupture. It is clearly seen that the NS moduli of rupture are greater than the EW. This indicates a 'tougher' tensile behavior of the inner surface of the culm which has a significantly lower fiber volume. It is hypothesized that the high fiber volume of the outer surface results in reduced matrix bridging and therefore failure at a lower stress. Such behavior is typical of other fiber reinforced materials (Agarwal and Broutman 1990).

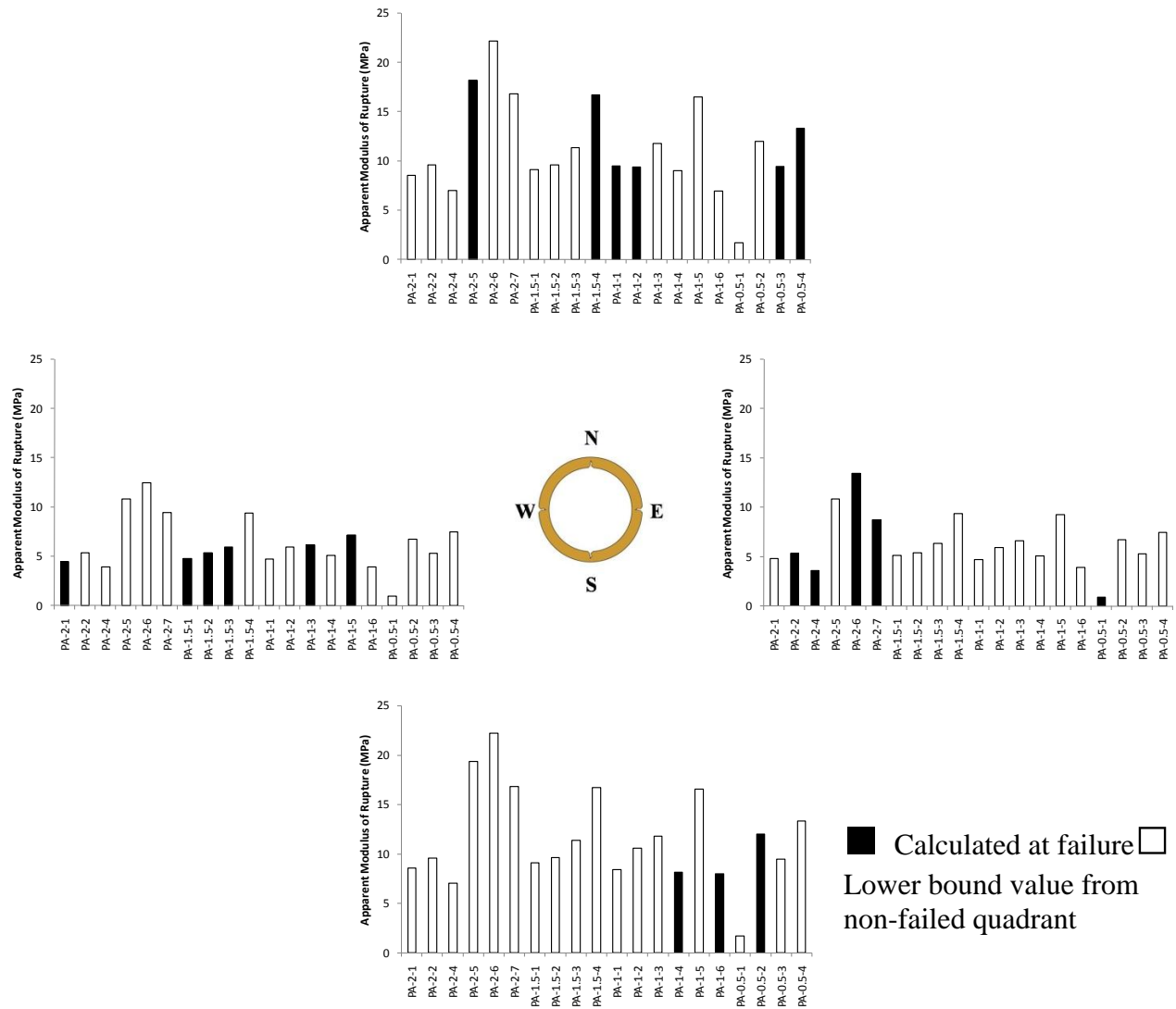


Figure 4.9 Location of failures and apparent modulus of rupture values for *P. aurea*.

Table 4.4 Measured and calculated results from edge bearing tests on *P. aurea*.

Specimen	L	R	t	wL	S	E _φ	Failure Location	t _r	M _{NS}	M _{EW}	f _{rNS}	f _{rEW}
	mm	mm	mm	N	N/mm	N/mm ²		mm	Nmm	Nmm	N/mm ²	N/mm ²
PA-2-1	42.0	17.7	4.3	179	83.6	371	W	4.3	1121	-647	>8.3	4.8
PA-2-2	44.0	17.9	4.1	196	90.7	490	E	4.0	1244	-716	>10.2	5.4
PA-2-4	45.0	18.3	4.8	189	104.7	358	E	4.8	1234	-713	>6.9	3.9
PA-2-5	44.0	17.1	4.1	410	125.0	485	N	4.3	2489	-1437	17.7	>10.8
PA-2-6	42.0	17.5	3.8	366	164.9	1286	E	3.5	2271	-1306	>25.7	12.5
PA-2-7	43.0	17.3	4.0	326	157.2	785	E	4.0	1996	-1150	>16.8	9.4
PA-1.5-1	33.5	18.4	4.0	130	72.1	542	W	4.0	841	-485	>9.1	5.1
PA-1.5-2	34.5	18.0	4.1	151	78.2	555	W	4.0	963	-555	>10.3	5.4
PA-1.5-3	34.0	18.1	4.0	162	75.6	553	W	4.0	1033	-595	>11.3	6.4
PA-1.5-4	33.0	17.7	4.0	166	102.6	1038	N	4.0	1037	-598	16.7	>9.4
PA-1-1	22.5	18.4	4.3	93	46.1	519	N	4.0	608	-350	9.6	>4.7
PA-1-2	23.0	18.6	4.3	115	44.3	358	N	4.5	753	-434	9.3	>5.9
PA-1-3	23.0	18.5	4.0	115	45.8	509	W	4.0	748	-431	>11.8	6.6
PA-1-4	23.0	18.6	4.8	122	43.1	267	S	5.0	808	-467	8.1	>5.1
PA-1-5	21.0	17.8	4.4	182	82.1	530	W	4.8	1136	-657	>13.5	9.3
PA-1-6	21.0	17.4	3.8	58	36.2	548	S	3.5	356	-205	8.1	>3.9
PA-0.5-1	11	17.8	4.0	23	7.6	80	E	4.0	144	-83	>2.4	1.3
PA-0.5-2	10.8	17.8	4.0	57	18.3	392	S	4.0	358	-206	12.0	>6.7
PA-0.5-3	10.0	17.6	4.0	42	17.1	384	N	4.0	261	-150	9.5	>5.3
PA-0.5-4	11.0	17.6	4.0	65	23.4	477	N	4.0	404	-233	13.3	>7.5
\bar{x}	28.5	17.9	4.1	157	70.9	526		4.1	991	-571	11.5	6.5
s	11.87	0.45	0.26	105	44.7	262		0.38	640	369	4.7	2.7
COV (%)	41.6	2.5	6.4	66.7	63.0	49.7		9.1	64.6	64.6	41.0	41.0

Results from the specimens having strain gages allowed for comparison of the strain longitudinal and transverse to the fibers. In Figure 4.10a and b, the calculated transverse stress versus the longitudinal (L) and transverse (T) strains for PA-2 and PA-1 gaged specimens are shown. This data was recorded at the W location, although with the exception of PA-1-5, rupture did not occur at this location (Table 4.4). As should be expected in such a test, strain longitudinal to the fiber is minimal in comparison to the transverse strain. To ensure behavior was symmetric, specimen PA-2-7 was instrumented with an additional strain rosette on the E side (Figure 4.10c). The E longitudinal strain gage failed during the test, however the transverse strains show excellent agreement with the W-side transverse gage indicating symmetric behavior. This specimen ruptured at the E location. The ratio between the longitudinal and transverse strains (L/T) for the PA-1 and PA-2 specimens was approximately 0.040 and 0.026, respectively,

indicating a very nominal Poisson effect associated with tensile behavior transverse to the longitudinal culm axis. This result is consistent with that found for most unidirectional fiber reinforced materials having a relatively weak matrix (Agarwal and Broutman 1990).

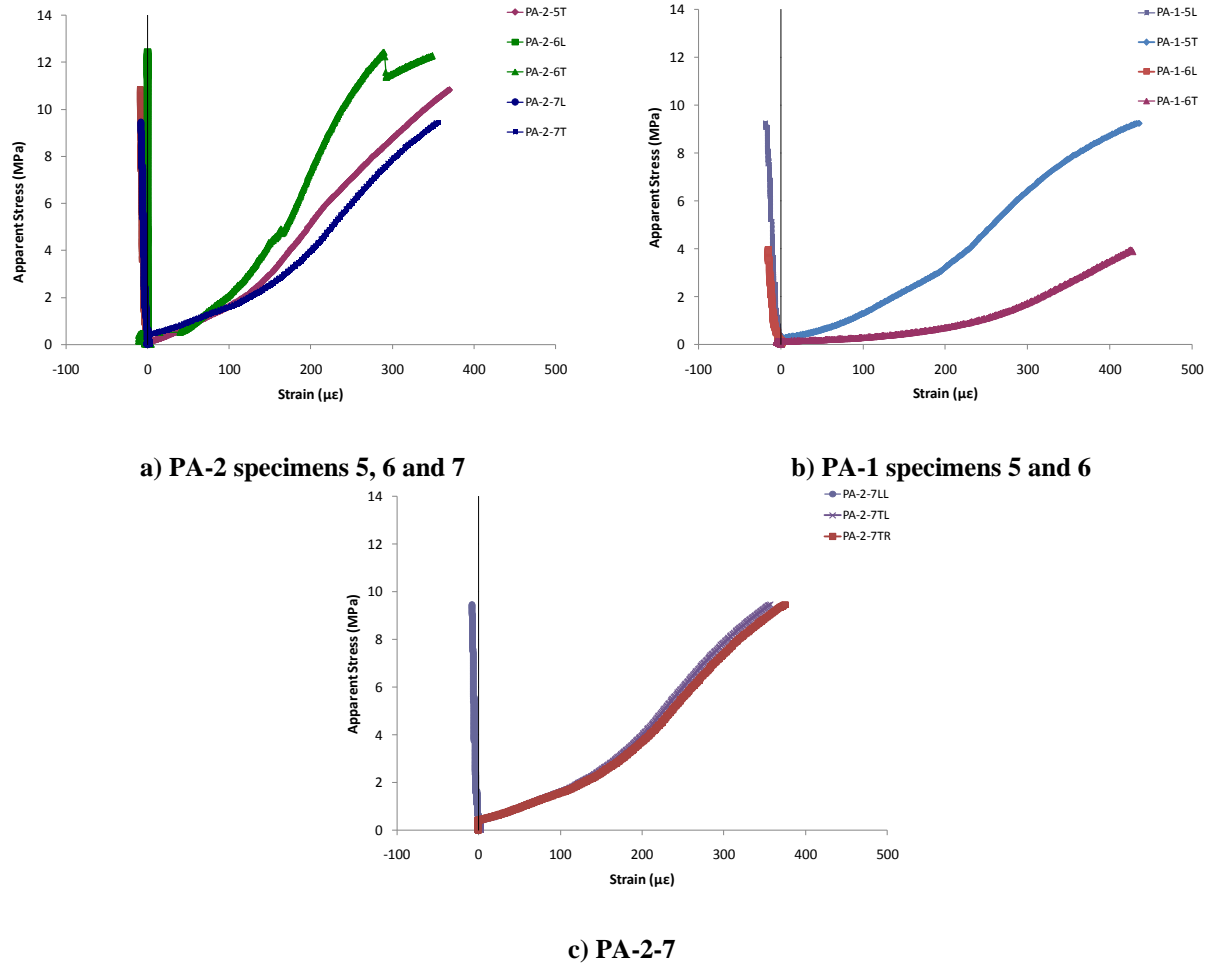


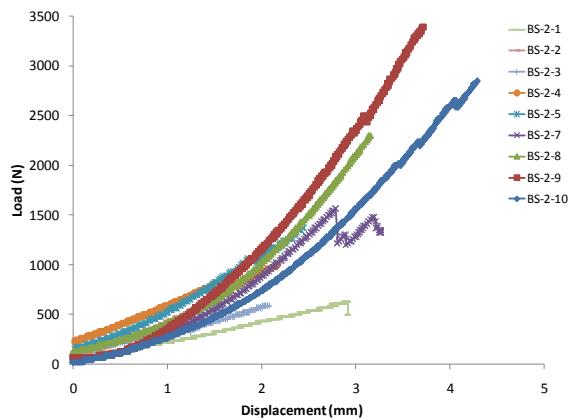
Figure 4.10 Apparent stress vs strain results for strain-gage instrumented edge bearing specimens for *Phyllostachys aurea*.

The strain gage readings and outer fiber tension stress (i.e. f_r) may also be used to estimate the tensile modulus of elasticity. For the five specimens having reliable strain data (Figure 4.10), the average tensile modulus of elasticity was calculated to be 3297 MPa. This result is six times greater than the calculated value of E_ϕ . The discrepancy is due to the fact that E_ϕ is effectively an average value accounting for the tension and compression behavior inherent

in the culm wall flexure. Additionally, E_{ϕ} is calculated based on the assumption of a linear isotropic material. The value determined from the strain gages represents the modulus only at the extreme tension fiber. This difference underlines the complex through-thickness behavior of the culm.

4.7.2 *Bambusa stenostachya*

The load-displacement curves for the 9 specimens tested are presented in Figure 4.11a. The data for specimen BS-2-6 only recorded the ultimate load. The traces, in general, show good repeatability. Specimen BS-2-3 had a pre-existing crack in the outer face of the specimen resulting in a reduced capacity and a softer load-displacement response, as shown in Figure 4.11a.



a) Load – displacement curves for all specimens.



b) Specimen BS-2-9 following failure showing rupture at all four quadrants, under applied load.

Figure 4.11 Edge bearing tests results for *B. stenostachya*.

All specimens were tested until failure. Figure 4.11b shows the multiple location failure of specimen BS-2-9. The photo was taken after the initial crack on the right (E) side developed and the applied load had been stopped. In this case, cracks are visible at all four quadrants of the

culm section. Table 4.5 provides measured and calculated results from this test series. The value of the slope of the load-deflection curve, $S = wL/D_v$, was determined from a best fit line between about 40% and 70% of experimental data (Figure 4.11a). While the modulus of rupture, f_r , may be calculated at the rupture location, corresponding lower bound values may be calculated at the other locations around the culm. These values are given in Table 4.5. Lower bound values are indicated using the ‘>’ inequality. The locations of the actual rupture failure (solid bars) and the lower bound values (open bars) are presented in Figure 4.12. Each graph represents the stress in each specimen at the designated location at the time of rupture.

Table 4.5 Measured and calculated results from edge bearing tests on *B. stenostachya*.

Specimen	L	R	t	wL	S	E_ϕ	Failure location	t_r	M_{NS}	M_{EW}	f_{rNS}	f_{rEW}
	mm	mm	mm	N	N/mm	N/mm ²		mm	Nmm	Nmm	N/mm ²	N/mm ²
BS-2-1	79.0	33.6	9.8	630	239	248	S	9.0	6690	-3894	5.1	>2.9
BS-2-2	76.5	33.3	10.5	738	558	481	W	11.0	7746	-4524	>5.2	2.9
BS-2-3	74.5	34.0	11.5	413	239	176	E	12.0	4427	-2594	>2.5	1.4
BS-2-4	76.5	33.9	12.3	999	517	306	E	11.5	10645	-6263	>5.2	2.9
BS-2-5	77.5	33.6	13.3	1455	1069	499	N	13.0	15358	-9086	6.3	>3.6
BS-2-6	77.5	32.9	14.3	1629	--	--	E	13.5	16764	-9992	>5.9	3.4
BS-2-7	77	33.0	13.5	1564	1609	695	S	12.5	16199	-9607	6.4	>3.6
BS-2-8	77	32.5	17.0	2302	2833	688	N	18.5	23271	-14137	5.7	>3.3
BS-2-9	76	31.6	17.3	3388	3496	746	E	16.5	33226	-20304	>8.0	4.6
BS-2-10	77	31.3	16.0	2845	2375	586	N	16.5	27681	-16772	7.7	>4.4
\bar{x}	77	33.0	13.5	1596	1448	492		13.6	16201	-9717	5.8	3.3
s	1.16	0.93	2.62	984	1225	208		2.62	9452	5826	1.53	0.88
COV (%)	1.5	2.8	19.4	61.7	84.6	42.4		19.3	58.3	60.0	26.2	26.8

The wall thickness of the *B. stenostachya* specimens increases from specimen BS-2-1 to BS-2-10 since the specimens are taken in order from the top to the bottom of the culm (see inset in Figure 4.12e). The results shown in Figure 4.12 and Table 4.5 suggests an increasing modulus of rupture with increasing wall thickness. Although effects associated with ‘height along the culm’ cannot be ruled out, it is noted that all *B. stenostachya* used was cut at least 1 year prior to testing and has been stored in a dry laboratory environment for at least 8 months prior to testing.

Unfortunately specimen history beyond this is not available. Once again, the NS modulus of rupture was greater than the EW.

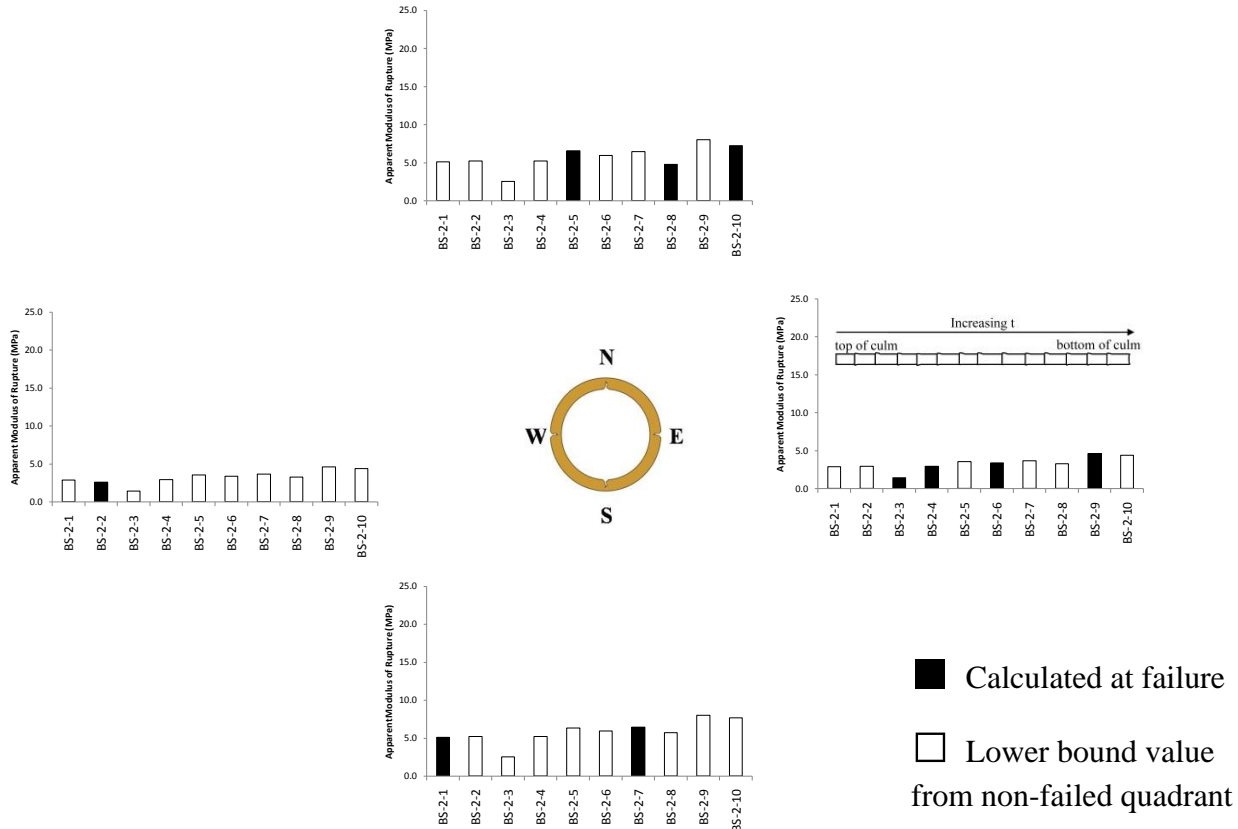


Figure 4.12 Location of failures and apparent modulus of rupture values for *B. stenostachya*.

Three *B. stenostachya* specimens were instrumented with strain gages and the results are presented in Figure 4.13. The gage on specimen BS-2-1 failed during the test. Figure 4.14 illustrates the strain gradient through the thickness of the wall based on interior and exterior strain gage readings. The diagrams clearly indicate that the neutral axis is located between approximately $0.65t$ and $0.80t$ and is shifted to the outside of the culm wall section. This observation reflects the combined moment and axial force applied at this section as described by Equation 4.9. Additionally, the high compressive strain in the inner wall indicates the significant

compressibility of the interior surface, which is attributed to the compressibility of the interior wall parenchyma cells (Obataya et al. 2007).

The strain gage readings and outer fiber tension stress (i.e. f_r) may also be used to estimate the tensile modulus of elasticity. For the two specimens having reliable strain data (BS-2-7 and -8), the average tensile modulus of elasticity was calculated to be 2113 MPa. These results are four times larger than the calculated value of E_ϕ . Again, the results demonstrate that the E_ϕ equation does not fully capture the bending capacity of the bamboo culm.

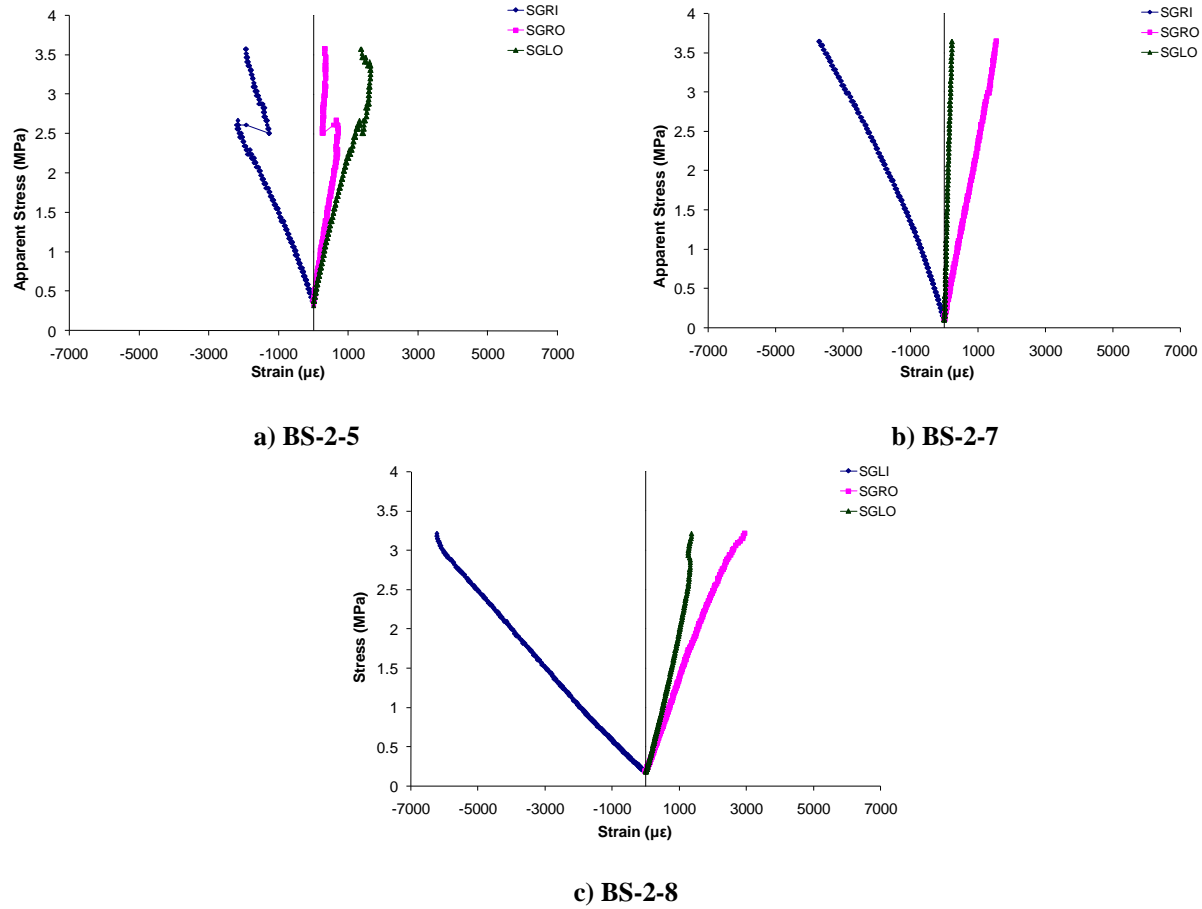


Figure 4.13 Apparent stress vs strain results for strain-gage instrumented edge bearing specimens for *B. stenostachya*.

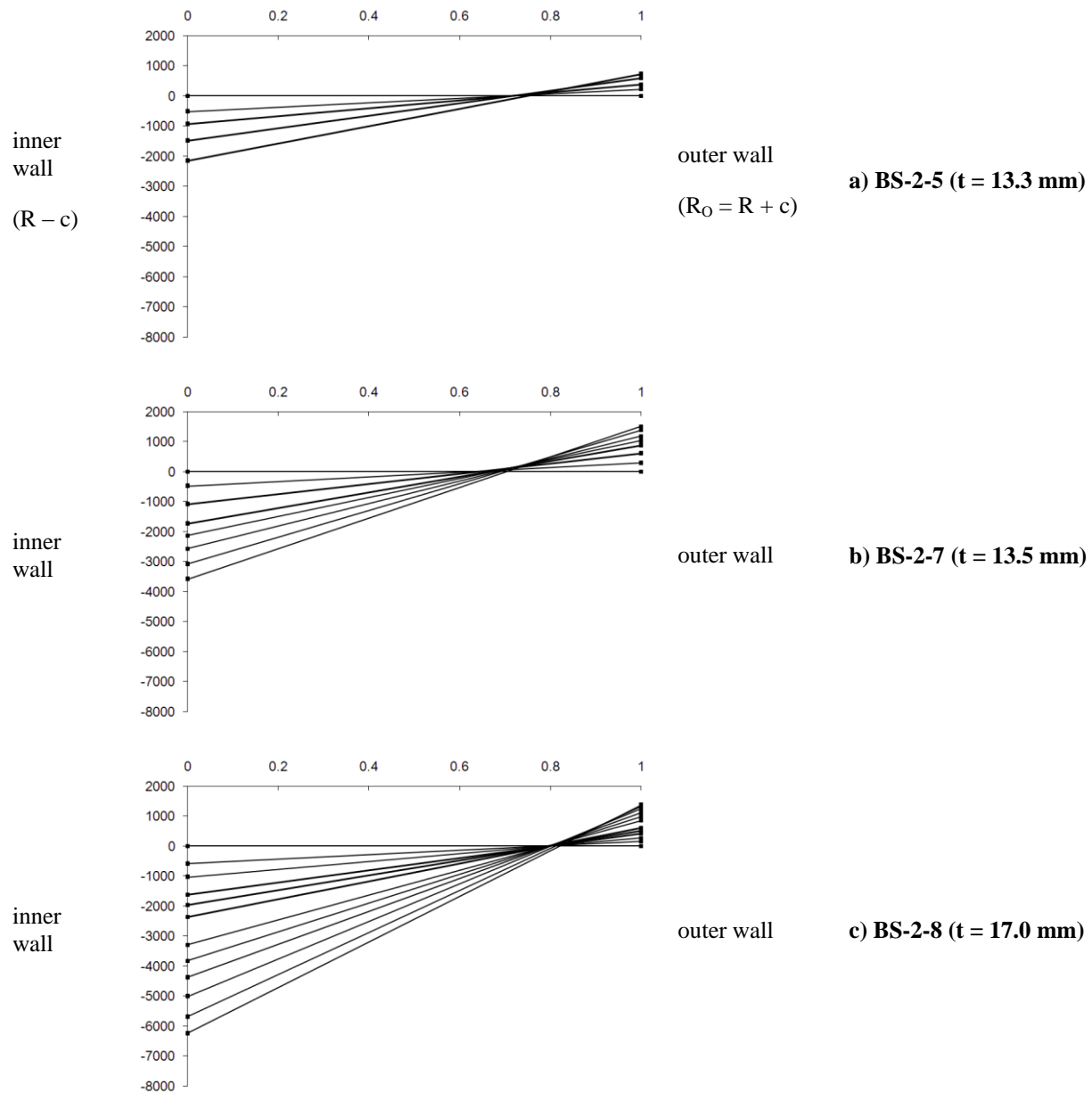


Figure 4.14 Strain distribution through wall thickness in edge bearing specimens *B. stenostachya*. Gradient lines are shown at various load levels through test; the outermost line is the gradient corresponding to the last load at which both required gages worked (failure passes through the gages).

4.7.3 Comparison of Edge Bearing Results for *P. aurea* and *B. stenostachya*.

The load-displacement curve differs for the two species of bamboo, as illustrated in Figure 4.8 and Figure 4.11a. The *P. aurea* specimens exhibit a softer response (Fig. 4.8a) in comparison to the *B. stenostachya* specimens, which increase in stiffness with increased applied load (Figure 4.11a); possible due to the development of ‘arching’ action in the thick-walled culm. The softer response of the *P. aurea* is attributed to the thinner wall section and therefore greater flexibility of the culm section.

4.8 SPLIT PIN TEST

Split pin testing was conducted on *Bambusa stenostachya* specimens cut from the same culm as the previously described edge bearing specimens. Ten specimens were tested for each test method and the specimens were taken from alternate adjacent locations along the culm (i.e: A-B-A-B-etc. where A specimens were edge bearing and B specimens were split-pin tests). Five split-pin specimens were tested with a strain gage positioned at the edge of the notch oriented to capture strain transverse to the longitudinal culm axis. The overall length of the split pin specimens was $2w = 3R_o$. As shown in Figure 4.1, a hole, with a diameter of 38.1 mm, is drilled through the specimen and a 3 mm crack initiator is cut on either side of this. The 2a dimension (Figure 4.1b) is therefore 44 mm. A split-pin is inserted and a tensile load is applied using a universal test machine in displacement control at a rate of 0.3 mm/min.

The resulting load-displacement plots (Figure 4.15a) recorded by the test frame controller indicate good agreement between the specimens. The failure of the specimens occurred along the notched edge of the specimens. The direct tension rupture stress of the culm is:

$$\sigma_{failure} = \frac{P}{2((2w-2a)t)} \quad (\text{Eq. 4.10})$$

where P is the maximum applied load, 2w is the specimen length, 2a is the initial length of the crack, t is the thickness of the wall and the leading coefficient ‘2’ accounts for the two culm walls engaged in tension. The Mode I stress intensity factor, K_I , is calculated as (Mitch et al. 2010):

$$K_I = \sigma_{gross} \sqrt{\pi a} \left[\frac{2w}{\pi a} \tan \left(\frac{\pi a}{2w} \right) \right]^{1/2} \quad (\text{Eq. 4.11})$$

where σ_{gross} is the tensile stress measured over the gross culm wall area: $\sigma_{gross} = \frac{P}{2(2w \cdot t)}$

4.8.1 Split Pin Test Results

The results from the split pin tests are presented in Table 4.6. Both the K_I and $\sigma_{failure}$ values are about 75% of those reported by Mitch (2009) for the same material coming from a different batch of culms. Additionally the variation in this test series was greater (COV = 0.28 as compared to 0.22 in Mitch). The present batch of culms was qualitatively drier and had more splitting evident than that tested by Mitch. Because the bamboo is commercially supplied, no history for the material can be established. Five of the specimens were instrumented with strain gages and the results are presented in Figure 4.15b. The gage on Specimen BS-3-9 failed during the test. The maximum strains reported ranged from 178 to 1021 microstrain ($\mu\epsilon$) indicating a very brittle failure mode. The modulus of elasticity values determined from these strain gage readings are reported in Table 4.6.

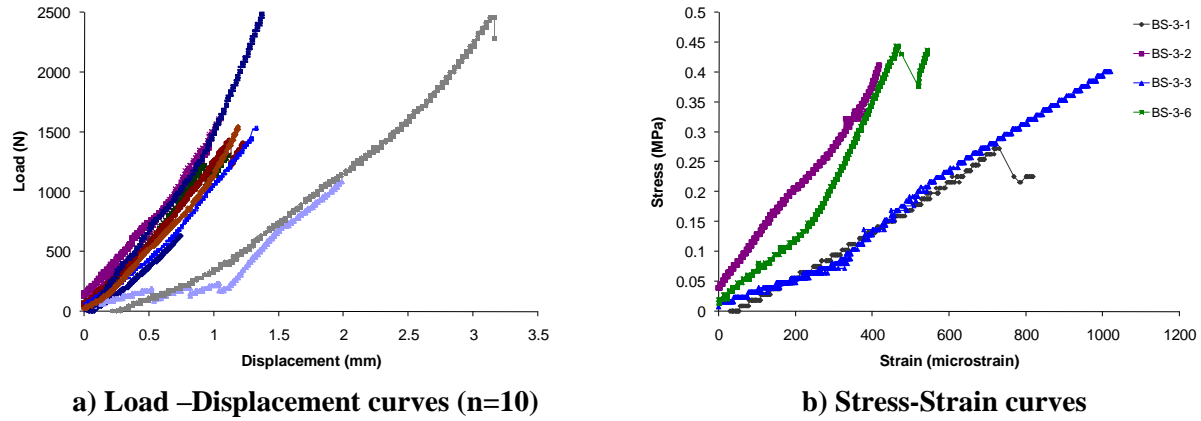


Figure 4.15 Test results for *B. stenostachya* split pin specimens.

Table 4.6 Split pin specimen results for *B. stenostachya*.

Specimen	Length	Wall Thickness	Crack Length	Ultimate Load	Failure Stress	Stress Intensity Factor	Tensile Modulus
	2w	t	2a	P	σ_{failure}	K_I	E
	mm	mm	mm	N	MPa	$\text{MPa}\cdot\text{m}^{1/2}$	MPa
BS-3-1	117	9.9	44.8	630	0.44	0.08	349
BS-3-2	122	13.9	45.0	1390	0.65	0.12	853
BS-3-3	112	12.1	45.5	1085	0.68	0.12	528
BS-3-4	115	12.3	44.8	1303	0.76	0.13	n.r.
BS-3-5	115	13.2	44.8	1629	0.88	0.15	n.r.
BS-3-6	116	14.0	44.0	1432	0.71	0.12	760
BS-3-7	115	14.5	44.5	2454	1.20	0.21	n.r.
BS-3-8	115	15.2	44.5	1455	0.68	0.12	n.r.
BS-3-9	115	18.0	44.8	2476	0.99	0.17	n.r.
BS-3-10	114	17.8	45.0	1542	0.63	0.11	n.r.
\bar{x}	116	14.1	44.8	1540	0.76	0.13	623
s	2.49	2.50	0.39	563	0.21	0.04	228
COV (%)	2.2	17.8	0.9	36.6	27.9	27.7	36.6

4.9 CORRELATION BETWEEN EDGE BEARING AND SPLIT PIN TEST RESULTS

A primary objective of this test program is to develop a test that not only quantifies bamboo splitting behavior but is also practical for field use. Both the split pin and edge bearing tests yield the transverse tensile capacity. Additionally, modulus of elasticity may be calculated if strain gages are employed although this would be unlikely in a simple field test. While, the modulus of

elasticity calculated from Equation 4.2 yields lower values compared to those calculated from strain readings, the modulus calculated from strain readings is representative of the flexural stiffness of the bamboo culm.

To assess the overall transverse tensile capacity of a full bamboo culm, the edge bearing test demonstrates the ultimate behavior. By comparison, the split pin test provides specific values for the transverse tensile strength of a notched, thus crack-initiated, failure. The edge bearing test provides information on the bamboo splitting behavior and the test setup is also practical for field use. Additional testing is needed to fully investigate the relationship between the split pin tensile stress and the edge bearing modulus of rupture. This then needs to be correlated with observations of bolted connection behavior and other splitting modes (Figure 4.2).

4.10 TRANSVERSE TENSION STRAIN

The fact that this study recorded some transverse rupture strain data permits a brief comment on a hypothesis promulgated by Arce-Villalobos (1993). Arce-Villalobos proposed, based on an experimental investigation that included two bamboo species (however not either *P. aurea* or *B. stenostachya*) that the transverse tension *strain* capacity of bamboo is 1200 $\mu\epsilon$ regardless of species and other material properties. Such a generalization, if true, would prove useful in interpreting material test results and mitigating the need for employing strain gages on standard tests. Table 4.7 summarizes the tensile rupture strains recorded in this test program. The recorded data shows a significant difference between the tensile strains recorded in the *B. stenostachya* edge bearing and split pin tests. The difference is attributed to the test method used. It should also be noted that the tests from which Arce-Villalobos arrived at his conclusions result in

transverse stress distribution through the culm wall that likely falls between the uniform tension condition of the split-pin test and the moment-induced gradient of the edge bearing test.

In the edge bearing test, the tensile rupture strain reflects the strain capacity of the outer layer of bamboo and is affected by the beneficial effects of the through-thickness strain gradient (Figure 4.14). Additionally, the organization of the fibers on the outer layer provides stiffness, while allowing the culm to demonstrate ductile bending behavior (Obataya et al. 2007). This relatively ductile behavior was visually demonstrated in the *P. aurea* edge bearing specimens. By comparison, in the split pin test, the through-thickness strain gradient should be relatively uniform in which case the measured strain may be viewed as the average strain capacity through the culm wall. Based on this interpretation, one would anticipate the direct tension capacity of *P. aurea* to be lower than the reported edge bearing strains.

Table 4.7 Observed tension rupture strain values.

	<i>P. aurea</i>	<i>B. stenostachya</i>	
	edge bearing test	edge bearing test	split pin test
recorded tension rupture strain values ($\mu\epsilon$)	349-436	1362-3011	178-1021
\bar{x} ($\mu\epsilon$)	388	1972	592
s ($\mu\epsilon$)	41	904	311
COV(%)	10.6	45.9	52.5

Based on the limited experimental results it may be concluded that the transverse rupture strain of bamboo is affected by the through-thickness strain gradient induced by the test method. Additionally, the degree of this gradient (curvature), as affected by the culm wall thickness also appears to affect the results. More study, both experimental and analytical is required on this issue.

4.11 SUMMARY

The presented study investigated the splitting failure of bamboo of *Bambusa stenostachya* through three test methods: the bolt hole, edge bearing and split pin tests. The bolt hole test results were comparable to the split pin test results from Mitch et al. (2010) and indicated a decrease in ultimate bearing stress with decreasing angle, i.e. loading oriented more transversely to the fibers. The edge bearing test was also compared to the split pin test and suggested that the edge bearing can be used as a surrogate for field tests to approximate the ultimate transverse tensile capacity of the culm, however additional work is required to fully investigate the correlation between the two test values.

5.0 STATISTICAL ANALYSIS OF MATERIAL PROPERTIES OF BAMBOO

5.1 INTRODUCTION

The mechanical and geometrical properties of bamboo vary within and between species. Available literature on mechanical properties of bamboo sporadically present the statistical variation for the species being researched (e.g.: Talla et al. 2004 and Shao et al. 2009), but few publications compare variation between species. Similarly, empirical relationships between mechanical and geometrical properties have been proposed, such as defining longitudinal tensile modulus of elasticity based on fiber content (Silva et al. 2006), but their basis for application beyond the species considered is generally not established. Indeed the earlier work of Janssen (1981) and Arce-Villalobos (1993) often points out a distinct lack of relationship between mechanical properties that are often related in other materials such as timber (see Section 2.2). A major barrier to the statistical comparison of bamboo mechanical properties is the lack of available data from a variety of species, as well as the variability of testing parameters, such as specimen size and loading rate. In some cases, the test methods used to determine a particular property are different from study to study.

The work presented in this chapter considers data collected by the Group for Non-Conventional Materials (GNOCMAT) at PUC-Rio and the author's group at the University of Pittsburgh. In total, the data collected represents nine bamboo species, and a variety of geometric and mechanical properties. The sources present tests on a variety of bamboo species, however

the available data sets are limited for most of the species. Only two species, *Phyllostachys aurea* and *Dendrocalamus giganteus*, which represent the two data sets with the largest number of samples, will be examined in detailed. Through this comparison, the significance of the statistical variability between these species will be assessed. This will provide at least one benchmark for interspecies variation.

The objective of this exercise is to reduce the epistemic uncertainty, due to variations in geometry and material properties, for a finite element model of a bamboo frame structure. The epistemic uncertainty in the material and geometric properties will be addressed using a sampling technique and assigning properties that result in ‘nominally identical but statistically different’ bamboo culm properties for the model (Shinozuka et al. 2000b). The distribution of the material properties, such as tensile and compressive stress, and the modulus of elasticity, will be determined. The properties can then be sampled to compare the effect of the variability in material properties.

The statistics from each data set are represented in Table 5.1 through Table 5.5. The tables are organized by mechanical or geometric property, with the mean and standard deviation listed for each sample set, as well as for the entire population. Although, some publications reported a mechanical or geometric property, the result was not always presented in a manner from which the statistical variation may be derived. Thus, the statistical analysis presented here focuses on the tensile and compressive stress and modulus of elasticity. The following sections briefly describe the test methods used to obtain the various mechanical properties reported.

Table 5.1 Longitudinal tensile properties of bamboo coupon specimens.

Source	Species	Treatment	Coupon Dimensions	Load Rate	Tensile Stress				Modulus of Elasticity				Poisson Ratio			
					n	\bar{x}	s	COV	n	\bar{x}	s	COV	n	\bar{x}	s	COV
			mm	mm/sec		MPa	MPa	%		GPa	GPa	%		MPa	MPa	%
Culzoni 1985 ^a	<i>B. multiplex</i> var. <i>disticha</i>	Air	20 x 1	0.1	4	88.8	17.8	20	4	13.0	1.8	14				
Culzoni 1985 ^a	<i>B. multiplex</i> var. <i>raeusch</i>	Air	20 x 1	0.1	2	110.0	20.8	19	2	11.1	1.5	13				
Culzoni 1985 ^a	<i>B. tuldooidos</i>	Air	20 x 1	0.1	4	111.6	20.6	18	4	10.6	1.8	17				
Culzoni 1985 ^a	<i>B. vulgaris</i> var. <i>Imperial</i>	Air	20 x 1	0.1	4	91.2	56.8	62	4	6.9	1.1	16				
Culzoni 1985 ^a	<i>B. vulgaris</i> var. <i>Schard</i>	Air	20 x 1	0.1	6	149.2	28.3	19	6	9.9	1.6	16				
Guatibonza 2009 ^b	<i>D. giganteus</i>	Air	22 x 1.2		4	100.6	22.7	23	4	11.3	0.3	3				
Ghavami and Marinho 2001 ^b	<i>D. giganteus</i>	Borax	20 x 1	0.01	9	149.4	49.4	33	5	17.5	4.8	27				
Culzoni 1985 ^a	<i>D. giganteus</i>	Air	20 x 1	0.1	10	129.4	22.9	18	10	13.1	2.3	18				
Krause 2009 ^a	<i>D. giganteus</i>	Air	20 x 1	0.02	3	205.2	14.6	7	3	18.7	1.31	7				
Ghavami and Marinho 2002 ^b	<i>G. angustifolia</i>	Borax	20 x 1	0.01	6	102.7	21.9	21	6	15.1	3.3	21	3	0.26	0.07	27
Culzoni 1985 ^a	<i>G. superba</i>	Air	20 x 1	0.1	4	94.6	64.0	68	4	10.0	1.5	15				
Cruz 2002 ^{b,c}	<i>P. aurea</i>	Air	20 x 1	0.01	6	210.4	38.9	19	6	18.9	3.1	16	6	0.29	0.04	15
Cruz 2002 ^{b,c}	<i>P. aurea</i>	Heat	20 x 1	0.01	6	175.4	56.1	32	6	21.9	2.4	11	6	0.33	0.04	13
Cruz 2002 ^{b,c}	<i>P. aurea</i>	Water	20 x 1	0.01	6	238.9	63.4	27	6	21.4	3.6	17	6	0.30	0.09	29
Sharma 2010	<i>P. aurea</i>	Water	20 x 1	0.02	13	251.1	36.7	15								
Krause 2009	<i>P. aurea</i>	Water	20 x 1	0.02	3	260.9	3.4	0.01								

^a Modulus of elasticity determined from clip gage mounted on specimens;

^b Modulus of elasticity determined from electrical resistance strain gages mounted on specimens;

^c Poisson ratio determined from electrical resistance strain gages mounted on specimens.

Table 5.2 Longitudinal compressive properties of full culm bamboo.

Source	Species	Treatment	Height	Load Rate	Compressive Stress				Modulus of Elasticity				Poisson Ratio			
					n	\bar{x}	s	COV	n	\bar{x}	s	COV	n	\bar{x}	s	COV
			mm	mm/sec		MPa	MPa	%		GPa	GPa	%		MPa	MPa	%
Culzoni 1985 ^a	<i>B. multiplex</i> var. <i>disticha</i>	Air	2Dia	0.03	4	24.3	4.8	20	4	3.8	0.57	15				
Culzoni 1985 ^a	<i>B. multiplex</i> var. <i>raeusch</i>	Air	2Dia	0.03	2	3.1	0.4	12	2	3.1	0.36	12				
Mitch 2009	<i>B. stenostachya</i>	Borax	Dia	0.01	12	56.7	7.0	12								
Culzoni 1985 ^a	<i>B. tuldoidos</i>	Air	2Dia	0.03	4	34.1	4.6	13	4	3.0	0.20	7				
Moreira 1991	<i>B. vulgaris</i>	Air	2Dia	0.001	5	33.6	3.8	11								
Culzoni 1985 ^a	<i>B. vulgaris</i> var. <i>Imperial</i>	Air	2Dia	0.03	4	26.7	18.2	68	4	2.3	0.23	10				
Culzoni 1985 ^a	<i>B. vulgaris</i> var. <i>Schard</i>	Air	2Dia	0.03	6	46.2	8.4	18	6	2.9	0.46	16				
Ghavami and Marinho 2001 ^{b,c}	<i>D. giganteus</i>	Borax	Dia	Manual	6	78.0	9.6	12	6	21.0	4.3	21	5	0.31	0.10	33
Culzoni 1985 ^a	<i>D. giganteus</i>	Air	2Dia	0.03	10	42.3	8.8	21	10	3.8	0.69	18				
Moreira 1991	<i>D. giganteus</i>	Air	2Dia	0.001	6	34.0	3.1	9								
Krause 2009	<i>D. giganteus</i>	Air	Dia	Manual	5	55.1	11.4	2								
Ghavami and Marinho 2002 ^{b,c}	<i>G. angustifolia</i>	Borax	Dia	Manual	6	32.9	5.3	16	6	12.6	2.39	19	5	0.42	0.13	31
Culzoni 1985 ^a	<i>G. superba</i>	Air	2Dia	0.03	4	41.8	7.4	18	4	3.0	0.46	16				
Cruz 2002 ^{b,c}	<i>P. aurea</i>	Air	Dia	Manual	6	69.3	9.9	14	6	24.8	4.3	17	6	0.23	0.03	12
Cruz 2002 ^{b,c}	<i>P. aurea</i>	Heat	Dia	Manual	6	69.1	9.7	14	6	26.8	4.1	15	6	0.30	0.07	22
Cruz 2002 ^{b,c}	<i>P. aurea</i>	Water	Dia	Manual	6	68.1	13.5	20	6	21.5	7.1	33	6	0.27	0.07	27
Krause 2009	<i>P. aurea</i>	Water	Dia	Manual	3	55.1	3.0	5								

^a Modulus of elasticity determined from clip gage mounted on specimens;

^b Modulus of elasticity determined from electrical resistance strain gages mounted on specimens;

^c Poisson ratio determined from electrical resistance strain gages mounted on specimens.

Table 5.3 Transverse shear properties determined from bamboo coupon specimens.

Source	Species	Treatment	Dimensions	Load Rate	Transverse Shear Stress			
					n	\bar{x}	s	COV
			mm	mm/sec		MPa	MPa	%
Culzoni 1985	<i>B. multiplex</i> var. <i>disticha</i>	Air	12 x 1	Manual	2	53.0	5.66	11
Culzoni 1985	<i>B. multiplex</i> var. <i>raeusch</i>	Air	12 x 1	Manual	1	62.0		
Culzoni 1985	<i>B. tuldooidos</i>	Air	12 x 1	Manual	2	59.0	0.00	0
Culzoni 1985	<i>B. vulgaris</i> var. Imperial	Air	12 x 1	Manual	2	40.8	2.55	6
Culzoni 1985	<i>B. vulgaris</i> var. Schard	Air	12 x 1	Manual	3	41.2	1.89	5
Culzoni 1985	<i>D. giganteus</i>	Air	12 x 1	Manual	5	46.2	1.87	4
Culzoni 1985	<i>G. superba</i>	Air	12 x 1	Manual	2	48.0	2.83	6
Cruz 2002	<i>P. aurea</i>	Air	20 x 1	Manual	6	45.4	4.37	10
Cruz 2002	<i>P. aurea</i>	Heat	20 x 1	Manual	6	46.2	4.34	9
Cruz 2002	<i>P. aurea</i>	Water	20 x 1	Manual	6	46.9	6.38	14

Table 5.4 Interlaminar shear properties determined from bamboo tensile-type notched coupons.

Source	Species	Treatment	Dimensions	Number of Cuts	Load Rate	Interlaminar Shear Stress			
						n	\bar{x}	s	COV
			mm		mm/sec		MPa	MPa	%
Moreira 1991	<i>B. vulgaris</i>	Air	20 x 8	2		6	6.55	0.75	11
Guatibonza 2009	<i>D. giganteus</i>	Air	15 x 1.5	2		11	3.7	0.81	22
Ghavami and Marinho 2001	<i>D. giganteus</i>	Borax	20 x 1	2	Manual	6	3.5	0.70	20
Ghavami and Marinho 2001	<i>D. giganteus</i>	Borax	20 x 1	3	Manual	5	4.1	0.63	15
Moreira 1991	<i>D. giganteus</i>	Air	20 x 8	2		6	6.85	0.71	10
Ghavami and Marinho 2002	<i>G. angustifolia</i>	Borax	20 x 1	2	Manual	6	2.0	0.38	19
Cruz 2002	<i>P. aurea</i>	Air	20 x 1	2	0.02	18	4.0	0.68	17
Cruz 2002	<i>P. aurea</i>	Heat	20 x 1	2	0.02	18	4.4	0.52	12
Cruz 2002	<i>P. aurea</i>	Water	20 x 1	2	0.02	18	3.6	0.50	14

Table 5.5 Full culm geometrical properties.

Source	Species	Treatment	External Diameter				Wall Thickness				Internodal Length			
			n	\bar{x}	s	COV	n	\bar{x}	s	COV	n	\bar{x}	s	COV
				mm	mm	%		mm	mm	%		mm	mm	%
Culzoni 1985	<i>B. multiplex</i> var. <i>disticha</i>	Air	2	31.25	5.30	17	2	3.75	0.82	22	2	475	106.07	22
Culzoni 1985	<i>B. multiplex</i> var. <i>raeusch</i>	Air	1	20.00			1	3.67			1	450		
Culzoni 1985	<i>B. tuldoidos</i>	Air	2	32.50	5.89	18	2	5.67	1.89	33	2	400		0
Moreira 1991	<i>B. vulgaris</i>	Air	6	91.97	0.97	1	6	6.62	0.11	2				
Culzoni 1985	<i>B. vulgaris</i> var. <i>Imperial</i>	Air	2	67.50	10.14	15	2	7.67	3.30	43	2	335	35.36	11
Culzoni 1985	<i>B. vulgaris</i> var. <i>Schard</i>	Air	3	71.11	19.88	28	3	8.94	1.42	16	3	343.3	50.33	15
Ghavami and Marinho 2001	<i>D. giganteus</i>	Borax	3	103.22	26.16	25	3	9.00	7.57	84				
Culzoni 1985	<i>D. giganteus</i>	Air	5	109.67	28.66	26	5	9.20	1.91	1	5	486	60.66	12
Moreira 1991	<i>D. giganteus</i>	Air	6	99.85	1.60	2	6	6.64	0.08	7				
Guatibonza 2009	<i>D. giganteus</i>	Air	8	98.67	1.28	1	8	14.17	0.93	21	8	362.50	53.25	15
Ghavami and Marinho 2002	<i>G. angustifolia</i>	Borax	6	76.68	43.29	56	6	13.19	7.51	57	6	271.65	103.39	38
Culzoni 1985	<i>G. superba</i>	Air	2	90.50	27.58	30	2	7.83	2.12	27	2	330	98.99	30
Ghavami and Marinho 2001	<i>G. tagoara</i>		3	79.11	30.08	38	3	16.32	9.20	56	3	331.70	123.88	37
Ghavami and Marinho 2001	<i>Matake</i>		3	66.32	53.98	81	3	12.36	11.48	93	3	303.27	223.48	74
Ghavami and Marinho 2001	<i>Moso</i>		3	78.59	53.21	68	3	11.12	8.77	79	3	241.98	182.64	75
Mitch 2009	<i>B. stenostachya</i>	Boric Acid	6	90.54	4.52	5	6	16.95	3.24	19				

5.2 EXPERIMENTAL DESIGN AND STUDY PROCEDURES

5.2.1 Tensile Properties

The data sources all used the same test methodology, however some of the test parameters varied between sources as shown in Table 5.1. In general, specimen dimensions and test protocol were based on guidelines from INBAR (1999) and ISO (2004b). Modulus of elasticity and Poisson ratio were determined using electrical resistance strain gages. The exception are the results reported by Culzoni (1985), which referenced no standard, were tested at a significantly faster load rate than ISO (2004b) specifies (0.01 mm/s), and utilized a clip gage to determine the modulus of elasticity. A schematic of the tension test method is shown in the second entry of Table 4.1.

5.2.2 Compressive Properties

All data sources used the same test methodology to determine full culm compressive strength, modulus of elasticity and Poisson ratio data, however test parameters varied between sources as shown in Table 5.2. INBAR (1999) and ISO (2004b) recommend specimens have a height of one culm diameter and that modulus and Poisson ratio be determined using electric resistance strain gages. The results reported by Culzoni (1985) and Moreira (1991) referenced no standard for the test. These tests utilized a specimen dimension having a height of two culm diameters and were tested at a load rate greater than specified (0.01 mm/s). Culzoni utilized a clip gage to determine the modulus of elasticity. A schematic of this test method is shown in the first entry of Table 4.1.

5.2.3 Transverse Shear Properties

The transverse shear properties (Table 5.3) were obtained by Culzoni (1985) and Cruz (2002) using the INBAR (1999) standard. The test method is a simple two-plane shear arrangement which restricts the flexure of the specimen (fifth entry in Table 4.1). The load was applied manually until the specimen failed resulting in a specimen broken into three pieces.

5.2.4 Interlaminar Shear Properties

The interlaminar shear tests conducted by Moreira (1991) were based on the ASTM D2733 (1976) *Method of Test for Interlaminar Shear Strength of Structural Reinforced Plastics at Elevated Temperatures*. The tests conducted by Ghavami and Marinho (2001, 2002) and Cruz (2002) used the INBAR (1999) standard. The specimens were rectangular coupons that had two symmetrical cuts that did not penetrate beyond the axis of symmetry (sixth entry in Table 4.1).

5.2.5 Geometric Properties

A sample of measured geometric properties, from the previous presented data sources (Table 5.1-Table 5.4) is summarized in Table 5.5. Conventionally, diameter is measured at two orthogonal locations across a section. Wall thickness and intermodal length is typically measured at four locations around a section (at 90° increments).

5.3 STATISTICAL METHODOLOGY

The data presented in the previous tables represents a small population of data from multiple laboratory sources. The variability between results is attributed to the differences in testing parameters, as summarized previously, and the multiple operators used to obtain the data. ASTM E177 (2008) indicates the use of accepted reference values, however these values do not exist for bamboo material properties. The generally accepted method of assessing bamboo data is to compare obtained data with published data to see if the results are in the same range. Considering the variation shown in Table 5.1 to Table 5.4, one must conclude that this is a flawed approach for bamboo. For most construction materials, the acceptable variability within single or multiple data sets is often determined by the two standard deviations limit ($2s$), which relates to 95% repeatability (r – within a laboratory and R – between laboratories) or confidence (ASTM E177 2008). The standard also indicates that comparison of test results follow the difference two-sigma limit ($d2s$) or a precision within twice the standard deviation (s_r – within a laboratory and s_R – between laboratories). These limits assume normal distribution of the data and are independent of the number of tests included. For design values, the AC 162 *Acceptance Criteria for Structural Bamboo* (ICBO 2000) notes that the experimental values are reduced in proportion to their standard deviation in the same manner as timber: defined by ASTM D2915 (2003). To apply the ASTM limits, the distribution of the data must be assessed.

5.3.1 Preliminary Analysis

The data shown in Table 5.1 to Table 5.4 represents a small population of material test data from various species. The data represents information mostly from secondary sources, which indicates that there is increased uncertainty in the data. Issues of varying definitions, measurement error,

source bias and reliability all affect the uncertainty of the data. The data was filtered based on the following criteria: 1) at least two data sources for a species; 2) the results were in an acceptable range in comparison to other data; and, 3) the testing parameters represented up-to-date methods for testing, however they are not required to be identical. The data sets that will be included in the analysis represent two species, *D. giganteus* and *P. aurea*. Excluded data is the compressive modulus from Culzoni (1985) which did not fall into the apparent acceptable range. This data will be excluded for the statistical analysis to reduce the uncertainty. Since the type of treatment is disregarded, the three data sets from Cruz (2002) will be pooled into a single source.

The criterion removed the majority of data and creates a very small data population for each species. Since the types of mechanical tests that are conducted by each data source are limited, only four mechanical properties will be investigated with focus placed on the tensile and compressive stresses and modulus. Table 5.6 and Table 5.7 indicate the data sources and averages for each property. In some instances, the data source was limited to a single property. Comparison of the four data sets illustrates the variation in the mean and the standard deviations, boxplots of this data are shown in Figure 5.1. The shaded sections of the boxplots indicate the 2nd and 3rd quartiles, or 25-75%, of the data. The error bars indicate the maximum and minimum values in the data, as indicated in the legend in Figure 5.1h. The distribution for data sources with a limited number of samples is difficult to assess in histograms. All of the sources were analyzed and the data is within the 2s limit. Only one data set from the *P. aurea* sources (Cruz (2002) tensile stress) had a single data point that was outside the 2s limit.

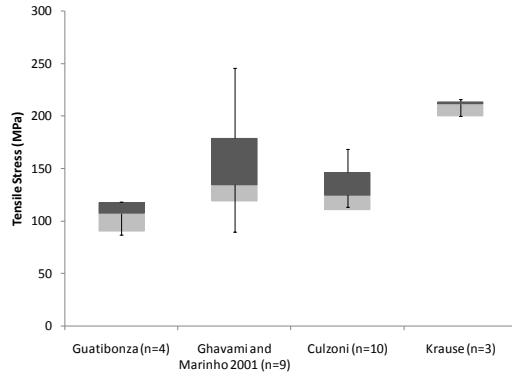
Table 5.6 Selected data sources for the longitudinal tensile stress and modulus.

	Source	Treatment	Dimensions	Load Rate	Tensile Stress				Modulus of Elasticity			
					n	\bar{x}	s	COV	n	\bar{x}	s	COV
			mm	mm/sec		MPa	MPa	%		GPa	GPa	%
<i>D. giganteus</i>	Guatibonza 2009 ^b	Air	22 x 1.2		4	100.6	22.7	23	4	11.3	0.3	3
	Ghavami and Marinho 2001 ^b	Borax	20 x 1	0.01	9	149.4	49.4	33	5	17.5	4.8	27
	Culzoni 1985 ^a	Air	20 x 1	0.1	10	129.4	22.9	18	10	13.1	2.3	18
	Krause 2009 ^a	Air	20 x 1	0.02	3	205.2	14.6	7	3	18.7	1.31	7
<i>P. aurea</i>	Cruz 2002 ^{b,c}	Air	20 x 1	0.01	6	210.4	38.9	19	6	18.9	3.1	16
	Cruz 2002 ^{b,c}	Heat	20 x 1	0.01	6	175.4	56.1	32	6	21.9	2.4	11
	Cruz 2002 ^{b,c}	Water	20 x 1	0.01	6	238.9	63.4	27	6	21.4	3.6	17
	Sharma 2010	Water	20 x 1	0.02	13	251.1	36.7	15	3	16.2	2.3	14
	Krause 2009	Water	20 x 1	0.02	3	260.9	3.4	0.01				

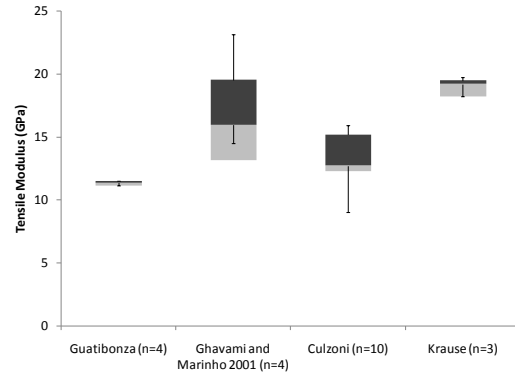
^a Modulus of elasticity determined from clip gage mounted on specimens;^b Modulus of elasticity determined from electrical resistance strain gages mounted on specimens;^c Poisson ratio determined from electrical resistance strain gages mounted on specimens.**Table 5.7 Selected data sources for longitudinal compressive stress and modulus.**

	Source	Treatment	Height	Load Rate	Compressive Stress				Modulus of Elasticity			
					n	\bar{x}	s	COV	n	\bar{x}	s	COV
			mm	mm/sec		MPa	MPa	%		GPa	GPa	%
<i>D. giganteus</i>	Ghavami and Marinho 2001 ^{b,c}	Borax	Dia	Manual	6	78.0	9.6	12	6	21.0	4.3	21
	Culzoni 1985 ^a	Air	2Dia	0.03	10	42.3	8.8	21				
	Moreira 1991	Air	2Dia	0.001	6	34.0	3.1	9				
	Krause 2009	Air	Dia	Manual	5	55.1	11.4	2				
<i>P. aurea</i>	Cruz 2002 ^{b,c}	Air	Dia	Manual	6	69.3	9.9	14	6	24.8	4.3	17
	Cruz 2002 ^{b,c}	Heat	Dia	Manual	6	69.1	9.7	14	6	26.8	4.1	15
	Cruz 2002 ^{b,c}	Water	Dia	Manual	6	68.1	13.5	20	6	21.5	7.1	33
	Krause 2009	Water	Dia	Manual	3	55.1	3.0	5				

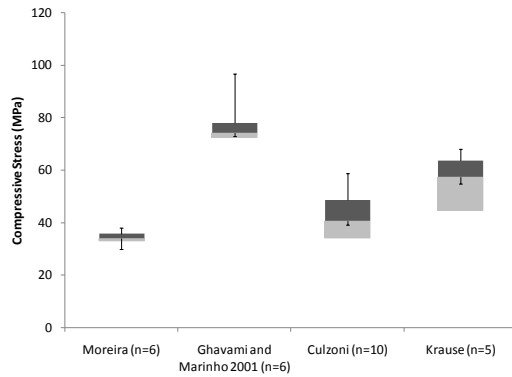
^a Modulus of elasticity determined from clip gage mounted on specimens;^b Modulus of elasticity determined from electrical resistance strain gages mounted on specimens;^c Poisson ratio determined from electrical resistance strain gages mounted on specimens.



a) Tensile Stress for *D. giganteus*



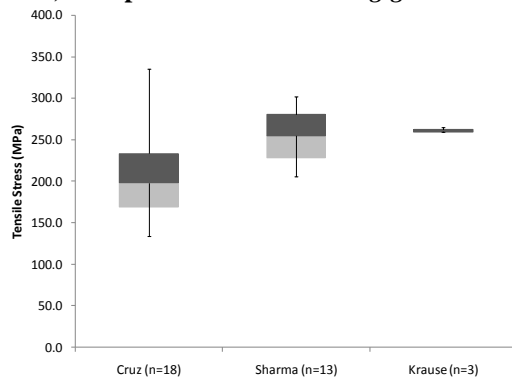
b) Tensile Modulus for *D. giganteus*



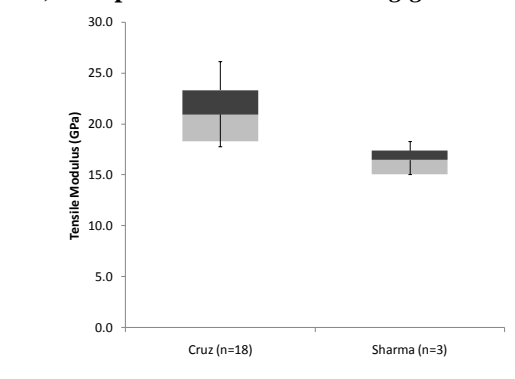
c) Compressive Stress for *D. giganteus*



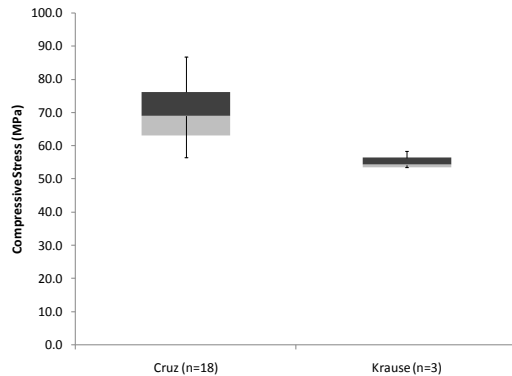
d) Compressive modulus for *D. giganteus*



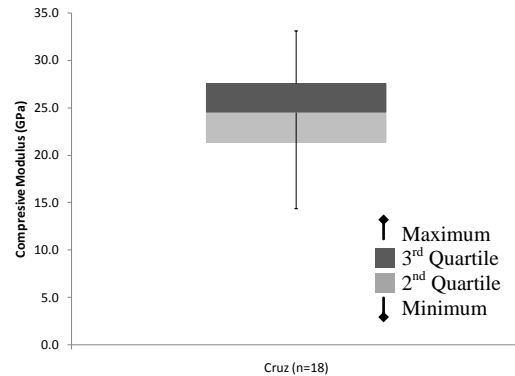
e) Tensile Stress for *P. aurea*



f) Tensile Modulus for *P. aurea*



g) Compressive Stress for *P. aurea*



h) Compressive modulus for *P. aurea*

Figure 5.1 Mechanical properties boxplots for *D. giganteus* and *P. aurea*.

5.3.2 Primary analysis

The primary objective of the statistical analysis was to determine the material properties for the two species with a given level of confidence. The analysis will provide a range of properties through sampling techniques which will serve as input for the *OpenSees* model described in Chapter 6.0 .

5.3.2.1 Homogeneity of variances

Table 5.6 and Table 5.7 list the descriptive statistics for the selected data sources. The comparison of the sources by their respective means demonstrates the high variability between samples. The variability can be attributed to multiple sources, but is often a result of the material itself. The data sources will instead be compared by the homogeneity of variances. The analysis of variances (ANOVA) considers the stress or modulus for two bamboo species from different operators, or data sources. The null hypothesis (H_0) is that the variance of the k^{th} group is equal to the variance of group $k+1$:

$$H_0: \sigma_1 = \sigma_2 = \dots = \sigma_k \quad (\text{Eq. 5.1a})$$

and

$$H_1: \text{at least one of the variances are not equal} \quad (\text{Eq. 5.1b})$$

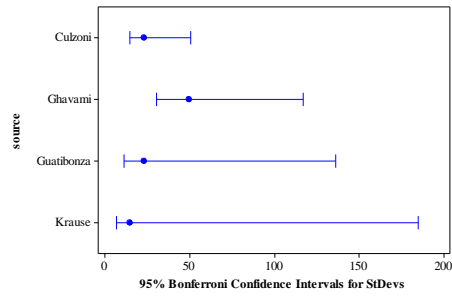
Two tests were explored, Levene's test (Minitab 2008) and Bartlett's test (Cooper 1969). The Levene test was used to reduce the effect of the departures from normality of the data sets found in the Bartlett test (NIST 2010). Analysis of the significance in the variation between the variance of data sources was tested at a confidence level of 95%.

The ANOVA results are presented in Table 5.8 and in Figure 5.2. The Bartlett statistic and p-value (Minitab 2008) is provided for comparison. Based on the Levene statistic and p-

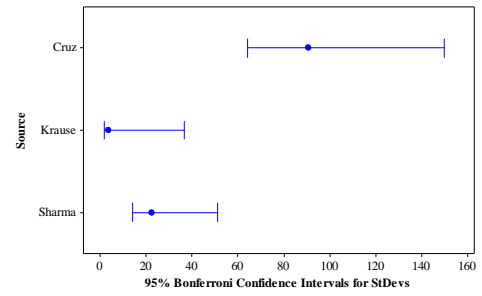
value, the null hypothesis was accepted or rejected. One data set was rejected: *D. giganteus* tensile modulus. The compressive modulus for *D. giganteus* and *P. aurea* were not tested due to the single data source. To pool the data, the means from each data source were compared to determine if the variation is significant.

Table 5.8 ANOVA test for equal variances.

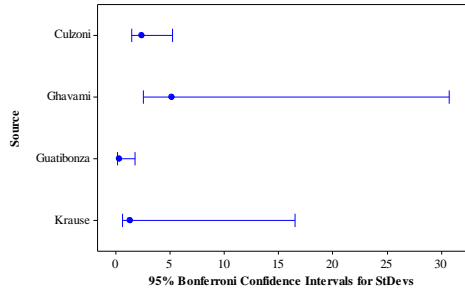
	Property	Bartlett	p-value	Levene	p-value	H ₀ or H ₁
<i>D. giganteus</i>	Tensile Stress	6.86	0.077	1.55	0.229	H ₀
	Tensile Modulus	14.04	0.003	5.76	0.007	H ₁
	Compressive Stress	6.41	0.093	1.5	0.24	H ₀
	Compressive Modulus	n.a.				
<i>P. aurea</i>	Tensile Stress	21.44	0	2.66	0.088	H ₀
	Tensile Modulus	1.87	0.808	0.98	0.335	H ₀
	Compressive Stress	12.31	0.155	2.74	0.114	H ₀
	Compressive Modulus	n.a.				



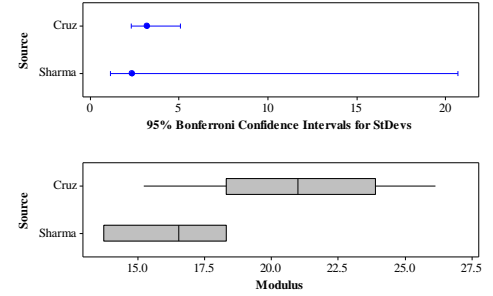
a) *D. giganteus* Tensile Stress



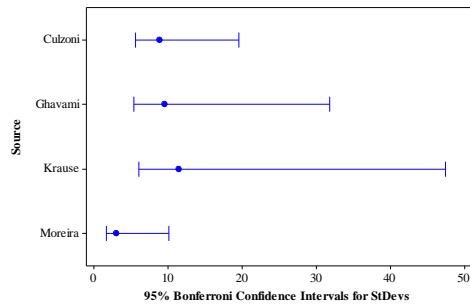
b) *P. aurea* Tensile Stress



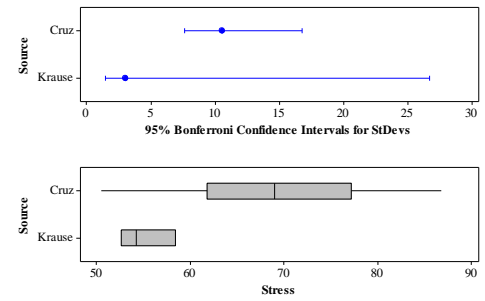
c) *D. giganteus* Tensile Modulus



d) *P. aurea* Tensile Modulus



e) *D. giganteus* Compressive Stress



f) *P. aurea* Compressive Stress

Figure 5.2 ANOVA test for equal variances.

5.3.2.2 Analysis of Variance for equal means

ANOVA compares means from two or more independent groups ($k = 2$ or more). The analysis considers the stress or modulus for two bamboo species from different operators, or data sources.

The null hypothesis is that the mean of the k^{th} group is equal to the mean of group $k+1$:

$$H_0: \mu_1 = \mu_2 = \dots = \mu_k \quad (\text{Eq. 5.2a})$$

and

$$H_1: \text{at least one mean is not equal} \quad (\text{Eq. 5.2b})$$

Additionally, the variance within the group and between groups was assessed to determine if there is a significant difference. The null hypothesis for the variance is (Devore 2000):

$$H_0: \sigma_B^2 \leq \sigma_W^2 \quad (\text{Eq. 5.3a})$$

$$H_1: \sigma_B^2 > \sigma_W^2 \quad (\text{Eq. 5.3b})$$

To calculate the variance between groups:

$$s_B^2 = \frac{SS_B}{df_B} \quad (\text{Eq. 5.4a})$$

where

$$SS_B = \sum_{i=1}^k n_i (\bar{x}_i - \bar{x})^2 \quad (\text{Eq. 5.4b})$$

$$df_B = k - 1 \quad (\text{Eq. 5.4c})$$

To calculate the variance within groups:

$$s_W^2 = \frac{SS_W}{df_W} \quad (\text{Eq. 5.5a})$$

where

$$SS_W = \sum_{i=1}^k (n_i - 1) s_i^2 \quad (\text{Eq. 5.5b})$$

$$df_W = N - k \quad (\text{Eq. 5.5c})$$

To calculate the ANOVA F statistic:

$$F_{stat} = \frac{s_B^2}{s_W^2} \quad (\text{Eq. 5.6})$$

The critical value of F , F_{crit} , is obtained from a table based on the degree of freedoms between and within groups (dfw and dfb, respectively), as well as the selected confidence level in the form of the value of alpha (F_{dfw,dfb,α_c}).

5.3.2.3 Results

Dendrocalamus giganteus Tensile Stress and Modulus

The results for the ANOVA test for equal means is discussed below and summarized in Table 5.9. For the tensile stress, the results indicate that the F_{stat} is greater than F_{crit} , thus the finding is significant and the null hypothesis is rejected. The p-value is less than the critical alpha ($\alpha_c=0.05$), $p_{stat} = 0.004$. For the tensile modulus, the analysis indicates that the F_{stat} is greater than F_{crit} . The finding is significant and the null hypothesis is rejected. The p-value is less than critical alpha ($p_{stat} = 0.007$).

Dendrocalamus giganteus Compressive Stress and Modulus

For the compressive stress the variance within the sample is less than the variance between samples, thus the null hypothesis is rejected and there is significant difference between and within the groups. The analysis for the compressive stress rejected the null hypothesis. The compressive modulus was limited to one data source and thus was not tested.

Phyllostachys aurea

The null hypothesis was rejected for the tensile stress, modulus and compressive stress. The compressive modulus was limited to one data source and thus was not tested.

5.3.2.4 Summary

The ANOVA analysis rejected the null hypothesis and indicated that the significance is borderline ($0.01 \leq p \leq 0.05$) for the *P. aurea* sources, while the *D. giganteus* sources were highly significant ($p \leq 0.005$). The initial hypothesis was that the mean for the data from the multiple data sources would be equal, which is not probable even if the samples were conducted by the same operator. The distribution of the data will be analyzed to determine the best fit. The results indicate that there is significant variation between the individual data sources and thus they will not be pooled. The data source's distributions were investigated individually to obtain a range of design values.

Table 5.9 Summary of ANOVA test for *D. giganteus* and *P. aurea*, with null hypothesis $\mu_1 = \mu_2 \dots = \mu_k$.

Dendrocalamus giganteus	Tension						Phyllostachys aurea	Tension							
	Stress	Source	Sum of Squares	Degrees of Freedom	Mean Squares			Stress	Source	Sum of Squares	Degrees of Freedom	Mean Squares			
		Between (SSB)	20888	3	6963				Between (SSB)	17134	2	8657			
		Within (SSW)	26232	22	1192				Within (SSW)	72126	31	2327			
		Total	47120	25					Total	89259	33				
		F _{stat}	5.84						F _{stat}	3.68					
		F _{crit}	3.05						F _{crit}	3.31					
		p _{critical}	0.004	Significant					p _{critical}	0.037	Significant				
		Modulus	Between (SSB)	132	3	44			Modulus	Between (SSB)	54	1	54		
	Within (SSW)		132	17	8			Within (SSW)		182	19	10			
	Total		264	20				Total		236	20				
	F _{stat}		5.68					F _{stat}		5.65					
	F _{crit}		3.20					F _{crit}		4.38					
	p _{critical}		0.007	Significant				p _{critical}		0.028	Significant				
Compression	Stress	Between (SSB)	6946	3	2315		Compression	Stress	Between (SSB)	484	1	484			
		Within (SSW)	1731	23	75				Within (SSW)	1890	19	99			
		Total	8678	26					Total	2374	20				
		F _{stat}	30.76						F _{stat}	4.87					
		F _{crit}	3.03						F _{crit}	4.38					
		p _{critical}	0.000	Significant					p _{critical}	0.04	Significant				

5.3.3 Distribution

Each of the data sources was evaluated to determine the appropriate distribution (Minitab 2008). A goodness-of-fit test was conducted using the Anderson-Darling (A-D) statistic to compare three distributions: Normal, Weibull and the three-parameter Weibull (Weibull-3). The p-value was used to determine the best fit. The results are presented in Table 5.10. The results indicate that the majority of the data is best fit to a Normal distribution. In the cases of the three-parameter Weibull, the next best fit was considered due to the additional computation associated with a three-parameter Weibull distribution. The Anderson-Darling statistic was used to compare the Normal and Weibull distributions, with the lower statistic selected.

Table 5.10 Comparison of distributions for goodness-of-fit.

		Source	Normal		Weibull		Weibull-3		Distribution
			A-D	p-value	A-D	p-value	A-D	p-value	
<i>D. giganteus</i>	TS	Gautibonza	0.351	0.253	0.451	0.230	0.435	0.195	Normal
		Ghavami	0.258	0.623	0.268	>0.250	0.246	>0.500	Normal
		Culzoni	0.270	0.592	0.324	>0.250	0.248	>0.500	Normal
		Krause	0.355	0.174	0.449	0.226	0.442	0.184	Weibull
		Gautibonza	0.349	0.256	0.476	0.205	0.477	0.141	Normal
		Ghavami	0.217	0.619	0.262	>0.250	0.268	>0.500	Normal
		Culzoni	0.390	0.311	0.390	>0.250	0.349	0.361	Weibull-3
		Krause	0.296	0.285	0.354	>0.250	0.342	0.379	Weibull-3
		Moreira	0.204	0.770	0.189	>0.250	0.198	>0.500	Normal
		Ghavami	0.797	0.017	0.88	0.017	0.353	0.479	Weibull-3
		Culzoni	0.341	0.415	0.374	>0.250	0.387	0.414	Normal
		Krause	0.280	0.478	0.332	>0.250	0.345	0.390	Normal
		Ghavami	0.563	0.081	0.645	0.075	0.493	0.227	Weibull-3
<i>P. aurea</i>		Cruz	1.040	0.007	0.969	0.012	0.617	0.113	Weibull-3
		Sharma	0.163	0.915	0.205	>0.250	0.191	>0.500	Normal
		Krause	0.304	0.266	0.408	>0.250	0.377	0.337	Weibull-3
		Cruz	0.248	0.710	0.64	>0.250	0.280	>0.500	Normal
		Sharma	0.207	0.555	0.256	>0.250	0.250	>0.500	Normal
		Cruz	0.229	0.777	0.188	>0.250	0.218	>0.500	Normal
		Krause	0.261	0.378	0.359	>0.250	0.343	0.401	Weibull-3
		Cruz	0.280	0.603	0.322	>0.250	0.328	0.443	Normal
TS = tensile strength TM= tensile modulus CS = compressive strength CM = compressive modulus									

5.3.4 Normal distribution

The data was analyzed as a normal distribution with the respective mean and standard deviation used for each data source. The normal distribution is often used to represent the distribution of the material strength data. The probability distribution density function for a normal distribution is:

$$f(q) = \frac{1}{\sqrt{2\pi}s} \exp \left[-\frac{1}{2} \left(\frac{q-\mu}{s} \right)^2 \right] \quad (\text{Eq. 5.7})$$

where μ is the mean and s is the standard deviation.

5.3.5 Weibull Distribution

The Weibull distribution is also commonly used to model the distribution of material properties (Barbero et al. 2000). The cumulative distribution function (CDF) of a two-parameter Weibull distribution is:

$$F(q; \alpha, \beta) = 1 - \exp \left[- \left(\frac{q}{\alpha} \right)^\beta \right] \quad (\text{Eq. 5.8})$$

in which F is the probability of failure, q is the property under investigation, α is the scale parameter and β is the shape parameter. An approximate estimate of the median rank, $F(q_i)$, was calculated using Bernard's median rank estimator (Zhang et al. 2006).

$$F(q_i) = \frac{(i-0.3)}{(n+0.4)} \quad (\text{Eq. 5.9})$$

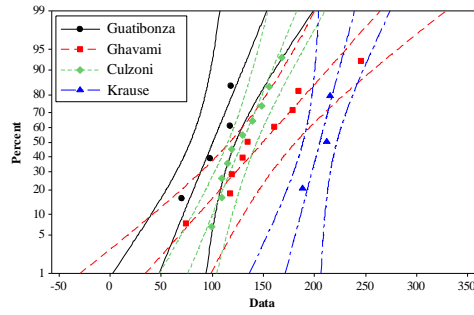
To estimate the parameters for the Normal and Weibull distributions the maximum likelihood estimates (MLE) method was used in Minitab (2008). The Anderson-Darling adjusted statistic was used to test goodness-of-fit with a confidence interval of 95%. For comparison, the Normal (μ and s) and Weibull distribution parameters (α and β) were calculated in Microsoft Excel.

5.3.6 Results

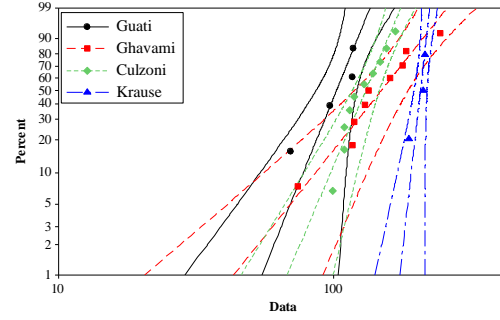
The Normal and Weibull distributions were compared to test goodness-of-fit. The results are presented in Table 5.10. The Anderson-Darling (A-D) statistic indicated that the majority of the data fit a Normal distribution. The few sources that were better fit to a Weibull distribution only had a slightly lower A-D statistic than the Weibull distributions. The comparison of the two distributions is shown in Figure 5.3 and Figure 5.4. The p-value for the Normal distribution was calculated to test the null hypothesis (H_0) that the data fit the distribution. The p-value for the majority of data sources was well above $\alpha_c=0.05$ and the hypothesis was accepted (Table 5.11). Three sources were below or near to the rejection level: Ghavami and Marinho (2001) for compressive stress and modulus and Cruz (2002) for tensile stress. Based on the generated parameters, the Normal probability density function and the reliability of the mechanical property was determined. The plots are shown in Figure 5.5.

Table 5.11 Calculated and estimated parameters for the Normal and Weibull distributions.

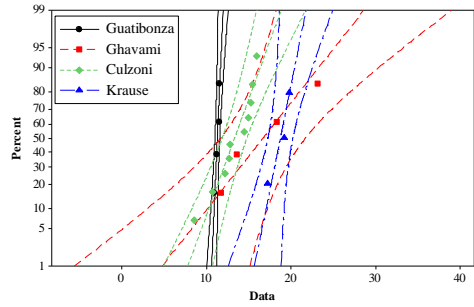
			Normal						Weibull						
			Calculated		Maximum Likelihood Estimate				Calculated		Maximum Likelihood Estimate				
		Source	\bar{x}	s	\bar{x}	s	A-D	P-value	Shape	Scale	Shape	Scale	A-D	P-value	Dist.
<i>D. giganteus</i>	TS	Gautibonza	100.6	22.7	100.6	22.7	0.351	0.253	3.92	111.2	6.74	108.4	0.451	0.230	N
		Ghavami	149.4	49.4	149.4	49.4	0.258	0.623	3.16	167.5	3.43	166.2	0.268	>0.250	N
		Culzoni	129.4	22.9	129.4	22.9	0.270	0.592	6.12	139.0	6.43	138.8	0.324	>0.250	N
		Krause	205.2	14.62	205.2	14.6	0.355	0.174	12.60	212.4	24.47	210.5	0.449	0.226	N
	TM	Gautibonza	11.3	0.29	11.3	0.29	0.256	0.256	37.24	11.4	58.81	11.4	0.476	0.205	N
		Ghavami	16.7	5.12	16.7	5.12	0.619	0.619	3.22	18.7	4.15	18.4	0.262	>0.250	W
		Culzoni	13.1	2.34	13.3	2.37	0.311	0.311	5.64	14.1	7.71	14.2	0.380	>0.250	N
		Krause	18.7	1.31	18.7	1.31	0.285	0.285	13.20	19.4	23.99	19.2	0.354	>0.250	N
	CS	Moreira	34.0	3.05	34.0	3.05	0.204	0.770	11.35	35.4	14.52	35.2	0.189	>0.250	W
		Ghavami	78.0	9.58	78.0	9.58	0.797	0.017	7.31	83.0	8.04	82.2	0.888	0.017	N
		Culzoni	42.3	8.84	42.3	8.84	0.341	0.415	5.09	45.9	5.34	45.8	0.374	>0.250	N
		Krause	55.1	11.44	55.1	11.44	0.280	0.478	4.68	60.2	6.43	59.4	0.332	>0.250	N
CM	Ghavami	21.0	4.33	21.0	4.33	0.563	0.081	4.73	23.0	5.73	22.7	0.645	0.075	N	
<i>P. aurea</i>	TS	Cruz	208.2	57.4	225.1	90.55	1.040	0.007	4.01	230.0	2.61	253.2	0.969	0.012	W
		Sharma	251.1	36.7	270.2	22.5	0.163	0.915	7.39	267.0	14.67	279.9	0.205	>0.250	N
		Krause	260.9	3.4	260.9	3.35	0.304	0.266	69.33	262.6	97.25	262.2	0.408	>0.250	N
	TM	Cruz	20.8	3.2	20.8	3.17	0.248	0.710	7.31	22.1	7.73	22.1	0.264	>0.250	N
		Sharma	16.2	2.3	16.2	2.32	0.207	0.555	6.56	17.2	10.46	16.9	0.256	>0.250	N
	CS	Cruz	68.8	10.5	68.8	10.49	0.229	0.777	7.24	73.3	7.87	73.1	0.188	>0.250	W
		Krause	55.1	3.0	55.1	2.99	0.261	0.378	17.0	56.5	23.59	56.3	0.359	>0.250	N
	CM	Cruz	24.4	5.5	24.4	5.52	0.280	0.603	4.41	26.8	5.25	26.5	0.322	>0.250	
TS = tensile strength TM= tensile modulus CS = compressive strength CM = compressive modulus N = normal distribution W = Weibull distribution															



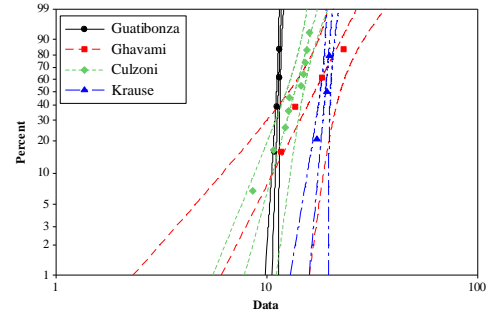
a) Normal plot Tensile Stress



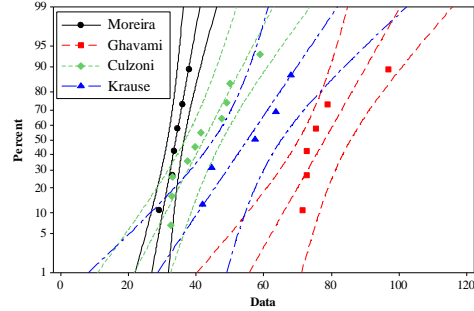
b) Weibull plot Tensile Stress



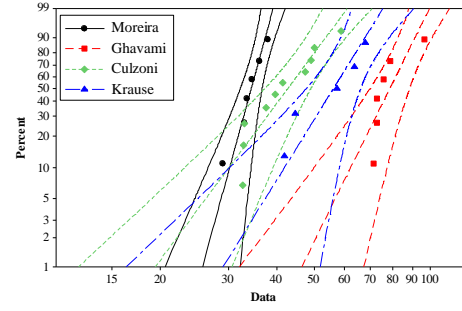
c) Normal plot Tensile Modulus



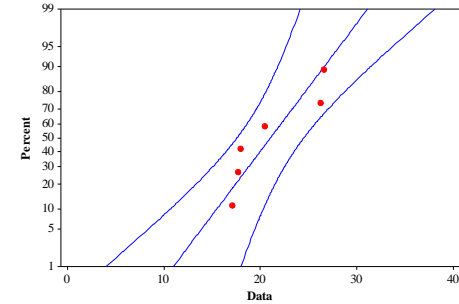
d) Weibull plot Tensile modulus



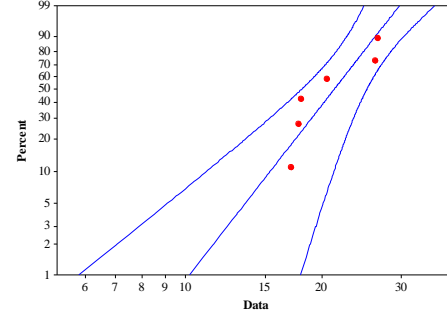
e) Normal plot Compressive stress



f) Weibull plot Compressive stress

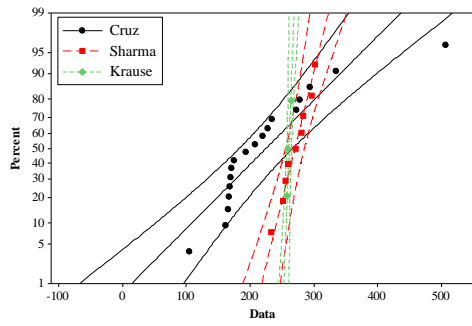


g) Normal plot Compressive modulus

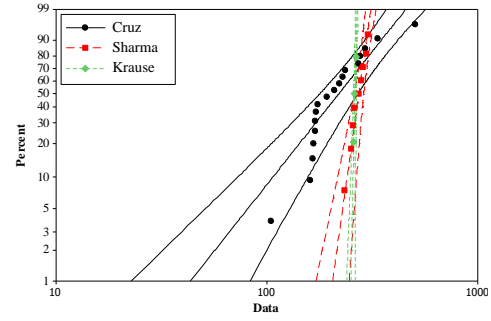


h) Weibull plot Compressive modulus

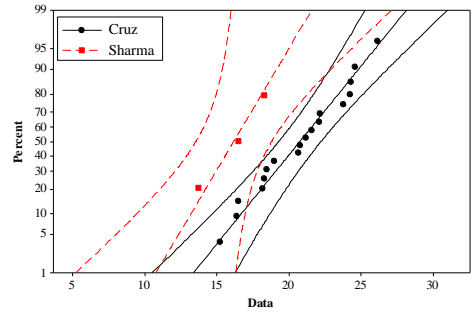
Figure 5.3 Normal and Weibull probability plots for *D. giganteus*.



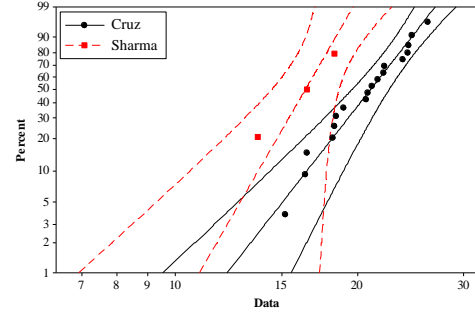
a) Normal plot Tensile Stress



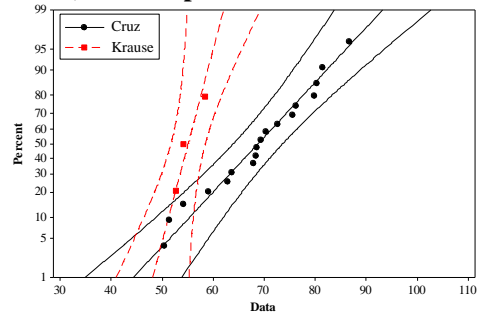
b) Weibull plot Tensile Stress



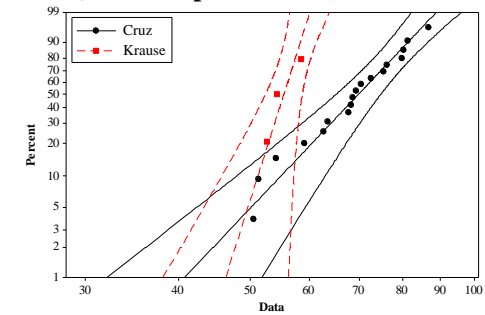
c) Normal plot Tensile Modulus



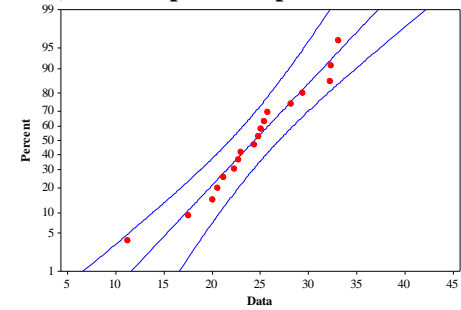
d) Weibull plot Tensile modulus



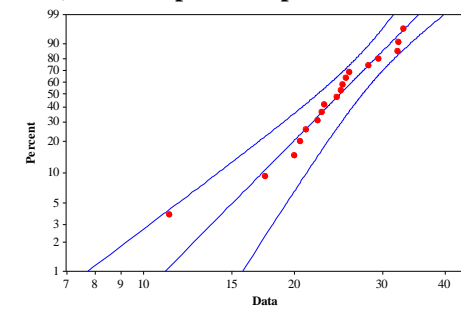
e) Normal plot Compressive stress



f) Weibull plot Compressive stress

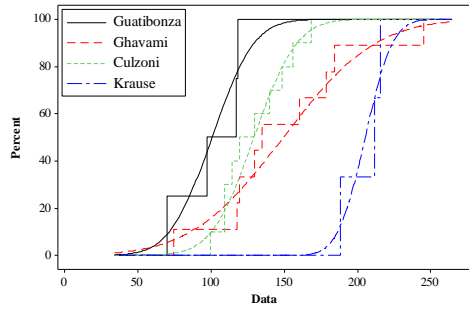


g) Normal plot Compressive modulus

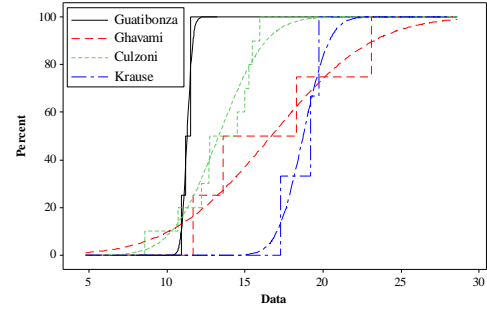


h) Weibull plot Compressive modulus

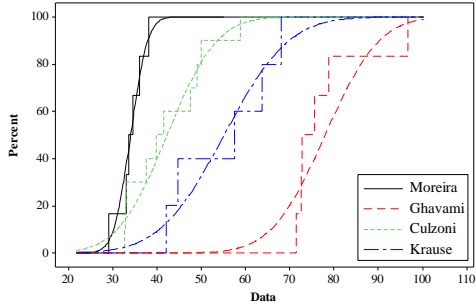
Figure 5.4 Normal and Weibull probability plots for *P. aurea*.



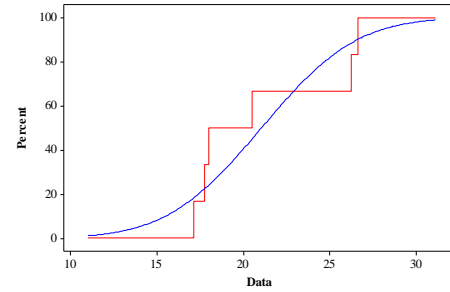
a) Tensile stress for *D. giganteus*



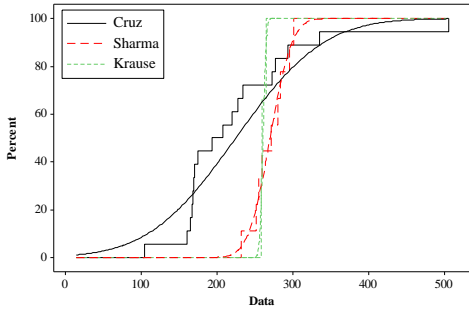
b) Tensile modulus for *D. giganteus*



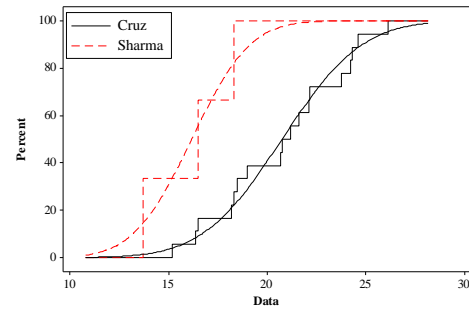
c) Compressive stress for *D. giganteus*



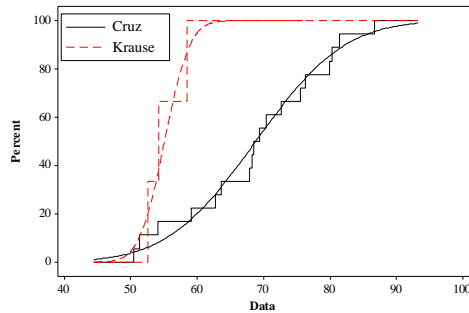
d) Compressive modulus for *D. giganteus*



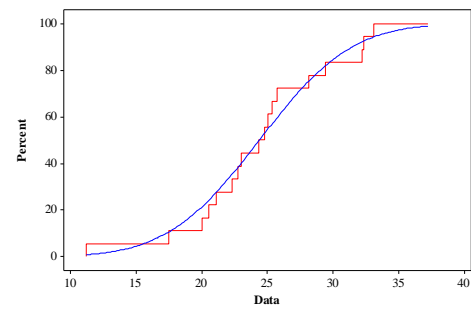
e) Tensile stress for *P. aurea*



f) Tensile modulus for *P. aurea*



g) Compressive stress for *P. aurea*



h) Compressive modulus for *P. aurea*

Figure 5.5 Normal empirical cumulative distribution functions.

5.3.7 Summary

The statistical analysis illustrated the inherent variability between and within data sources from two bamboo species. The statistical tests indicated that:

1. The source (the operator, testing parameters and conditions) has a significant effect on the variability of the data, thus data from multiple sources cannot be pooled and considered to be from the same population.
2. There is need for standardization of key parameters in testing and reporting bamboo mechanical properties.
3. For a complete statistical analysis, there is a need for greater published data on bamboo mechanical properties.
4. Nonetheless, the majority of the data follows a normal distribution.

The analysis provided a range on material properties that can be used as input for the *OpenSees* model. Using the Normal cumulative distribution functions, multiple random material property values will be generated for each species. The ranges will be sampled to create models that will be ‘nominally identical but statistically different.’

6.0 SEISMIC ANALYSIS OF BAMBOO PORTAL FRAME

6.1 MODELING THE PROTOTYPE BAMBOO STRUCTURE

A finite element model (FEM) of the prototype structure described in Section 3.2 is developed. Material properties presented in Chapter 5.0 will be used. In order to validate the modeling approach, a FE model of the tested portal frame (described in Sections 3.4-3.6) is first assembled.

6.1.1 Modeling the Column Base

As described in Section 3.6, the column base behavior was more complex than initially hypothesized. Mitch (2010) therefore investigated the push-over behavior of four-culm grouted-bar bamboo column bases and his recommendations with respect to modeling this connection are adopted here. Mitch expressed the column stiffness of the bases in terms of the relationship between I_{culm} , I_{column} , and $I_{apparent}$.

For a single culm, the moment of inertia is:

$$I_{culm} = \frac{\pi}{4} (R_o^4 - R_i^4) \quad (\text{Eq. 6.1})$$

For the symmetric four-culm column considered in this study, the moment of inertia is:

$$I_{column} = 4 \left[\left(\frac{\pi}{4} (R_o^4 - R_i^4) \right) + Ay^2 \right] \quad (\text{Eq. 6.2})$$

Where R_o and R_i are the outer and inner culm diameters ($R_i = R_o - 2t$, where t is the culm wall thickness), A is a single culm cross sectional area and y is the distance from a single culm centroid to the centroid of the four-culm group.

For the prototype structure geometry and the tested frame geometry, the ratio I_{column}/I_{culm} is approximately 42 (for comparison, this ratio was approximately 40 in the Mitch study). Mitch concludes that the apparent, fixed-base cantilever stiffness of the four-culm grouted-bar column base, $I_{apparent}$, is approximately $0.2I_{column}$. From this result, an appropriate rotational spring behavior for the column base may be determined. This spring is then used to model the column base behavior while I_{culm} and appropriate column geometry, effectively resulting in I_{column} , is used to model the column itself resulting in a partially restrained boundary condition at the column base (Figure 6.1).

6.1.2 Validation Using Tested Prototype Portal Frame

A two-dimensional model of the tested portal frame (Sections 3.4-3.6) was assembled using the open source code *OpenSees* (Mazzoni et al. 2009). Individual bamboo culms were modeled using beam elements having appropriate section properties (see Table 6.1). A diagram of the frame, showing element and node numbering, is shown in Figure 6.1. The material and geometrical properties of the *Phyllostachys aurea* culms were those of the tested frame and are reported in Chapter 3.0. The apparent full-culm modulus was taken as the compressive modulus, $E = 21,600$ MPa for all members. To account for the two-dimensional model, the moments of inertia of the culms comprising the columns were doubled to account for the two-column out-of-plane arrangement (Table 6.1). A pushover load was conducted with the load applied to the top

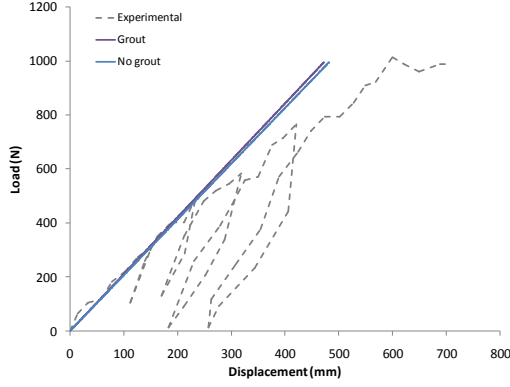
left-hand column joints (nodes 2 and 15). This load arrangement is the same used in the experimental program.

Figure 6.2a illustrates the resulting load-displacement pushover curve (solid line) in comparison to the results discussed in Chapter 3.0 (Figure 3.24, indicated by dashed line). The results indicated good agreement in comparison with the experimental results, although the elastic model does not capture the degradation of the stiffness.

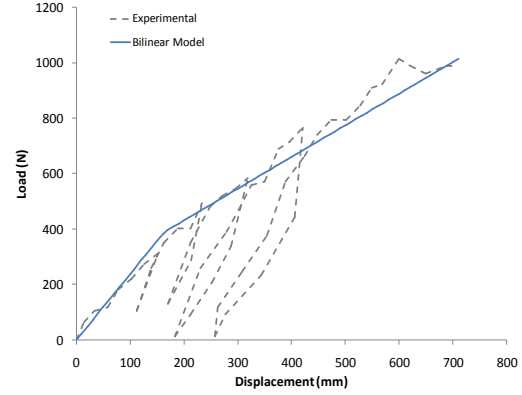
Figure 6.1 OpenSees model node and member (noted in squares) numbering.

of inertia; thus his recommendations implicitly include the effect of grout on the bamboo section properties. Also, as discussed in Chapter 3.0 and in Mitch (2010), there is some slip between the culm and the grout, resulting in a violation of the plane sections assumption. There is presently insufficient data to develop a model that adequately describes this slip. Finally, the modulus of the grout varies significantly and was not determined in the work described in Chapter 3.0. To evaluate the effect of the grout plug, the modulus is estimated to be $550f_c'$ (ASCE 41 2006), where f_c' is approximately 8.5 MPa. Figure 6.2a compares the behavior of a transformed section and a solely bamboo section, both with elastic rotational spring boundary conditions. The results indicated that the transformed section contributed little additional stiffness to the frame and thus will be neglected hereafter.

To capture the nonlinear behavior of the frame, a bilinear material model was created in *OpenSees* (discussed in greater detail in Section 6.1.4). Mitch (2010) notes that the maximum proportional rotation for the column occurs at 0.05 radians, however the experimental results and observations indicated that the *Phyllostachys aurea* frame demonstrated considerable flexibility. The difference in behavior is attributed to the thinner wall and smaller diameter section of the *P. aurea* bamboo used. The bilinear model was established using the yield rotation (0.18 radians) obtained from the experimental results. Based on the rotational spring stiffness, the parameters for the bilinear curve were obtained. The model was compared to the experimental results, as shown in Figure 6.2b. The figure illustrates that the model was able to capture the backbone curve of the experimental results. Based on the results presented, it is concluded that the basic portal frame behavior is captured by the model.



a) elastic behavior with and without grout plug



b) behavior using bilinear rotational springs

Figure 6.2 Pushover behavior of the experimental frame.

Table 6.1 OpenSees model geometric and material properties for PUC-Rio comparison.

Element	Member ID (see Fig 6.1)	R_o	t	Length	Area	moment of inertia	spring constant
		mm	mm	mm	mm ²	mm ⁴	N-m
Rotational Spring	Springs 24-27	-	-	0	-	-	$2K_\theta = 4692$
Column Base with grout	1,4,6,20	25	4.5	700	$2A_{culm} = 1538$	$2I_{culm} = 572,557$	-
Column base without grout	1,4,6,20	29	4.5	700	$2A_{culm} = 1287$	$2I_{culm} = 336,714$	-
Lower Column	2,5,7,21	25	4.5	680	$2A_{culm} = 1287$	$2I_{culm} = 336,714$	-
Upper column outside	8,18,19,22	25	4.5	1470	$2A_{culm} = 1287$	$2I_{culm} = 336,714$	-
Upper column inside	9,10,23,24	25	4.5	1400	$2A_{culm} = 1287$	$2I_{culm} = 336,714$	-
Lower Lateral	30	20	4.75	5800	$A_{culm} = 526$	$I_{culm} = 83,185$	-
Upper Lateral	25	20	4.75	6000	$A_{culm} = 526$	$I_{culm} = 83,185$	-
Column-roof joint outside	11 & 17	20	4.75	170	$A_{culm} = 1287$	$I_{culm} = 336,714$	-
Column-roof joint inside	12 & 16	20	4.75	300	$A_{culm} = 1287$	$I_{culm} = 336,714$	-
Roof	13 & 14	20	4.75	3700	$A_{culm} = 526$	$I_{culm} = 83,185$	-
Tension Tie	15	20	4.75	2200	$A_{culm} = 526$	$I_{culm} = 83,185$	-

6.1.3 Mungpoo Prototype Model Parameters

A second model was created based on the *in situ* geometric and bamboo material properties observed at the St. Joseph's School in Mungpoo (described in Section 3.2). The bamboo species, *Bambusa nutans*, was not discussed in Chapter 5.0 due to the lack of information on the structural material properties of this species. For the model, the apparent full culm compressive

modulus is assumed equal to the tensile modulus; thus $E = 10,700 \text{ MPa}$ (Paudel 2008). The geometric properties are listed in Table 6.2. The exterior wall infill panels were excluded from the model due to their unknown stiffness and the observation that the wall panels in the prototype structures were supported by the grade beams (Figure 3.8). Additionally, the model assumes an interior frame (see Figure 3.9); these do not necessarily have infill panels.

Table 6.2 OpenSees model geometric and material properties for Mungpoo.

Element	Member ID (see Fig. 6.1)	R_o	t	Length	Area	moment of inertia	spring constant
		mm	mm	mm	mm^2	mm^4	N-m
Rotational Spring	Springs 24-27	-	-	0	-	-	$2K_\theta = 24,308$
Column base without grout	1,4,6,20	40	15	700	$2A_{\text{culm}} = 6126$	$2I_{\text{culm}} = 3,407,646$	-
Lower Column	2,5,7,21	40	15	680	$2A_{\text{culm}} = 6126$	$2I_{\text{culm}} = 3,407,646$	-
Upper column outside	8,18,19,22	40	15	1470	$2A_{\text{culm}} = 6126$	$2I_{\text{culm}} = 3,407,646$	-
Upper column inside	9,10,23,24	40	15	1400	$2A_{\text{culm}} = 6126$	$2I_{\text{culm}} = 3,407,646$	-
Lower Lateral	30	35	10	5800	$A_{\text{culm}} = 1885$	$I_{\text{culm}} = 871,792$	-
Upper Lateral	25	35	10	6000	$A_{\text{culm}} = 1885$	$I_{\text{culm}} = 871,792$	-
Column-roof joint outside	11 & 17	40	15	170	$A_{\text{culm}} = 6126$	$I_{\text{culm}} = 3,407,646$	-
Column-roof joint inside	12 & 16	40	15	300	$A_{\text{culm}} = 6126$	$I_{\text{culm}} = 3,407,646$	-
Roof	13 & 14	35	10	3700	$A_{\text{culm}} = 1885$	$I_{\text{culm}} = 871,792$	-
Tension Tie	15	35	10	2200	$A_{\text{culm}} = 1885$	$I_{\text{culm}} = 871,792$	-

As this is to be a seismic assessment, the mass carried by the portal frame must be determined. The majority of the seismic mass results from the corrugated steel roofing. The roof weight carried by a single interior frame was calculated based on the tributary area of an interior portal frame. The steel roofing was assumed to have a weight of 143.6 N/m^2 (ASCE 7 2005) and the density of the *B. nutans* was taken as 890 kg/m^3 including an allowance to account for the rafters (Naik 2005). The design values and tributary areas are listed in Table 6.3. The lumped masses were placed along the ridgeline, at the tension tie, and at the top of the columns in proportion shown in Figure 6.3.

Damping was selected to be 5% based on recent studies on timber frame construction (Ellingwood et al. 2004; Li and Ellingwood 2007). For wood frame structures, the damping ratio varies significantly from 2% to 15% (Rosowsky 2002); similar variability may be expected in bamboo structures but is not the subject of the present work.

The resulting dynamic model was found to be dominated by first mode behavior characterized as the lateral drift of the frame. The fundamental period was found to be 0.817 seconds and the first mode mass participation factor was essentially 100%.

Table 6.3 Structural materials and associated nodal masses.

Location	Nodes	Material	Tributary area	Design load	Weight	Mass	Mass per node
			m ²	N/m ²	N	kg	kg
Ridgeline	10	Deck Metal, 18 Gage	3.1	143.6	446	45.5	52.1
		<i>Bambusa nutans</i>		21.1	65	6.6	
Left Tension Tie	11	Deck Metal, 18 Gage	3.9	143.6	560	57.1	65.5
		<i>Bambusa nutans</i>		21.1	82	8.4	
Right Tension Tie	9	Deck Metal, 18 Gage	3.9	143.6	560	57.1	65.5
		<i>Bambusa nutans</i>		21.1	82	8.4	
Left Column-roof joint	12 & 13	Deck Metal, 18 Gage	10.1	143.6	1450	147.8	84.8
		<i>Bambusa nutans</i>		21.1	213	21.7	
Right column-roof joint	6 & 8	Deck Metal, 18 Gage	10.1	143.6	1450	147.8	84.8
		<i>Bambusa nutans</i>		21.1	213	21.7	

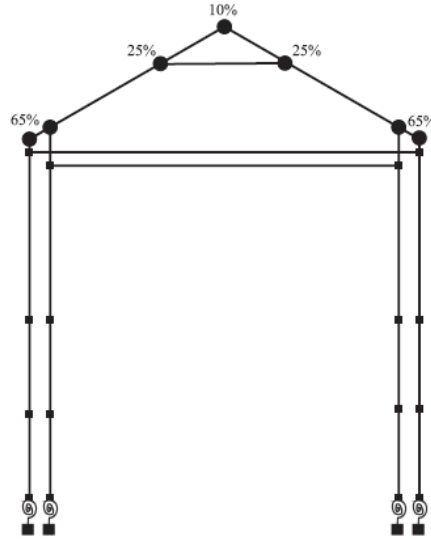
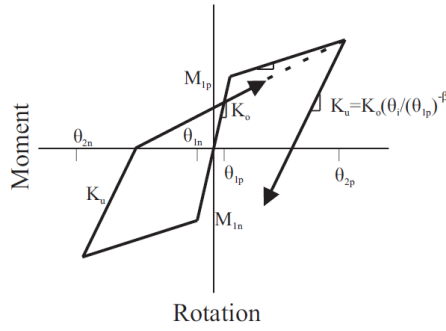


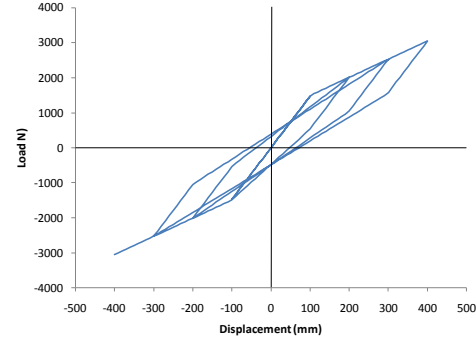
Figure 6.3 Location of nodal masses in OpenSees Mungpoo model.

6.1.4 Moment-rotation bilinear hysteretic relationship

Based on the spring stiffness ($2EI_{\text{culm}}/L$) used in the initial modeling and recommended by Mitch (2010), a bilinear moment rotation relationship for the culm base springs was established. Again, based on the observations of Mitch, a hysteretic model similar to a Modified Takeda hysteresis (Otani 1974 as reported in Carr 2002) was established to capture the observed ‘pinching’ and degrading stiffness (upon reloading) behaviors. The relationship is illustrated in Figure 6.4. Mitch notes that the maximum proportional rotation for the column occurs at 0.05 radians (θ_{1P}), which corresponds to a moment of 1215 N-m (M_{1P}). Values of the model parameters shown in Figure 6.4 used in this study are given in Table 6.4. Based on the dominance of the base rotation behavior and observed experimental behavior, the culms were modeled using the elastic properties given in Table 6.2.



a) hysteretic model (adopted from Carr 2002)



b) hysteretic behavior model input

Figure 6.4 Bilinear hysteretic material model input parameters for *OpenSees*.

Table 6.4 *OpenSees* hysteretic model parameters.

	M_{1p}	θ_{1p}	M_{2p}	θ_{2p}	β	$2K_0$
	N-m	rad	N-m	rad	--	N-m
base spring	1215	0.02	1215	0.05	0	24,308

6.2 SEISMIC INPUT PARAMETERS

6.2.1 Ground Motion Suite for NE India

Ground motion records are available globally, especially for major earthquakes, however for remote regions and those experiencing only moderate or rare events, very little or no ground motion data may be available. If data is unavailable, synthetic ground motion records can be generated using different methods that utilize predefined response spectra and regression analysis to create a ground motion suite (Hu et al. 1996). The primary objective of this section, however, is to obtain an accurate representative seismic demand spectra for the region under investigation. Demand spectra from the National Building Code of India (NBCI) (2005) and those generated from the limited ground motion records available for northeastern India will be used for this purpose.

The horizontal seismic design spectra from the NBCI (2005) is represented by the design horizontal acceleration spectrum value, A_h , which is a function of the site zone factor, importance factor, response reduction factor, and the average response acceleration based on the soil type, natural period and 5% damping; this is similar to the ASCE 7 (2005) response spectra approach. The NBCI also notes that the design vertical acceleration spectrum may be represented as two-thirds of the horizontal acceleration spectrum, A_h , although vertical accelerations are not considered in the present work. The Darjeeling – Gangtok region is located in Indian Seismic Zone IV. Jayanetti (2004) noted the design spectrum for the IPRITI and TRADA (UK) full-scale test (see Section 3.1) was obtained from Indian Standard 1893: Criteria for Earthquake Resistant Design of Structures (1984). The test design spectrum was based on a seismic zone IV having 5% damping and was located on soft soil.

Representative ground motions from the region were not available to the author. The closest station on the Incorporated Research Institutions for Seismology (IRIS) network is the Lhasa (LSA) station in Tibet, approximately 416 km northeast of Darjeeling. To allow comparison to the work of others, ground motion records from the 1995 Kobe (PEER record 1043) and 1994 Northridge (PEER record 0935) earthquakes (shown in Figure 6.10a and Figure 6.11a, respectively), in addition to those developed based on NBCI spectra (see below) were used. In this manner, the model is comparable to the IPRITI and TRADA (UK) full-scale shake table tests reported by Jayanetti (2004).

Pal et al. (2008) used GIS to create an earthquake hazard zonation of the Sikkim Himalayas. The authors noted that the 2002 Bureau of Indian Standards (BIS) classifies peak ground acceleration, with 10 % probability of exceedance in 50 years, for Zone IV as 0.25g and Zone V as 0.40g. Pal et al. also notes the shear wave velocity (β_s) as 700 – 1500 m/s for soil

Zone IC and 350–700 m/s for Zone II; these are equivalent to ASCE 7-05 Site Classes B-C and C-D, respectively. The Mungpoo (see Section 3.2) site classification is assumed to fall between ASCE Site Classes B and C due to the presence of hard greenschist upon which the grade beam foundations bear (confirmed during 2008 site visit). Nath et al. (2000) describe the microzonation of Sikkim and the generation of representative ground motions based on the seismological characteristics of the region. Nath (2004, 2005) also incorporated GIS mapping to generate seismic microzonation maps of Sikkim. Nath et al. (2008) produced artificial ground motion suites for a $M_W = 8.3$ for Jorhang, Sikkim, shown in Figure 6.5. The Nath et al. simulation is based on records of the December 2, 2001 event at the same location having a magnitude: $M_L = 5.6$. The data for the original and artificial events are not available to the author, however the similarity between the artificial event shown in Figure 6.5 and those used in this study, particularly the Northridge event (Figure 6.11a), is noted. Data for the northeast region of India is difficult to obtain.

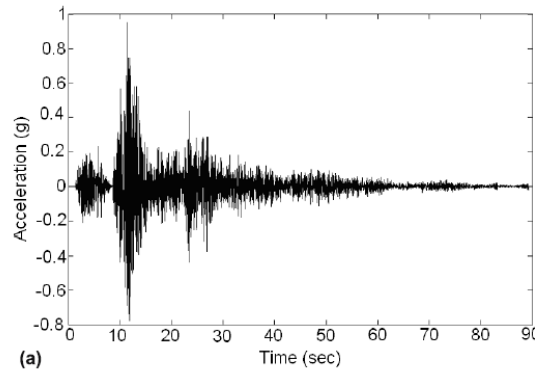


Figure 6.5 Artificial accelerogram for the MW 8.3 scenario earthquake located at Jorhang (Nath et al. 2008).

6.2.2 Response Spectra

Using the values of peak ground acceleration and the Site Classes described above, design level response spectra were developed using the methods of ASCE 7 (2005) and NBCI (2005). In the NBCI, a factor of 0.5 is used to reduce the maximum considered earthquake (MCE) to a design basis earthquake (DBE). The ratio of the peak short period ground acceleration to peak ground acceleration at 1 second period (S_s/S_1) was assumed to be 2.5 to obtain the equivalent S_{DS} and S_{D1} design values. Based on these values, the response spectra were calculated for zones IV and V and site class C (Figure 6.6).

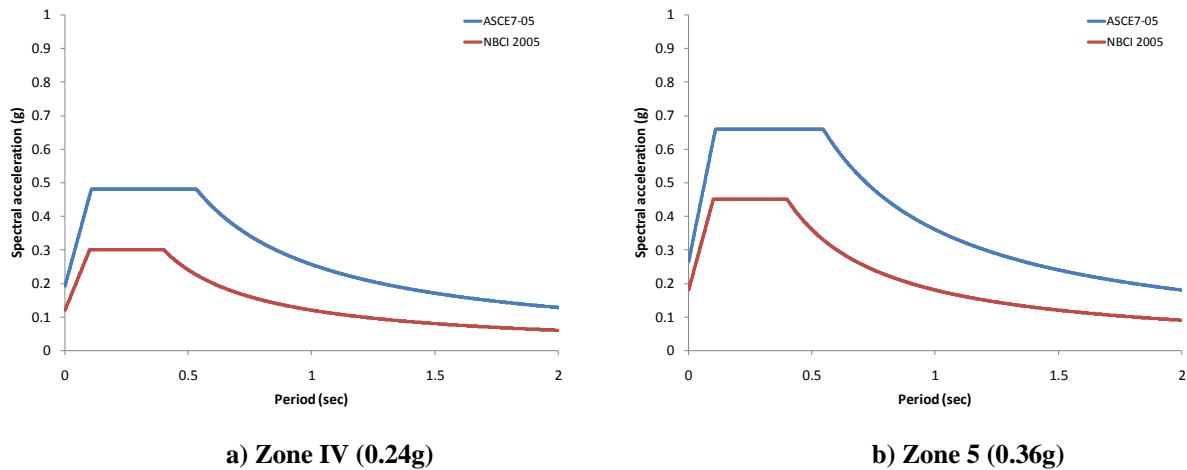


Figure 6.6 Spectral acceleration based on ASCE 7-05 and NBCI (2005) for site class C.

6.2.3 Artificial Ground Motion

Using the more conservative ASCE 7 spectra, artificial ground motion records designed to match the spectra shown in Figure 6.6 were generated using the program SIMQKE (Carr 2002). The SIMQKE manual notes the program's ability to generate statistically independent artificial acceleration time histories and tries, by iteration, to match the specified response spectrum (Carr 2002). To generate the records, a compound intensity envelope, shown in Figure 6.7, was used.

The input values are shown in the figure and are based on typical records such as that shown in Figure 6.5. The resulting two artificial ground motions and their calculated and target spectra are shown in Figure 6.8.

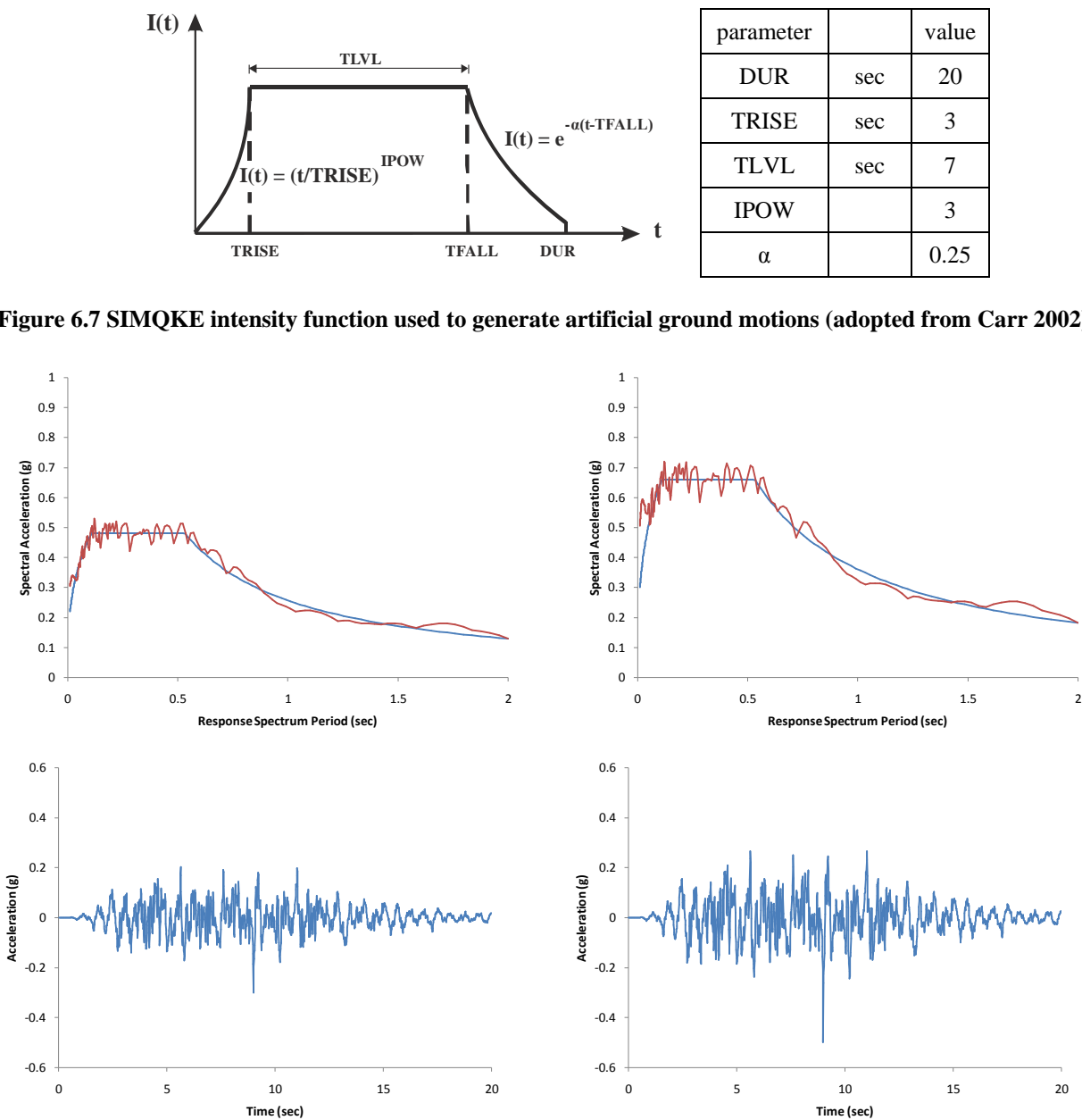


Figure 6.8 Response spectrum and artificial ground motions generated by SIMQKE.

6.3 SEISMIC ANALYSIS

6.3.1 Nonlinear Static (Pushover) Analysis

A pushover analysis on the Mungpoo (*Bambusa nutans*) model that included the effects of gravity load was first performed. The lateral load was applied at the left column-lateral joints (nodes 2 & 15; see Figure 6.1). The pushover was conducted until the equivalent modulus of rupture load at the column bases was reached. The modulus of rupture was taken as 53 MPa (Ahmad 2000), and the ultimate lateral displacement of a single culm corresponded to an applied pushover load of approximately 400 N.

The base shear versus lateral drift results for pushover analysis is shown in Figure 6.9. The symmetric frame results in an essentially bilinear behavior which approximates that observed experimentally (Figure 3.25). The response remains elastic until a lateral drift of 101 mm, which corresponds to a lateral drift ratio of 3.5%. The relatively stiff ‘post-yield’ (or secondary stiffness) response reflects the considerable reserve flexural capacity of the column section as compared to the base rotation behavior.

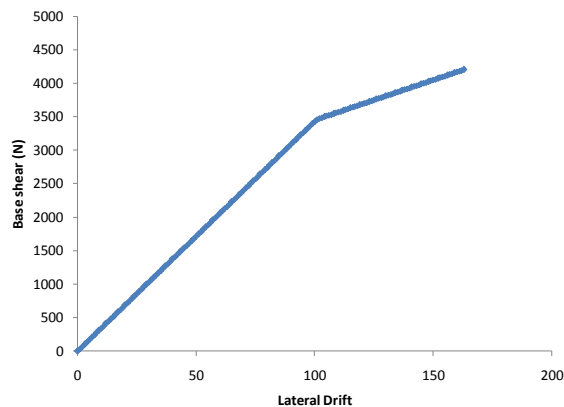


Figure 6.9 Nonlinear static analysis results for Mungpoo frame.

6.3.2 Nonlinear Dynamic Analysis

A nonlinear dynamic analysis was conducted using *OpenSees* (Mazzoni et al. 2009). The dynamic analysis included Newton-Raphson tangent stiffness iteration and an integration method based on the Newmark average acceleration method. The model included 5% Rayleigh proportional damping. The four ground motion histories (Kobe, Northridge and two artificial events) were applied to the model. The lateral drift was recorded at the left outside column- joint (node 2). The base shear was measured at the culm bases (nodes 1, 7, 10, and 3).

6.4 PERFORMANCE ASSESSMENT

Based on the seismic analysis conducted, the roof drift was investigated as the engineering demand parameter for the performance assessment. As is shown, the model remained essentially elastic through all analyses indicating generally excellent performance of the prototype structure.

6.4.1 Nonlinear Dynamic Response

The results from the nonlinear dynamic analyses are presented in Figure 6.10 through Figure 6.13. Shown in these figures are: a) the input ground motion; b) the base shear-drift hysteresis; c) the drift time history; and d) the base shear time history. A summary of key performance criteria is presented in Table 6.5. The maximum drift ratio occurred in the Kobe event (Figure 6.10) at 0.50%. The lowest lateral drift ratio was 0.06% in the Indian seismic zone IV event (Figure 6.12). The seismic response coefficient, C_s , (shown in Table 6.5) is the proportion of the structural mass, W , represented by the base shear (i.e.: $V_{\text{base}} = C_s W$). This value ranged from

1.1% to 8.6% for the analyses conducted. The analyses indicated that the dynamic response for all four events was within the linear lateral drift response shown in Figure 6.9. The hysteresis shown in Figure 6.10 to Figure 6.13b reflects the 5% damping selected. As noted above, this value is felt to be appropriate for this modeling effort.

Table 6.5 Nonlinear dynamic response of the Mungpoo frame.

Event	Maximum base shear	Maximum seismic response coefficient	Maximum lateral drift	Maximum lateral drift ratio
	V_{\max} (N)	C_s	Δ (mm)	Δ (%)
Kobe	439.5	0.086	14.3	0.50
Northridge	251.6	0.049	7.91	0.28
Zone IV	56.6	0.011	1.84	0.06
Zone V	80.0	0.016	2.61	0.09

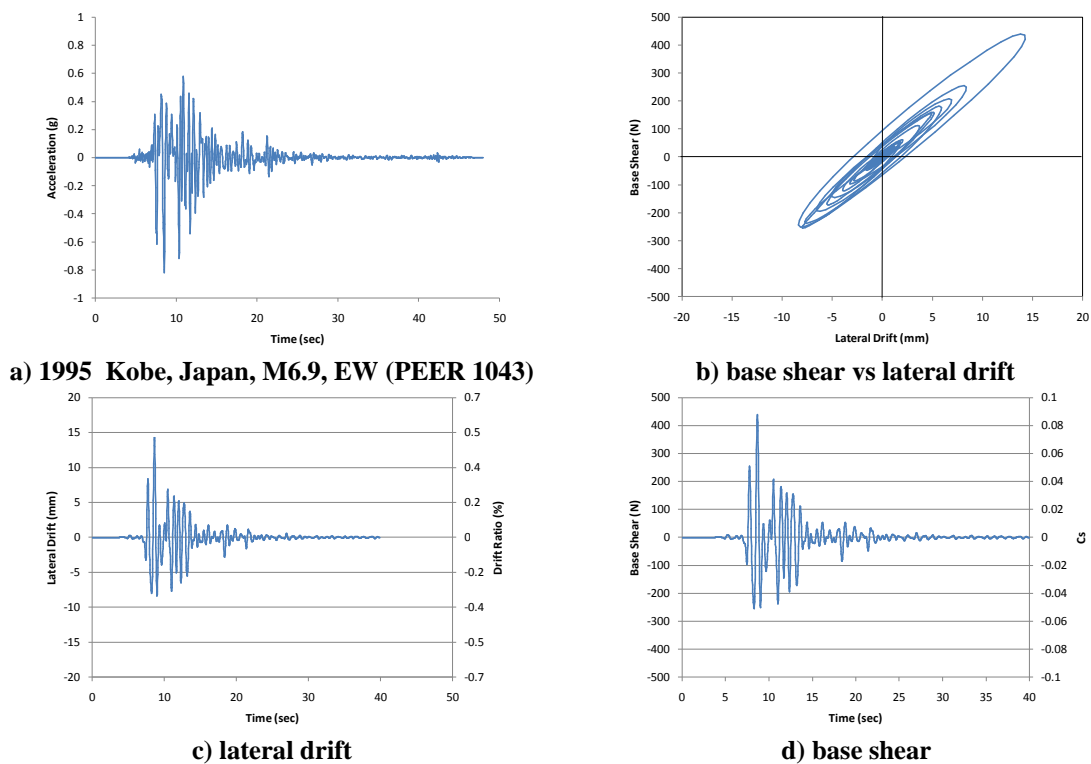
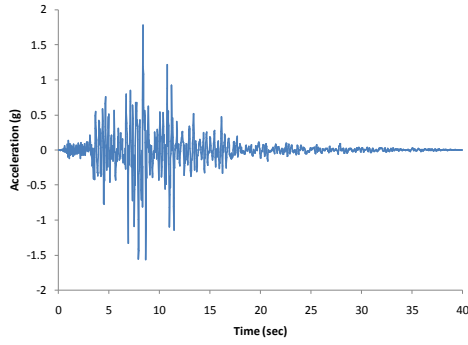
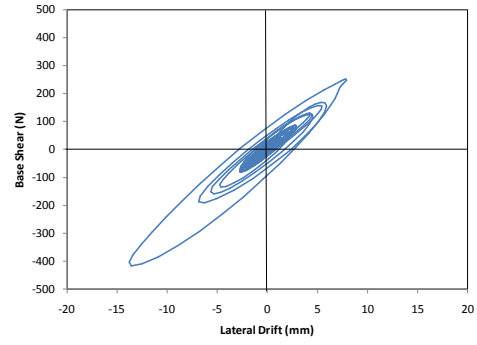


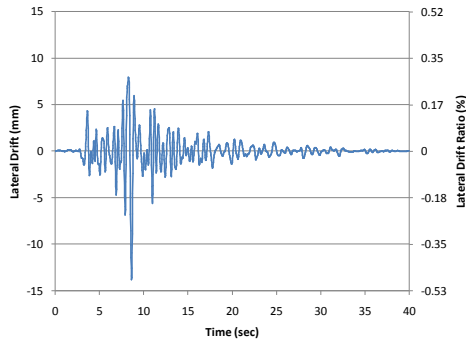
Figure 6.10 Kobe earthquake results.



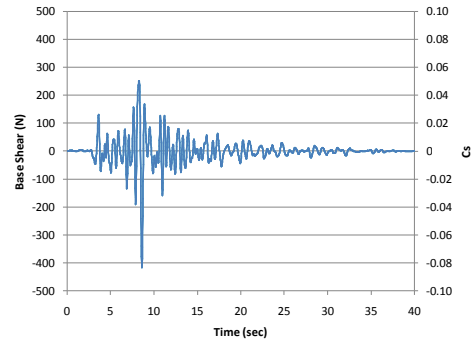
a) 1994 Northridge, California, M6.7, NS (PEER 0935)



b) base shear vs lateral drift

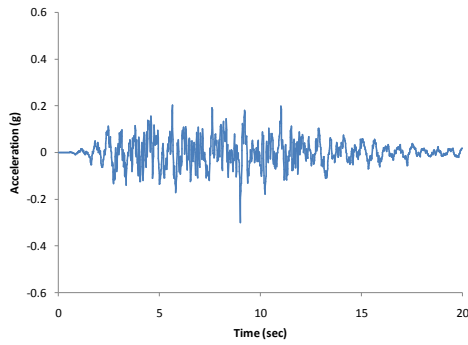


c) lateral drift

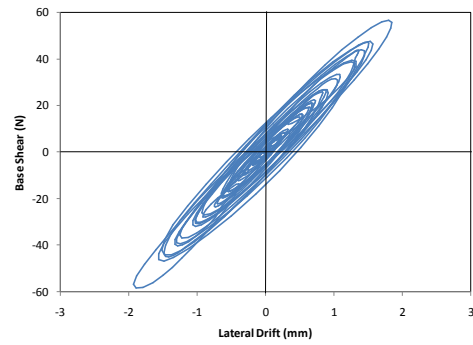


d) base shear

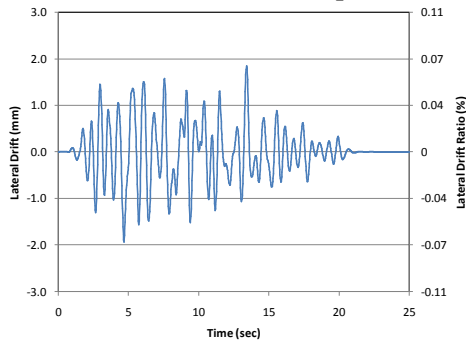
Figure 6.11 Northridge earthquake results.



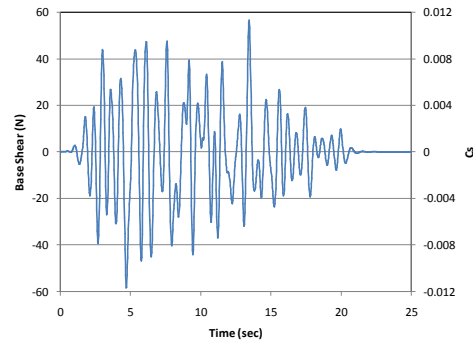
a) India Zone IV earthquake



b) base shear vs lateral drift



c) lateral drift



d) base shear

Figure 6.12 India Zone IV earthquake results.

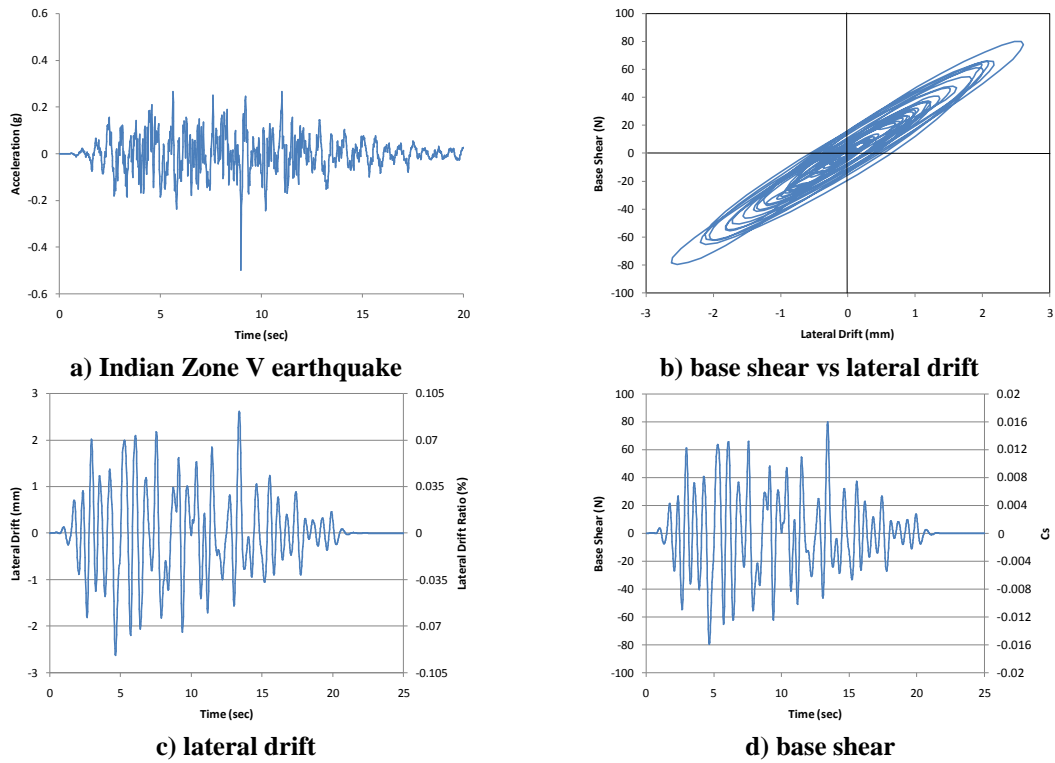


Figure 6.13 India Zone V earthquake results.

6.4.2 Capacity vs. Demand

The capacity spectrum method defines ‘performance points’ as the intersection of the capacity and the demand curves. The capacity curve is obtained by transforming the acceleration response spectrum (Figure 6.6) to an acceleration displacement response spectrum. The conversion is affected as follows (Shinozuka et al. 2000b):

$$S_d = \frac{S_a T^2}{(2\pi)^2} \quad (\text{Eq. 6.3})$$

For the demand curve, the conversion is (Shinozuka et al. 2000b):

$$S_a = \frac{V}{W\alpha} \quad (\text{Eq. 6.4})$$

$$\alpha = \frac{(\sum m_i \phi_i)^2}{\sum m_i \sum m_i \phi_i^2} \quad (\text{Eq. 6.5})$$

$$S_d = \frac{\Delta_i}{\Gamma} \quad (\text{Eq. 6.6})$$

$$\Gamma = \frac{\sum w_i \varphi_i}{\sum w_i \varphi_i^2} \quad (\text{Eq. 6.7})$$

Where: V = total base shear; W = total weight; m_i = mass at i^{th} floor; φ_i = the modal amplitude at i^{th} floor; Δ_i = lateral displacement at i^{th} floor; and w_i = weight at i^{th} floor. Since this structure is essentially a single degree of freedom problem, $\alpha = 1$ and $\Gamma = 1/\varphi_i$. Thus:

$$S_a = \frac{V}{W} \quad (\text{Eq. 6.8})$$

$$S_d = \Delta_i \varphi_i \quad (\text{Eq. 6.9})$$

The modal amplitude at node 2 was obtained from *OpenSees* as 0.042 for the first mode shape. The resulting capacity-demand spectrum is shown in Figure 6.14. The intersection of the capacity and demand curves represents the performance point.

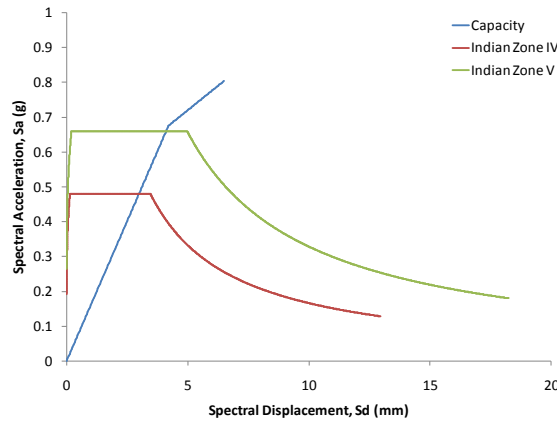


Figure 6.14 Capacity vs. demand curve in ADRS format.

While the performance point is clearly located within serviceability limits (see Figure 6.9), there is not enough information to adequately define the typical performance categories of immediate occupancy (IO), life safety (LS) and collapse prevention (CO). The performance points occur at lateral displacements of 3.10 mm and 4.21 mm for Zones IV and Zones V, respectively. These values correspond to drift ratios of 0.11% and 0.15%, respectively.

6.4.3 Effect of Species Selection and Variation of Material Properties

Based on the results in Chapter 5.0 , three random normal-distribution material property samples for *Dendrocalamus giganteus* and *Phyllotstachys aurea* were generated using Minitab (2008). The only material property generated for the model was the compressive modulus, E, of each species. Both species were limited to a single source for the material property, (Ghavami and Marinho (2001) and water treated Cruz (2002), respectively), as discussed in Chapter 5.0 . To create nominally identical and statistically different models, the material properties would typically be the only variation between models. For bamboo, however, the material properties are a function of the geometry, and thus cannot be separated from geometry.

For the geometric properties, it is difficult to ascertain the variability in the measurements from the individual studies, therefore the full culm geometrical properties associated with the respective studies (Table 5.5) were utilized in the model and remained the same for all three samples. For the *P. aurea* samples, the geometrical properties from the frame test (Chapter 3.0) were used.

In this analysis, the frame geometry remains the same (Figure 6.1) and the bamboo species is varied. *D. giganteus* would result in a larger culm size having significant variation in material properties. *P. aurea*, on the other hand, is more comparable in size to the *B. nutans* used in the Mungpoo model described in the previous sections, although it is significantly stiffer and demonstrates much less variation of material properties. A summary of the culm geometric and material properties used is given in Table 6.6.

Table 6.6 Summary of geometric and material properties for parametric analysis.

Species	Constant geometric properties					Varying material properties				
	Culm	D _o (mm)	t (mm)	A _{culm} (mm ²)	I _{culm} (mm ⁴)	Analysis ID	E _c (MPa)	K _θ (N-m)	M (N-m)	T _n (sec)
<i>B. nutans</i>	Mungpoo ¹	80.0 ²	15.00	3063	1,703,823	Mungpoo ¹	10,700	2346	235	0.817
		70.0 ³	10.00	1885	871,792			-	-	
<i>D. giganteus</i>	DG	103.2 ²	9.00	5328	2,983,158	DG1	19,400	38582	3858	0.508
						DG2	20,800	41367	4137	0.491
		90.0 ³	8.50	2176	1,826,628	DG3	28,100	55885	5589	0.422
<i>P. aurea</i>	PA	50.0 ²	4.50	1287	168,087	PA1	33,104	3710	371	1.454
						PA2	30,591	3428	343	1.512
		40.0 ³	4.75	526	83,185	PA3	32,563	3649	365	1.466

¹ parameters from Mungpoo model presented in previous sections (Table 6.2) presented here comparison

² vertical culms

³ horizontal culms

The analysis utilizes the four ground motion suites presented previously. As illustrated by the fundamental period (T_n) of each model shown in Table 6.6, the models considered resulted in significantly stiffer (*D. giganteus*) and more flexible (*P. aurea*) behavior than the *B. nutans* Mungpoo model. The results of these analyses are summarized in Table 6.7 and Table 6.8. The final column in each table provides the ratio of the values obtained from the parametric analyses with those from the Mungpoo model.

Table 6.7 Summary of parametric analysis of material properties for *D. giganteus*.

		DG1	DG2	DG3	\bar{x}	s	COV (%)	$\frac{\bar{x}}{\text{Mungpoo}}$
Kobe	V (N)	332.7	323.7	288.5	315.0	23.34	7	1.24
	C_s	0.07	0.06	0.06	0.06	0.00	7	0.72
	Δ (mm)	4.3	3.90	2.61	3.61	0.88	24	0.25
	Δ (%)	0.15	0.14	0.09	0.13	0.03	24	0.25
Northridge	V (N)	332.8	333.8	310.7	325.8	13.09	4	1.29
	C_s	0.07	0.07	0.06	0.06	0.00	4	1.30
	Δ (mm)	5.0	4.73	3.44	4.40	0.85	19	0.56
	Δ (%)	0.18	0.17	0.12	0.15	0.03	19	0.55
Indian Zone IV	V (N)	66.4	53.6	53.3	57.7	7.48	13	1.02
	C_s	0.01	0.01	0.01	0.01	0.00	13	0.10
	Δ (mm)	0.94	0.71	0.54	0.73	0.20	28	0.40
	Δ (%)	0.03	0.02	0.02	0.03	0.01	28	0.43
Indian Zone V	V (N)	65.1	66.5	65.2	65.6	0.81	1	0.82
	C_s	0.01	0.01	0.01	0.01	0.00	1	0.80
	Δ (mm)	1.07	0.87	0.65	0.87	0.21	24	0.27
	Δ (%)	0.04	0.03	0.02	0.03	0.01	24	0.28

Table 6.8 Summary of parametric analysis of material properties for *P. aurea*.

		PA1	PA2	PA3	\bar{x}	s	COV (%)	$\frac{\bar{x}}{\text{Mungpoo}}$
Kobe	V (N)	260.5	257.0	262.2	259.9	2.68	1	1.02
	C_s	0.05	0.05	0.05	0.05	0.00	1	0.59
	Δ (mm)	25.79	31.80	26.35	27.98	3.32	12	1.96
	Δ (%)	0.90	1.12	0.92	0.98	0.12	12	1.96
Northridge	V (N)	187.2	171.1	186.2	181.5	9.06	5	0.72
	C_s	0.04	0.03	0.04	0.04	0.00	5	0.72
	Δ (mm)	18.45	21.17	18.62	19.42	1.52	8	2.45
	Δ (%)	0.65	0.74	0.65	0.68	0.05	8	2.43
Indian Zone IV	V (N)	59.5	70.3	60.1	63.3	6.09	10	1.12
	C_s	0.01	0.01	0.01	0.01	0.00	10	0.11
	Δ (mm)	5.88	8.80	6.04	6.90	1.64	24	3.75
	Δ (%)	0.21	0.31	0.21	0.24	0.06	24	4.04
Indian Zone V	V (N)	80.5	95.4	81.4	85.7	8.35	10	1.07
	C_s	0.02	0.02	0.02	0.02	0.00	10	1.05
	Δ (mm)	7.95	11.92	8.17	9.35	2.23	24	2.93
	Δ (%)	0.28	0.42	0.29	0.33	0.08	24	2.98

6.4.4 Results

The results presented in Table 6.6 and Table 6.7 indicate that the *D. giganteus* samples resulted in base shear close to those of the Mungpoo (*B. nutans*) model. The displacements, however, are less than the Mungpoo model, reflecting the stiffer structure. In the *P. aurea* specimens the lateral displacement is significantly larger, 1.96 to 3.75 times greater than the Mungpoo model as expected for the more flexible structure. Since the frames considered are relatively simple and are responding in an essentially elastic manner to the excitation considered, the variability inherent in the material properties is reflected in the structural response. As can be seen in Table 6.6, the response of the *D. giganteus* model shows considerable variability in its response, reflective of the material variability (Chapter 5.0 for this species).

Figure 6.15 compares the resulting capacity-demand spectrum for all of the models. The figure reflects the range in the natural period, with the lines representing the *D. giganteus*, *B. nutans* (Mungpoo), and *P. aurea* samples in order of increasing period. The variability inherent in the material properties is evident in the range of the resulting performance points for each species.

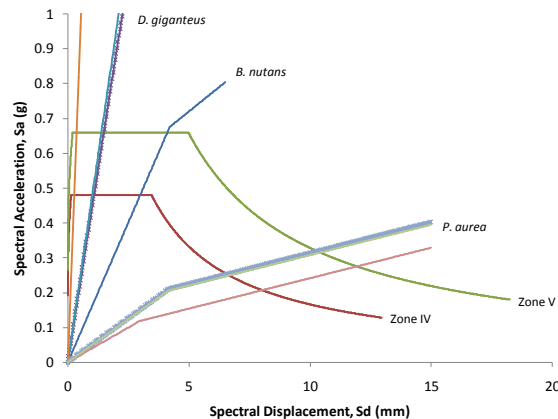


Figure 6.15 Capacity-demand spectrum for all models.

6.5 FRAGILITY FUNCTIONS

The basis for formulation of fragility curves is a lognormal cumulative distribution function (CDF) of building performance as a function of the seismic demand (Porter et al. 2007). Performance, in this case is subjective, and may be roughly defined as a damage level. Typically, fragility curves are based on experimental data or observations. For marginally and non-engineered structures, however, previous studies and data are limited. Formulation of fragility functions would therefore need to be based on derived fragility functions, established using an analytical model (Nielson and DesRoches 2003; Ellingwood et al. 2004; Kim and Rosokowsky 2005).

To create fragility functions, the response of the structure is obtained from a series of analyses. The damage to the individual components is evaluated and the capacity is determined from the response analysis (Aslani and Miranda 2005). Evaluation of the method of failure for the components is conducted to ascertain which damage indices adequately describe the damage to the component. The seismic demand is based on ground motion representative of the site under investigation. The assumptions and approximations in the model create uncertainty in the analyses. Material properties, structural configurations, the placement of nonstructural elements, as well as the ground motion suite can all contribute to this uncertainty (Aslani and Miranda 2005; Nielson and DesRoches 2003). Uncertainty can be addressed through generalizations of parameters or a more detailed analysis can be performed (Porter et al. 2007). The accuracy of the model may then be verified through exploration of the effect of uncertainty on the probability function. With considerably greater experimental and/or observational data (see Section 7.5), the described approach, using a probabilistic framework, may be appropriate for evaluation of the

seismic performance of bamboo structures. This would then establish a foundation for development of a reliability based method for design of bamboo structures.

The present work explored the parameters necessary to create analytically based fragility curves. While information on the seismic behavior of the frame was obtained, additional data is needed to establish the damage indices for a performance based design approach. Existing standards, such as lateral drift limits (ASCE 7 2005), are not necessarily directly applicable to bamboo structures: as has been seen, bamboo frame structures can undergo considerable drift without ‘structural’ damage. The established limit states, or damage measures, must reflect the material, the overall frame behavior, in addition to socio-cultural considerations and perspectives.

6.6 SUMMARY

A nonlinear model was created in *OpenSees*. Based on Mitch (2010), a rotational spring boundary condition was created to capture the observed rigid body behavior of the column bases. The model was validated by comparison to the experimental results presented in Chapter 3.0 . Once the model was validated, a static pushover and nonlinear dynamic analyses were conducted on several models of the Mungpoo (*B. nutans*) prototype structure. Four ground motions were utilized for the dynamic analyses, the Kobe, Northridge, and artificial Indian Zone IV and V events. The analyses indicated that the dynamic response for all four events was within the linear lateral drift response. A parametric analysis on *D. giganteus* and *P. aurea* emphasized the dependency of the frame behavior on the frame stiffness. While varying the material and

geometric properties provided a good sample range in properties, additional information is needed to fully explore the influence of the properties on the overall frame behavior.

7.0 CONCLUSIONS

The objective of this dissertation is to describe a wide-ranging research program aimed at identifying a method through which vernacular bamboo construction methods may be formalized into a performance based design framework. This requires an understanding of both material and structural behavior and an appreciation of the social and engineering context in which the structure is built. To accomplish this objective, several studies were completed.

7.1 PROTOTYPE STRUCTURE

An experimental study of the prototype structure, considered throughout the dissertation, was conducted to learn about the prototype frame behavior. The prototype frame test provided significant details for the modeling tasks and the results provided input parameters for the *OpenSees* model. Additional material testing provided additional insight to the pull-out behavior of the column bases, demonstrating the resistance of the nodal walls to prevent pull-out failure. Also, the tensile testing provided additional input for the statistical analysis. In the course of the research program presented in Chapter 3.0 and in a parallel study (Mitch 2009), it was determined that certain mechanical properties of bamboo are not well established and furthermore that there is no standard method for comparing these critical properties.

7.2 CHARACTERIZATION OF DESIGN VALUES

Chapter 4.0 reported on an experimental program aimed at filling the gaps in comparing critical properties in available knowledge and data. Initially a fracture mechanics approach to quantifying bamboo behavior was attempted in an effort to normalize for the significant variation expected in a natural material. While this method was successful, it was not felt to be practical for application outside a well-equipped laboratory environment. Thus a simpler, mechanics-based, materials test was pursued and an attempt to correlate results from this with the more reliable fracture mechanics approach was made. The presented study investigated the splitting failure of bamboo of *Bambusa stenostachya* through three test methods: the bolt hole, edge bearing and split pin tests. The bolt hole test results were comparable to the split pin tests reported by Mitch et al. (2010) and indicated a decrease in ultimate bearing stress with decreasing angle, i.e.: loading oriented more transversely to the fibers. The edge bearing test was also compared to the split pin test and suggested that the edge bearing can be used as a surrogate for field tests to approximate the ultimate transverse tensile capacity of the culm, however additional work is required to fully investigate the correlation between the two test values.

7.3 STATISTICAL ANALYSIS OF BAMBOO PROPERTIES

The work presented in Chapter 5.0 considered data collected by the Group for Non-Conventional Materials (GNOCMAT) at PUC-Rio and the author's group at the University of Pittsburgh. In total, the data collected represents nine bamboo species, and a variety of geometric and mechanical properties. The sources present tests on a variety of bamboo species, however the available data sets are limited for most of the species. Only two species, *Phyllostachys aurea*

and *Dendrocalamus giganteus*, which represent the two data sets with the largest number of samples, were examined in detailed. Comparison of the two species assessed the significance of the statistical variability between these species and provided at least one benchmark for interspecies variation. The statistical analysis illustrated the inherent variability between and within data sources from two bamboo species. The statistical tests indicated that:

1. the source (the operator, testing parameters and conditions) has a significant effect on the variability of the data, thus data from different sources cannot be pooled and considered to be from the same population.
2. there is need for standardization of key parameters in testing and reporting bamboo mechanical properties.
3. for a complete statistical analysis, there is a need for greater published data on bamboo mechanical properties.
4. nonetheless, the majority of the data follows a normal distribution.

7.4 SEISMIC ANALYSIS

A model was successfully developed in *OpenSees* and validated against the experimental results presented in Chapter 3.0 . Pushover and dynamic analyses provided information on the capacity and the demand on the structure. Performance points were obtained and are clearly located within serviceability limits, however there is not enough information to adequately define the typical categories of immediate occupancy (IO), life safety (LS) and collapse prevention (CP). To fully develop fragility curves to demonstrate the performance of the bamboo portal frame structure, additional experimental work is needed, as discussed in section 7.5.

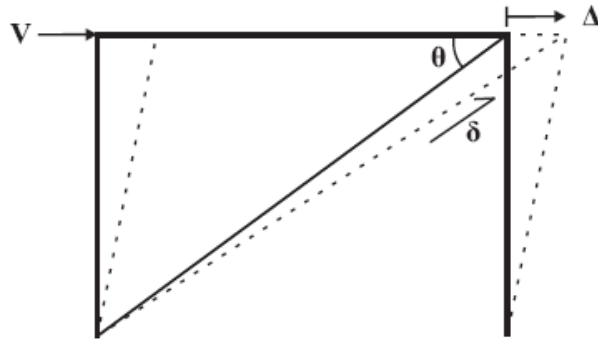
7.5 FUTURE WORK

7.5.1 Material Characterization

The inherent variability of bamboo geometric and material properties continues to be a disadvantage for engineering design. The variability, however, can be overcome with standardized testing and reporting methods that provide the necessary information to create engineering design standards. Additionally, testing methods, such as the edge bearing test discussed in Chapter 4.0, need to be fully developed. This test method provides a unique opportunity to obtain design values associated with the observed dominant bamboo behavior (splitting) and assess the potential of bamboo members in the field.

7.5.2 Panel Shear

The prototype bamboo portal test presented in Chapter 3.0 provided the basic input parameters for the seismic model. The model should, however, include the behavior of the frame with infill panels (Figure 7.1a). It is anticipated that the infill will not necessarily improve the overall behavior, but will alter the racking behavior of the frame. An experimental test program is proposed to obtain the shear capacity of the infill panels, shown in Figure 7.1c. The panels will be tested to obtain their overall stiffness that can be input into the model as a pin-ended brace (Figure 7.1d). The model will more accurately describe the structural behavior of the frame and is analogous to that used to model masonry infill walls (Madan et al. 1997).

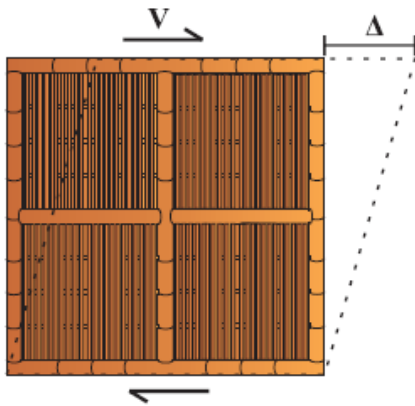


$$\delta = \Delta \cos \theta$$

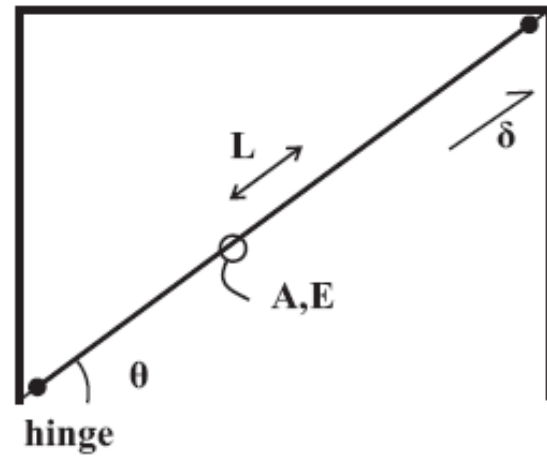
$$\frac{F}{\delta} = \frac{V / \cos \theta}{\Delta \cos \theta} = \frac{V}{\Delta \cos^2 \theta}$$

$$\frac{F}{\delta} = \frac{AE}{L} \rightarrow \frac{V}{\Delta \cos^2 \theta} = \frac{AE}{L}$$

a) pushover of bamboo portal frame



b) proposed experiment on infill panel



c) portal frame model

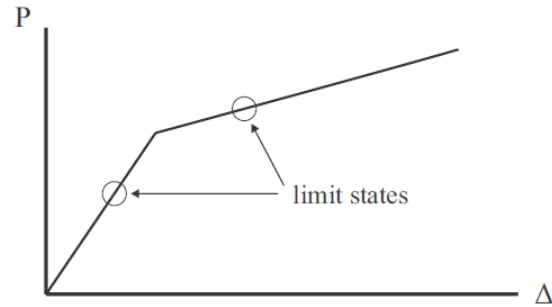
Figure 7.1 Portal frame analysis including bamboo infill.

7.5.3 Column-roof joint

An additional area for future work is the column-roof joint of the portal frame. The model presented in Chapter 6.0 did not include information on the degradation of this joint. As shown in Figure 7.2a, splitting failure is common in the bolted region of a multi-culm connection. By simplifying the connection for testing, a force-displacement relationship, shown in Figure 7.2b, can be obtained. Significant limit states such as bolt induced splitting, bamboo crushing, and block shear may be identified. The behavior will then be included in the model, and more importantly in the assessment of the capacity of the frame to determine its overall performance.



a) splitting failure observed at Mungpoo (Mitch 2009)



b) pushover curve for joint

Figure 7.2 Column-roof joint splitting failure and capacity curve.

7.6 SUMMARY

The work presented explored the seismic performance of bamboo structures. To develop the seismic model of the bamboo portal frame, parameters from the St. Joseph's school in Mungpoo, India were observed. Based on the observations, several experimental programs were undertaken. Additional material testing provided information about the global behavior of the frame, as well as the localized splitting failure of the full bamboo culm. To provide further input for the model, a statistical analysis of bamboo material properties was conducted on data sources from the NOCMAT group at PUC-Rio and work conducted at the University of Pittsburgh. The analysis demonstrated a normal distribution of the data sources investigated, as well as the need for standardized test and reporting methods.

Based on the input parameters developed in the experimental and statistical analysis, a seismic model of a bamboo portal frame was created in *OpenSees*. While the model provided information on the performance of the frame, additional experimental work is necessary to fully develop performance metrics. To establish the fragility curves to demonstrate the seismic performance, additional experimental work is needed to improve the model. The additional

information on the stiffness of the infill panels and the degradation of the column-roof joint will help to assess the overall behavior in event of an earthquake. The work established the need for additional testing and characterization of bamboo material properties to reduce the inherent variability to fully bring bamboo construction into engineering practice and design.

APPENDIX

DEFINITIONS AND ABBREVIATIONS

Definitions

culm	stem of bamboo, typically hollow although solid in some species
diaphragm	transverse interior section at node (see below)
fiber	cellulosic fibers
internode	region between two nodes in which fiber direction is longitudinal to axis of the culm
matrix	lignin that surrounds the fibers
node	region of bamboo culm where fibers are no longer only longitudinal and form a thickened section from which leaves and buds emerge
sympodial	root system from which culms emerge as shoots
wall	the radial thickness of the hollow cylinder

Abbreviations

ANOVA	analysis of variance
ASCE	American Society of Civil Engineers
ASTM	American Society for Testing and Materials
COV	coefficient of variation
DM	damage measure
EDP	engineering demand parameters
HAZUS	Hazards US
INBAR	International Network of Bamboo and Rattan
ISO	International Organization for Standardization
NBCI	National Building Code of India
PBD	Performance based design
PBSD	performance based seismic design
PGA	peak ground acceleration
STD DEV	standard deviation

CITED REFERENCES

- Agarwal, B.D. and L.J. Broutman (1990). *Analysis and Performance of Fiber Composites*, Second Edition. New York: Wiley.
- Ahmad, M. (2000). *Analysis of Calcutta bamboo for structural composite materials*. Doctoral Dissertation, Virginia Polytechnic Institute and State University.
- Ali, Z. (2007). *Sustainable Shelters for Post Disaster Reconstruction: An Integrated Approach for Reconstruction after the South Asia Earthquake*. Master's Thesis, Massachusetts Institute of Technology.
- Amada, S., Munekata, T., Nagase, Y., Ichikawa, Y., Kirigai, A. and Y. Zhifei (1996). The mechanical structures of bamboos in viewpoint of functionally gradient and composite materials. *Journal of Composite Materials*, **30**(7), pp. 800-819.
- Amada, S., Ichikawa, Y., Munekata, T., Nagase, Y. and Shimizu, H. (1997). Fiber texture and mechanical graded structure of bamboo. *Composites: Part B*, **28B**, pp. 13-20.
- Amada, S. and Untao S. (2001). Fracture properties of bamboo. *Composites: Part B*, **32**, pp. 451-459.
- Arce-Villalobos, O.A. (1993). *Fundamentals of the design of bamboo structures*. Master's Thesis, Eindhoven University of Technology, Netherlands.
- ASCE 7-05 (2005). *Minimum design loads for buildings and other structures*, ASCE 7-05. Reston, Virginia: American Society of Civil Engineers.
- ASCE 41-06 (2006). *Seismic Rehabilitation of Existing Buildings*, ASCE 41-06. Reston, Virginia: American Society of Civil Engineers.
- Aslani, H. and Miranda, E. (2005). Fragility Assessment of Slab-Column Connections in Existing Non-Ductile Reinforced Concrete Buildings, *Journal of Earthquake Engineering*, **9**(6), pp. 777-804.
- ASTM D2733-70 (1976). *Method of Test for Interlaminar Shear Strength of Structural Reinforced Plastics at Elevated Temperatures*. West Conshohocken, PA: ASTM International.

- ASTM D2915 (2003). *Standard Practice for Evaluating Allowable Properties for Grades of Structural Lumber*. West Conshohocken, PA: ASTM International.
- ASTM E177 (2008). *Standard Practice for Use of the Terms Precision and Bias in ASTM Test Methods*. West Conshohocken, PA: ASTM International.
- ATC-58 (Applied Technology Council) (2007). *Guidelines for Seismic Performance Assessment of Buildings 35% Complete Draft*. Redwood City, California: Applied Technology Council.
- Bamboostic (2004). Photos of Community Center, Camburi, Brazil. <<http://bamboostic.eu>>
- Barbero, E., Fernandez, J. and C. Navarro (2000). Statistical analysis of the mechanical properties of composite materials. *Composites Part B: Engineering*, **31**(5), pp. 375-381.
- Bilham, R., Gaur, V.K. and Molnar, P. (2001). Himalayan Seismic Hazard. *Science*, **293**(5534), pp. 1442-1444.
- British Standards (2002). *Structural use of timber, Code of practice for permissible stress design, materials and workmanship, BS 5268-2:2002*. United Kingdom: British Standards.
- Brown, J.L. (2004) Bamboo House Passes Seismic Test. *Civil Engineering*, November, p. 27.
- Carr, A.J. (2002). *RUAUMOKO: Inelastic Dynamic Analysis 2-Dimensional Version*. Department of Civil Engineering, Christchurch, New Zealand: University of Canterbury.
- Civil Engineering (2006). The Widening Gulf. *Civil Engineering Magazine*, American Society of Civil Engineers, **76**(8), pp. 56-61.
- Cooper B.E. (1969). *Statistics for experimentalists*. Oxford, UK: Pergamon.
- Cruz, M.L.S. (2002). *Caracterização física e mecânica de colmos inteiros do bambu da espécie phyllostachys aurea: comportamento à flambagem* (in Portuguese). Master's Thesis, Pontifícia Universidade Católica – Rio de Janeiro.
- Culzoni, R.A.M. (1985). *Características dos bambus e sua utilização como material alternativo no concreto* (in Portuguese). Master's Thesis, Pontifícia Universidade Católica.
- Devore, J.L. (2000). *Probability and statistics for engineering and the sciences*. Pacific Grove, CA: Duxbury.
- Ellingwood, B.R. et al. (2004). Fragility Assessment of Light-Frame Wood Construction Subjected to Wind and Earthquake Hazards. *Journal of Structural Engineering*, **130**(12), pp. 1921–1930.
- Faber Maunsell (2005). *Madras Project Feasibility Study*. United Kingdom: Faber Maunsell/AECOM.
- Finch, P. (2005). Coded for Design. *Architectural Review*, July, p. 28.

- Ghavami, K. and Moreira, L.E. (1996). Development of a new joint for bamboo space structures. *Proceedings of Mobile and Rapidly Assembled Structures II: Second International Conference on Mobile and Rapidly Assembled Structures*, **24**, pp. 201-210.
- Ghavami, K. and A.B. Marinho. (2001). *Determinação das propriedades mecânicas dos bambus das espécies: moso, matake, Guadua angustifolia, guadua tagoara e Dendrocalamus giganteus, para utilização na engenharia* (in Portuguese). Rio de Janeiro: PUC-Rio, Publicação RMNC-1 Bambu 01/2001.
- Ghavami, K. and A.B. Marinho. (2002). *Propriedades mecânicas dos colmos dos bambus das espécies: moso e guadua angustifolia para utilização na engenharia* (in Portuguese). Rio de Janeiro: PUC-Rio, Publicação RMNC-2 Bambu 02/2002.
- Ghavami, K., Allameh, S., Cruz, M.L.S. and Soboyejo, W.O. (2003a). Multiscale study of bamboo *Phyllostachys edulis*. *Proceedings of the First Inter American Conference on non-Conventional Materials and Technologies in the Eco-Construction and Infrastructure - IAC-NOCMAT 2003*.
- Ghavami, K., Rodrigues, C.S., and Paciornik, S. (2003b). Bamboo: Functionally Graded Composite Material. *Asian Journal of Civil Engineering (Building and Housing)*, **4**(1), pp. 1-10.
- Ghavami, K. (2005). Bamboo as reinforcement in structural concrete. *Cement and Cement Composites*, **27**, pp. 637-649.
- Guatibonza, C.A.R. (2009). *Determinação experimental da tenacidade do bamboo do modo I (KIC) e modo II (KIIC)*(in Portuguese). Master's Thesis, Pontifícia Universidade Católica.
- Gutierrez, J. (2004). Notes on the Seismic Adequacy of Vernacular Buildings. *Proceedings of the 13th World Conference on Earthquake Engineering*, Vancouver, B.C., Canada, Paper No. 5011.
- Guzman, D. and Morel, C. (2005). Connections and Slab for Bamboo Constructions. *Proceedings of the proceedings for the 2005 World Sustainable Building Conference*, Tokyo, Paper No.09-036.
- HAZUS (2003). *Earthquake loss estimation methodology*. Technical Manual, Washington D.C.: National Institute of Building for the Federal Emergency Management Agency.
- Hu, Y. et al. (1996). *Earthquake Engineering*. London, UK: E & FN SPON Ltd.
- ICBO (2000). Acceptance Criteria for Structural Bamboo (Acc 162). California: ICBO Evaluation Service Ltd.
- Inoue, M., Nakhara, M. et al. (2004). Development of Connecting Method for Natural Round Bamboo. *Proceedings for the World Conference on Timber Engineering*, p.331.

- INBAR (1999). In International Model Building Code for Bamboo, ed. Dr. Jules J. A. Janssen. Beijing: The International Network on Bamboo and Rattan.
- IS 1893 (1984). *Criteria for Earthquake Resistant Design of Structures* Indian Standard 1893. New Delhi, India: Bureau of Indian Standards.
- IS 6874 (1973). *Method of tests for round bamboos* IS: 9096-1973. New Delhi, India: Bureau of Indian Standards.
- IS 8242 (1976). *Methods of tests for split bamboos* IS: 8242-1976. New Delhi, India: Bureau of Indian Standards.
- IS 9096 (1979). *Code of practice for preservation of bamboos for structural purposes* IS: 9096-1979. New Delhi, India: Bureau of Indian Standards.
- ISO (International Organization for Standardization) (2004a). *International Standard ISO 22156:2004 (E), Bamboo – Structural Design*. Geneva, Switzerland: ISO.
- ISO (International Organization for Standardization) (2004b). *International Standard ISO 22157-1:2004 (E), Bamboo – Determination of Physical and Mechanical Properties – Part I: Requirements*. Geneva, Switzerland: ISO.
- ISO (International Organization for Standardization) (2004c). *International Standard ISO 22157-2:2004 (E), Bamboo – Determination of Physical and Mechanical Properties – Part II: Laboratory Manual*. Geneva, Switzerland: ISO.
- Janssen, J. (1981). *Bamboo in Building Structures*. Doctoral Thesis, Eindhoven University of Technology, Netherlands.
- Janssen, J.A. (2005). International Standards for Bamboo as a Structural Material. *Structural Engineering International*, **15**(1), pp. 48-48.
- Jayanetti, L. (2004). *Seismic testing of a bamboo based building system*. Buckinghamshire, UK: TRADA International.
- Kaushik, H. B., Dasgupta, K., Sahoo, D. R., and Kharel, G. (2006). Performance of Structures during the Sikkim Earthquake of 14 February 2006, *Current Science*, **91**(4), pp. 449-455.
- Kim, J.H. and Rosokowsky, D.V. (2005). Fragility Analysis for Performance-Based Seismic Design of Engineered Wood Shearwalls. *Journal of Structural Engineering*, **131**(11), pp. 1764–1773.
- Krause, J. (2009). *Desenvolvimento de elementos especiais de bambu para treliças espaciais* (in Portuguese). Master's Thesis, Pontifícia Universidade Católica.
- Laroque, P. (2007). *Design of a Low Cost Bamboo Footbridge*. Master's Thesis, Department of Civil and Environmental Engineering, Massachusetts Institute of Technology (MIT).

- Li, Y. and Ellingwood, B. (2007). Reliability of woodframe residential construction subjected to earthquakes. *Structural Safety*, 29, pp.294-307.
- Liese, W. (1998). *The anatomy of bamboo culms*. Beijing: International Network for Bamboo and Rattan.
- Liese, W. and Kumar, S. (2003). *Bamboo Preservation Compendium*. New Delhi, India: Center for Indian Bamboo Resource and Technology.
- Lobovikov, M., Paudel, S., Piazza, M., Ren, H., and Wu, J. (2007). *World Bamboo Resources: A thematic study prepared in the framework of the Global Forest Resources Assessment 2005*. Rome, Italy: Food and Agriculture Organization (FAO) of the United Nations.
- Low, I.M., Che, Z.Y. and Latella, B.A. (2006). Mapping the structure, composition and mechanical properties of bamboo. *Journal of Material Research*, **21**(8).
- Madan, A., Reihorn, A.M., Mander, J.B., and Valees, R.E. (1997). Modeling of masonry infill panels for structural analysis. *Journal of Structural Engineering*, **123**(10), pp. 1295-1303.
- Mazzoni, S., McKenna, F., Scott, M.H., Fenves, G.L. et al. (2009). *Open System for Earthquake Engineering Simulation User Command Language Manual*. Berkeley, CA: Pacific Earthquake Engineering Research Center, University of California Berkeley.
- Miles, C.A. (2002). *On-Farm Bamboo Production in the Pacific Northwest*. Washington State University Bamboo Research Report.
- Minitab (2008). *Minitab reference manual – Release 12 for Windows*. State College, PA: Minitab Inc.
- Mitch, D. (2009). Splitting Capacity Characterization of Bamboo Culms. *University of Pittsburgh Honors College Thesis*, March 2009. 88pp.
- Mitch, D., Harries, K.A., Sharma, B. (2010) (accepted for publication) Characterization of Splitting Behavior and Material Properties of Bamboo Culms. *ASCE Journal of Materials in Civil Engineering*.
- Mitch, D. (2010). Structural Behavior of Grouted-Bar Bamboo Column Bases. Master's Thesis, *University of Pittsburgh*. July 2010. 116 pp.
- Moreira, L.E. (1991). *Desenvolvimento de estruturas treliçadas espaciais de bamboo* (in Portuguese). Doctoral Dissertation, Pontifícia Universidade Católica – Rio de Janeiro.
- Naik, N.K. (2005). *Mechanical and physio-chemical properties of bamboo carried out by Aerospace Engineering Department*. Bombay, India: Indian Institute of Technology – Bombay.

- Nath, S.K., Sengupta, P. Sengupta, S. and Chakrabarti, A. (2000). Site response estimation using strong motion network: A step towards microzonation of the Sikkim Himalayas. *Current Science*, **79**(9/10), pp. 1316-1326.
- Nath, S.K. (2004). Seismic Hazard Mapping and Microzonation in the Sikkim Himalaya through GIS Integration of Site Effects and Strong Ground Motion Attributes. *Natural Hazards*, **31**, pp. 319–342.
- Nath, S.K. (2005). An initial model of seismic microzonation of Sikkim Himalaya through thematic mapping and GIS integration of geological and strong motion features. *Journal of Asian Earth Sciences*, **25**, pp.329–343.
- Nath, S.K., Thingbaijam, K.K.S, and Raj, A. (2008). Earthquake hazard in Northeast India – A seismic microzonation approach with typical case studies from Sikkim Himalaya and Guwahati city. *Journal of Earth System Science*, **117**(S2), pp. 809–831.
- NBCI (2005). *National Building Code of India*. India: Bureau of Indian Standards.
- NIST (2010). *NIST/SEMATECH e-Handbook of Statistical Methods*, <http://www.itl.nist.gov/div898/handbook/>, 2010.
- Nelson, C.W. (1939). *Stresses and Displacements in a Hollow Circular Cylinder*. Doctoral Thesis, University of Michigan.
- Nielson, B. and DesRoches, R. (2003). Seismic Fragility Curves for Bridges: a Tool for Retrofit Prioritization. *Advancing Mitigation Technologies and Disaster Response for Lifeline Systems: Proceedings of the sixth U.S. Conference and Workshop on Lifeline Earthquake Engineering*, Long Beach, California, Beavers, J.E. ed. Reston, Virginia: American Society of Civil Engineers, pp. 1060-1067.
- Nielson, B.G. and DesRoches, R. (2007). Seismic fragility methodology for highway bridges using a component level approach. *Earthquake Engineering and Structural Dynamics*, **36**, pp. 823-839.
- Obataya, E., Kitin, P. and H. Yamauchi (2007). Bending characteristics of bamboo (*Phyllostachys pubescens*) with respect to its fiber-foam composite structure. *Wood Science Technology*, **41**, pp. 385-400.
- Otani, S. (1974). *SAKE*, A computer program for inelastic response of R/C frames to earthquakes. *Report UILU-Eng-74-2029*, University of Illinois at Urbana Champaign, Civil Engineering, November 1974.
- Pal, I., Nath, S.K., Shukla, K., Pal, D.L., Raj, A., Thingbaijam, K.K.S. and Bansal, B.K. (2008). Earthquake hazard zonation of Sikkim Himalaya using a GIS platform. *Natural Hazards*, **45**, pp. 333-377.

- Paudel, S.K. (2008). Engineered bamboo as building material in modern bamboo structures. In *Proceedings of 1st international conference on modern bamboo structures (ICBS-2007)*, eds. Xiao, Y., Inoue, M., and Paudel, S.K. Changsha, China, October 28-30, 2007.
- PEER 1043. Kobe earthquake data, Peer Strong Motion Database.
<http://peer.berkeley.edu/smcat/data.html>
- PEER 0935. Northridge earthquake data. Peer Strong Motion Database.
<http://peer.berkeley.edu/smcat/data.html>
- Porter, K. et al. (2007). Creating Fragility Functions for Performance-Based Earthquake Engineering. *Earthquake Spectra*, **23**(2), pp. 471–489.
- Radio Cooperativa (2010). A 521 aumentaron los fallecidos por catástrofe en Chile (in spanish).
http://www.cooperativa.cl/prontus_notas/site/artic/20100515/pags/20100515121228.html
- Ranjan, M.P. et al. (1986). *Bamboo and Can Crafts of Northeast India*. New Delhi, India: Development Commissioner of Handicrafts, Government of India.
- Rohrbach & Gillmann (2002). ZERI Pavillion on the EXPO 2000, < bambus.rwth-aachen.de/>.
- Rosowsky, D.V. (2002). Reliability-based Seismic Design of Wood Shear Walls. *Journal of Structural Engineering*, **128**(11), pp. 1439–1453.
- Scott, M.H. and T. Haukaas. (2006). *Modules in OpenSees for the Next Generation of Performance-Based Engineering*, ASCE Conference. Proceedings, 202(33).
- Shao, Z.P., Fang, C.H., and Tian, G.L. (2009). Mode I interlaminar fracture property of moso bamboo (*Phyllostachys pubescens*). *Wood Science Technology*, **43**, pp. 527-536.
- Sharma B., Harries, K.A. and Kharel, G. (2008). Field Documentation and Survey of Bamboo Structures: Service Learning Opportunities in Sustainability Research. *Proceedings of Association for the Advancement of Sustainability in Higher Education (AASHE) 2nd Biennial Conference*, Raleigh, North Carolina, November 9-12, 2008.
- Sharma, B. (2010). Performance Based Design of Bamboo Structures. Doctoral Dissertation, *University of Pittsburgh*.
- Shinozuka, M. et al (2000a). Statistical Analysis of Fragility Curves. *Journal of Engineering Mechanics*, **126**(12), pp. 1224–1231.
- Shinozuka, M. et al (2000b). Nonlinear Static Procedure for Fragility Curve Development, *Journal of Engineering Mechanics*, **126**(12), pp. 1287–1295.
- Silbergliitt et al. (2006). *The Global Technology Revolution 2020, In-Depth Analyses Bio/Nano/Materials/Information Trends, Drivers, Barriers, and Social Implications*. Rand Corporation.

- Silva, E.C.N., Walters, M.C, and Paulino, G.H. (2006). Modeling Bamboo as a Functionally Graded Material: Lessons for the Analysis of Affordable Materials. *Journal of Material Science*, **42**, pp. 6991-7004.
- Talla, P.K., Tekougnening, J.R., Tangka, E. and A. Foudjet. (2004). Statistical model of strength in compression of *Raphia vinigera* L. (Arecacea). *Journal of Bamboo and Rattan*, **3**(3), pp. 6991-7004.
- Torres, L.A., Ghavami, K. and J.J. Garcia (2007). A Transversely Isotropic Law for the Determination of the Circumferential Young's Modulus of Bamboo with Diametric Compression Tests. *Latin American Applied Research*, **37**, pp 255-260.
- Trujillo, D. (2007). Bamboo Structures in Columbia. *The Structural Engineer*, **3**, pp. 25-30.
- Vlasov, V.Z. (1961). *Thin walled elastic beams*. 2nd ed. Washington, D.C.: National Science Foundation.
- Young, W.C. (1989). *Roark's Formulas for Stress & Strain*. 6th ed. New York: McGraw-Hill.
- Zhang, L.F., Xie, M. and L.C. Tang (2006). Robust Regression using Probability Plots for Estimating the Weibull Shape Parameter. *Quality Reliability Engineering International*, **22**, pp. 905-917.